T.C.

ANTALYA BILIM UNIVERSITY

INSTITUTE OF POSTGRADUATE EDUCATION

ELECTRICAL AND COMPUTER ENGINEERING

MASTER'S THESIS

DEVELOPMENT OF LOW-ION DOPED CR:LiCAF LASERS

Zekican ERTURK

JUNE 2023

ANTALYA

T.C.

ANTALYA BILIM UNIVERSITY

INSTITUTE OF POSTGRADUATE EDUCATION

ELECTRICAL AND COMPUTER ENGINEERING

MASTER'S THESIS

DEVELOPMENT OF LOW-ION DOPED CR:LiCAF LASERS

Zekican ERTURK

JUNE 2023

ANTALYA

T.C.

ANTALYA BILIM UNIVERSITY

INSTITUTE OF POSTGRADUATE EDUCATION

DEVELOPMENT OF LOW-ION DOPED CR:LiCAF LASERS

Zekican ERTURK

This study was supported by TUBITAK (The Scientific and Technological Research Council of Türkiye) Grant No: 119E264.

T.C.

ANTALYA BILIM UNIVERSITY

INSTITUTE OF POSTGRADUATE EDUCATION

DEVELOPMENT OF LOW-ION DOPED CR:LiCAF LASERS

Zekican ERTURK

This thesis was accepted by the jury (with unanimous vote / majority vote) on the date 22 /06/2023 in Electrical and Computer Engineering.

Asst. Prof. Dr. Yusuf ÖZTÜRK (Supervisor)

Prof. Dr. Ümit DEMIRBAS

Prof. Dr. Murat CANPOLAT

Director of The Institute

Prof. Dr. İbrahim Sani MERT

Thesis Submission Date:

DECLARATION

MSc Thesis of this study named “Development of Low Ion Doped Cr:LiCAF Lasers”, which I presented, I declare that scientific moral principles were followed in the preparation of this study, in case of benefiting from the works of others, reference is made in accordance with scientific norms, no falsification has been made in the data used, and that any part of this study is not presented as another academic study.

22/ 06 / 2023

Zekican ERTURK

CONTENTS

ABSTRACT

DEVELOPMENT OF LOW-ION DOPED CR:LiCAF LASERS

Zekican ERTURK

MSc Thesis in Electrical and Computer Engineering

Supervisor: Asst. Prof. Dr. Yusuf OZTURK

June 2023; 77 pages

Since the discovery of semiconductor lasers 50 years ago, these lasers have been found in numerous applications across various fields, including technology, scientific research, defense, healthcare, and more. These lasers required a great deal of aspects properties depending on the wavelength tunability and operation regimes. Based on this, for the femtosecond laser applications Ti:sapphire and Nd:YAG was one of the most prominent members of the solid-state laser family. Lately, as a low-cost alternative Cr:colquiirites lasers have been attracted. Cr:LiCAF laser, as a member of the colquiriite family, exhibits exceptional performance in terms of its physical properties, especially for power scaling applications. In this thesis, we have investigated diode pumped low ion doped Cr:LiCAF laser performance in terms of different laser operations. Power scaling potential of different lengths (10 mm, 12 mm, 15 mm, and 20 mm) Cr:LiCAF lasers tested with four multimode diode-pumped laser system. As a result, with a 10 mm 1.25% chromium doped gain medium 2.22 W output power was obtained. Continuous wave tuning range between 741-874 nm achieved. Afterward, in the gain switch experiments with a utilized pulse pumping setup 18% increase in the output power level was observed. We have also demonstrated the intracavity second harmonic generation. With different nonlinear crystals up to 441 mW, second harmonic power was generated. On the pulse generation parts, around 3 μs passively Q-switched Cr:LiCAF lasers were demonstrated. In passive mode-locking experiments, we have obtained a minimum of 65 fs pulses. Moreover, we have performed temperature estimation studies during lasing in Cr:LiCAF laser. Finally, off-surface birefringent filter plates two-color performance was tested on Cr:LiCAF laser numerically and experimentally. These studies show the potential of low-ion doped Cr:LiCAF laser for different applications.

KEYWORDS: Cr:LiCAF lasers, Diode pumped lasers, Mode-locked lasers, Second harmonic generation, Solid-State lasers

COMMITTEE: Asst. Prof. Dr. Yusuf ÖZTÜRK (Danışman)

Prof. Dr. Ümit DEMIRBAS

Prof. Dr. Murat CANPOLAT

ÖZET

DÜŞÜK İYON KATKILI CR:LiCAF LAZERLERİNİN GELİŞTİRİLMESİ

Zekican ERTÜRK

Yüksek Lisans Tezi, Elektrik ve Bilgisayar Mühendisliği Anabilim Dalı

Danışman: Dr. Öğr. Üyesi Yusuf ÖZTÜRK

Haziran 2023; 77 sayfa

50 yıl önce yarı iletken lazerlerin keşfiyle, bu lazerler teknoloji, bilimsel araştırma, savunma, sağlık ve daha fazlası dahil olmak üzere çeşitli alanlarda çok sayıda uygulamada kullanıldı. Bu lazerler, dalga boyu ayarlanabilirliğine ve çalışma rejimlerine bağlı olarak çok sayıda özellik gerektiriyordu. Buradan hareketle femtosaniye lazer uygulamaları için Ti:saphire ve Nd:YAG katı hal lazer ailesinin en öne çıkan üyelerinden biriydi. Son zamanlarda düşük maliyetli bir alternatif olarak Cr:colquiirites lazerler ilgi çekmektedir. Colquiriite ailesinin bir üyesi olan Cr:LiCAF lazer, fiziksel özellikleri açısından özellikle güç ölçeklendirme uygulamalarında olağanüstü performans sergilemektedir. Bu tezde diyot pompalı düşük iyon katkılı Cr:LiCAF lazer performansını farklı lazer operasyonları açısından inceledik. Farklı uzunluklarda (10 mm, 12 mm, 15 mm ve 20 mm) Cr:LiCAF lazerlerin güç ölçeklendirme potansiyeli, dört adet çok modlu diyot pompalı lazer sistemi ile test edilmiştir. Sonuç olarak 10 mm %1,25 krom katkılı kazanç kristali ile 2,22 W çıkış gücü elde edilmiştir. 741-874 nm arasında sürekli dalga ayar aralığı elde edildi. Daha sonra kazanç anahtarı deneylerinde çıkış gücü seviyesinde %18 artış gözlemlenmiştir. Ayrıca, kavite içi ikincil harmonik oluşturma deneyleri yapılmıştır. Farklı lineer olmayan kristaller ile 441 mW'a kadar çıkan ikincil harmonik güç üretilirmiştir. Darbe oluşturma deneylerinde, yaklaşık 3 μs pasif Q-anahtarlı Cr:LiCAF lazerler elde edilmiştir. Pasif mod kilitleme deneylerinde minimum 65 fs darbeli laser elde edildi. Daha sonra Cr:LiCAF lazerde lazerleme sırasındaki sıcaklık tahmin çalışmalarını gerçekleştirdik. Son olarak, yüzey dışı çift kırınımlı filtre kullanılarak iki-renkli Cr:LiCAF laser performansı deneysel ve numerik olarak test edildi. Bu çalışmalar, farklı uygulamalar için düşük iyon katkılı Cr:LiCAF lazerin potansiyelini göstermektedir.

ANAHTAR KELİMELER: Cr:LiCAF lazeri, Diyot pompalı lazerler, Ikincil harmonic üretimi, Katı-hal lazerleri, Kip-kilitli lazerler

JÜRİ: Asst. Prof. Dr. Yusuf ÖZTÜRK (Supervisor)

Prof. Dr. Ümit DEMIRBAS

Prof. Dr. Murat CANPOLAT

SYMBOLS AND ABBREVIATIONS

Symbols

E_1 : Energy level 1

E_2 : Energy level 2

h : Planck constant

v : Frequency of photon

τ : Lifetime

N_1 : Population of atoms in ground state

N_2 : Population of atoms in upper state

B_{12} : Einstein coefficient of absorption

ρ : Density of atoms

A_{21} : Einstein coefficient of spontaneous emission

B_{21} : Einstein coefficient of stimulated emission

k : Boltzmann constant

T : Temperature

c : Speed of light

R : Reflectivity

L : Length

g : Gain factor

λ : Wavelength

α : Absorption coefficient

η : Slope efficiency

σ_{ESA} : Excited state absorption cross section

σ_e : Emission cross section

L : Loss

P_{th} : Threshold power

w_p : Pump beam waist

w_c : Cavity beam waist

Abbreviations

LASER : Light amplification by stimulated emission of radiation

CW : Continuous wave

MASER : Microwave amplification by stimulation emission of radiation

MMD : Multimode diode

SMD : Single mode diode

BRF : Birefringent filter plate

BBO : Beta barium borate

BiBO : Bismuth borate

ML : Mode locking

RSD : Relative standard deviation

LIST OF TABLES

LIST OF FIGURES

PREFACE

This thesis presents my work on the topic of development of low-ion doped Cr:LiCAF lasers during the last 2 years. These years have been very educational in both a personal and professional way. I have had the privilege to work with amazing people. I would like to express my gratitude and appreciation to all the individuals who have contributed to the realization of this work. Their support, guidance, and collaboration have been instrumental in the completion of this project.

I would like to express my gratitude to my advisor Asst. Dr. Yusuf Öztürk, for his guidance and support since my undergraduate years. I am grateful for his mentorship and opportunities he has provided. I also would like to extend my deepest thanks to Prof. Umit Demirbas. within his limited time, he provided the opportunities of ABU-LTL and always enlightened the way that we are on. I need to thank to member of ABU-LTL, research assistant Serdar Okuyucu and M. Fetih Mekteplioğlu for their friendship and technical support. I would like to express my deepest appreciation to my dear friend Muharrem Kılınç. I have always felt his friendship and support from our undergraduates' years. His companionship has always been valuable in my personal and professional life.

Last but foremost, I would like to thank my family, especially my mother for her endless exertion on me.

1. INTRODUCTION

1.1. Overview

Over the years scientists have been working on understanding the principle and behavior of light. This pursuit of knowledge has led to the development of numerous technologies that harness the unique properties of light for a variety of applications. Among these technologies, the laser stands out as one of the most powerful and versatile. Engineers and scientists have been interested in lasers for their wide range of applications across various fields. Lasers have found utility in diverse areas, including communication, medicine, and manufacturing, and have played a pivotal role in revolutionary advancements in fields like biophotonics and quantum computing. One significant application of lasers is in telecommunication systems, where they are utilized to convert electrical signals into optical signals. These optical signals can be transmitted over long distances by means of fiber optic cables. Optical amplifiers, which use lasers to boost the optical signals along the way, help ensure that the signals remain strong and clear throughout the transmission. This allows for reliable and high-speed data transfer, making lasers a crucial component in modern communication networks. LASIK eye surgery is one of the most well-known applications of laser technology in medicine. During the procedure, a femtosecond pulsed laser is used to create a thin flap in the cornea, which is then lifted to allow for the reshaping of the underlying tissue with an ultraviolet laser. This precise reshaping of the cornea can correct common vision problems like nearsightedness, farsightedness, and astigmatism, and has become a popular alternative to traditional eyeglasses or contact lenses for many people.

While lasers have become popular in many fields, developing and optimizing laser systems still requires a deep understanding of the underlying physics that governs their behavior. This includes a thorough understanding of concepts such as stimulated emission, population inversion, and optical feedback, as well as the complex interactions between different components of a laser system. Without this fundamental knowledge, it would be difficult to develop new and improved laser technologies that meet the specific needs of different applications. Additionally, ongoing research in laser physics continues to drive innovation and advance our understanding of this fascinating area of science.

1.2. Thesis Organization

In this thesis, we focused on investigating the behavior of low-ion doped Cr:LiCAF laser systems under different operation conditions. This could involve exploring the various laser operation conditions, such as continuous wave (CW) operation, pulsed operation, and second harmonic generation, to understand how these systems behave and how they can be optimized. This thesis consists of 4 chapters. In the following Chapter, there is a brief history of the development of laser technology, including the evolution of the fundamental principles of laser operation. Involving key historical milestones in laser research, such as the work of Max Planck, Albert Einstein, and Charles Hard Townes. In Chapter II, the theoretical background of laser operations and underlying principles are discussed. This includes an overview of the basic principles of optical amplification, population inversion, and the stimulated emission process that is essential for laser operation. In addition, a brief literature review of Cr:LiCAF laser is

provided, which is a member of the colquiirite gain medium family. In Chapter III, the experimental results of different operations that were carried out during the thesis are presented. Chapter III of this thesis presents the experimental results of the various laser operations that were conducted during the research. This chapter includes a detailed description of the experimental setup, as well as the procedures and techniques used to achieve the desired laser behavior. Finally, in Chapter IV conclusion of the results obtained is presented. The fourth and final chapter of this thesis presents the conclusions drawn from the results obtained in the previous chapters. It summarizes the main findings and contributions of the study and discusses their significance and implications. Additionally, it provides recommendations for future research and directions for the field.

1.3. Brief History of Laser Technology

The origins of laser technology can be traced back to the early 1900s when Max Planck, a German scientist, made a groundbreaking discovery. Max Planck formulated the mathematical relationship that describes the energy distribution of electromagnetic radiation emitted by a blackbody, which came to be known as the “Planck Radiation Law.”. He proposed that electromagnetic energy can be emitted or absorbed in quantized amounts, known as “quanta”. Planck’s discovery of quantized energy was a major milestone that led to quantum theory’s development. In 1905, German-born physicist Albert Einstein used the quantum theory to develop the photoelectric effects. In his paper, he proposed that light delivers energy to the contacted surface (Einstein, 1905). Later on, he received the 1921 Nobel Prize in Physics for the discovery of the photoelectric effect. In 1917, Einstein build up his studies and provided the quantum theory of light-matter interaction (Einstein, 1917). This theory paved the way for the identification of the process of absorption, spontaneous emission, and stimulated emission of electromagnetic radiation. All these discoveries laid the foundation for the development of laser technology. Inspired by Einstein’s quantum theory, Charles Hard Townes began his search for a solution to create a microwave radiation oscillator with a higher frequency in 1951.

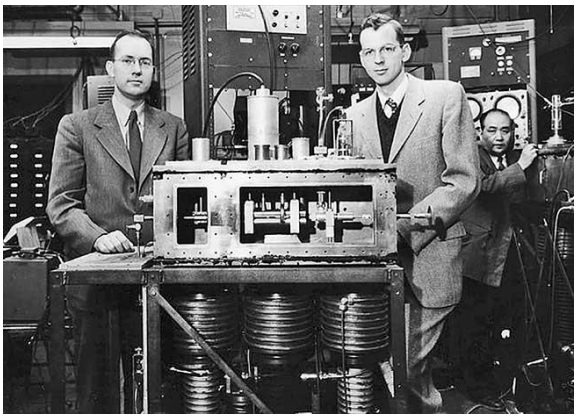

Figure 1.1. Charles Hard Townes (left) and James Power Gordon (right) with developed MASER device
Source: https://www.photonics.com/Articles/From_Masers_to_Lasers_in_Space_and_at_the/a61182

In 1954, Townes and his collaborator researchers James Power Gordon and Herbert Zeiger built the first MASER, which stands for “Microwave Amplification by Stimulated Emission of Radiation” operating at a wavelength of around 1.25 cm (Townes et al., 1955). Which was used for the stimulated emission of ammonia molecules to produce amplification of microwave emission. Later on, in 1958, Townes and Arthur Leonard Schawlow extended the study to the infrared and optical regions (Schawlow & Townes, 1958). These studies granted him to Nobel Prize in Physics in 1964, jointly with Nicolay Gennadiyevich Basov and Aleksandr Mikhailovich Prokhorov, for their pioneering work on the theory of stimulated emission and its application in the development of masers and lasers.

In the history of laser technology, one of the groundbreaking developments was achieved in 1960 by physicist Theodore Harold Maiman. The first working laser was constructed using a pink ruby crystal and optically pumped by a helical flashlamp surrounding the cylindrical laser crystal. This was the first time ever produced, coherent and in-phase electromagnetic radiation in the optical spectrum. The first laser produced by Maiman had a wavelength of 694.3 nm, which is in the red part of the visible spectrum. He published his study as “Stimulated Optical Radiation in Ruby” (Maiman, 1960). While the acronym “LASER” (Light Amplification by Stimulated Emission of Radiation) was first proposed by American physicist Gordon Gould, it was Theodore Maiman who first implemented the concept in real life by demonstrating the first working laser in 1960. Indeed, Maiman’s discovery of the solid-state laser was a major milestone in laser technology and led to the further development of various types of lasers for different applications. Today, lasers are used in many aspects of modern life, including in industry, medicine, telecommunications, and entertainment, to name just a few examples. The versatility and precision of lasers make them an important tool in many fields, and ongoing research continues to push the boundaries of what lasers can do.

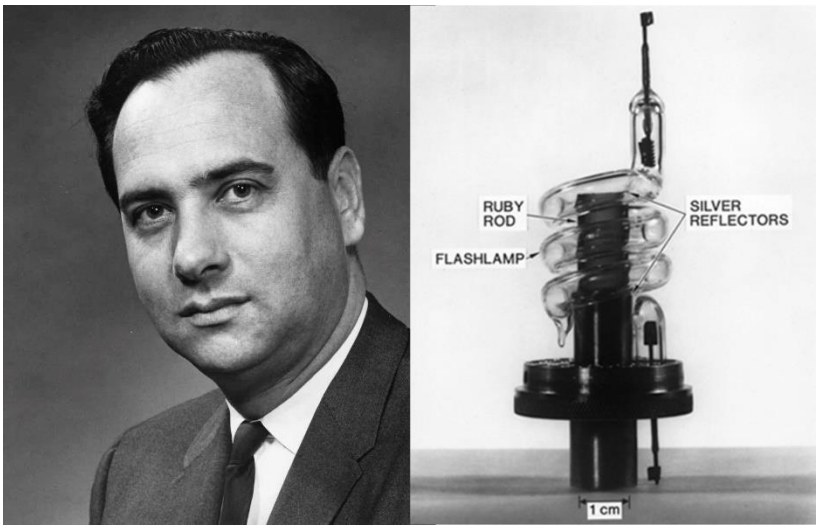

Figure 1.2. Theodore Harold Maiman (left) and first laser developed with ruby crystal (right)
Source: https://history.aip.org/phn/11606001.html

2. THEORETICAL BACKGROUND

In this chapter, we will begin by introducing the fundamental principles of solid-state lasers, including their construction, working mechanism, and unique properties. Next, we will dive into the concept of optical amplification, which is essential to understand how lasers can generate high-intensity beams of light. We will also discuss the fundamental processes of absorption, emission, and stimulated emission that governs the behavior of laser materials. Finally, we will explore the different operation regimes of solid-state lasers, including continuous wave, Q-switching, and mode-locking. Through this comprehensive discussion, we aim to provide a deeper understanding of solid-state lasers and their potential applications in various fields.

2.1. Introduction to Solid-State Lasers

In a solid-state laser, the gain medium commonly consists of a solid crystal or a glass material that is doped with ions. By utilizing an external energy source, such as a flashlamp or another laser, these ions within the gain medium can be excited to a higher energy level. Semiconductor lasers also use a solid-state material as the gain medium, but they differ from doped crystals in terms of their structure and mechanism of operation (Weber, 2000). In a semiconductor laser, applying the voltage across the p-n junction, with a movement of electron-hole pairs, results in the formation of population inversion. Populated inversion region triggers the stimulated emission of photons leading to laser action. The host material used in the gain medium of a solid-state laser should have good optical properties, such as high transparency at the laser wavelength, low optical absorption, and a broad emission band to facilitate the population inversion. In addition, it should have good mechanical and thermal properties to ensure stability and efficient heat dissipation. Sapphire and YAG (yttrium aluminum garnet) are among the most commonly used host materials for solid-state lasers. Sapphire is particularly well-suited for use in high-power laser systems due to its excellent thermal conductivity and mechanical properties (Moulton, 1986), while YAG has a high damage threshold (Gensic et al., 1964) and can be used to produce laser radiation in a wide range of wavelengths.

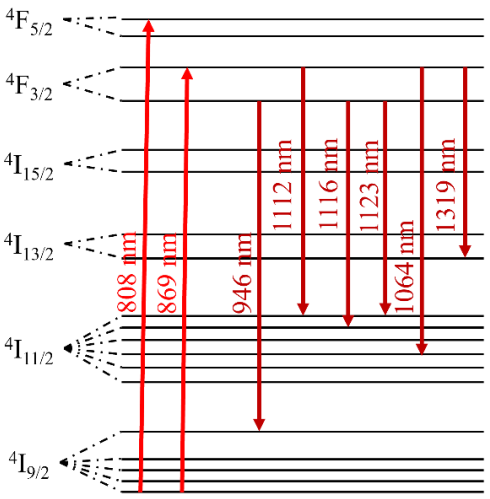

Figure 2.1. Energy level diagram of Nd^{3+}:YAG gain medium (Chaoyang et al, 2010)

The active ions in solid-state lasers are dopant atoms that are added to the host crystal or glass material. The interaction between the laser active-ions and the host material is crucial in determining the fundamental properties of lasers. This includes factors such as the spectral range of operation, the lifetime of excited states, the efficiency of the laser system, and other properties. Typically, rare earth ions and transition metal ions are the two categories of ions that are utilized as active ions. Along with the largest class of ions, due to their distinct fluorescent transition across a broad optical range, rare earth ions constitute the most extensive class of laser ions and are commonly employed (Koechner, 2006). Neodymium (Nd) is among the most recognizable members of rare earth ions and demonstrates multiple groups in the near-infrared spectrum, encompassing wavelengths around 900 nm, 1060 nm, and 1300 nm. Nevertheless, the most intense transition arises between $^4F_{3/2} \rightarrow {}^4I_{11/2}$ (figure 2.1) at 1050 nm and 1100 nm, which relies on the host lattice. Typically, 806 nm diode lasers are used as triggers for this transition. Besides, in the high-power application, ytterbium (Yb) ions are often used due to their short energy states, and better thermal solution (Denker & Shklovsky, 2013). Table 2.1 shows the most commonly used rare earth ions doped host material and corresponding wavelengths (Paschotta, 2008).

Table 2.1. Most commonly used rare earth ions doped host material and emission wavelengths

Ion	Common Host Media	Emission Wavelength
Neodymium (Nd^{3+})	YAG, YVO_4, YLF, Silica	1030-1100 nm, 900-950 nm, 1320-1350 nm
Ytterbium (Yb^{3+})	YAG, Tungstates, Silica	1000-1100 nm
Erbium (Er^{3+})	YAG, Silica	2940 nm, 1500-1600 nm, 550 nm
Thulium (Tm^{3+})	YAG, YLF, Silica, Fluoride Glasses	1700-2100 nm, 1450-1530 nm, 480 nm, 800 nm
Holmium (Ho^{3+})	YAG, YLF, Silica	2100 nm, 2800-2900 nm
Cerium (Ce^{3+})	YLF, LiCAF, LiluF, LiSAF	280-330 nm
Praseodymium (Pr^{3+})	Silica, Fluoride Glasses	1300 nm, 600nm, 520 nm, 490 nm

Compared to rare earth ion-doped crystals, transition metal ions possess transitions between the 3d-3d shell and offer outstanding characteristics for broadband laser operations. Additionally, they have a broader gain bandwidth and, because of the electron shell vibration of the host medium, are preferred for generating few-cycle pulses (Sorokin, 2004). Transition metal ions commonly employed as active ions include titanium (Ti), chromium (Cr), vanadium (V), nickel (Ni), manganese (Mn), cobalt (Co), and iron (Fe) (Weber,1998). Ti^{3+} doped sapphire is the most common illustration in this group and recognized for its broad emission range. The laser has a wide gain bandwidth in between 660-1180 nm, making it operable over a broad range of wavelengths. Moreover, the reported highest peak power obtained from the laser is around 10 petawatt (PW) with a pulse duration of 21 fs (Wenqi et al., 2018). Table 2.2 shows the frequently

utilized transition metal ions doped host material and their corresponding wavelengths (Paschotta, 2008a; Weber,1998).

Table 2.2. Most commonly used transition metal ions doped host material and emission wavelengths

Ion	Common Host Media	Emission Wavelength
Titanium (Ti^{3+})	Sapphire	650-1100 nm
Divalent Chromium (Cr^{2+})	ZnS, ZnSe	3000-3400 nm
Trivalent Chromium (Cr^{3+})	Ruby (Al_2O_4), Alexandrite ($BeAl_2O_4$), LiCAF, LiSAF, LiSGAF	800-900 nm
Vanadium (V^{2+})	$KMgF_3$	1064 nm

2.2. Optical Amplification, Absorption & Stimulated Emission

The term LASER stands for Light Amplification by Stimulated Emission of Radiation, which refers to a source of light that uses optical amplification of electromagnetic waves to produce a coherent and monochromatic beam of light. The fundamental principle underlying lasers is the phenomenon of stimulated emission of radiation. To grasp the concept of stimulated emission, it is crucial to have knowledge of the different processes that can take place when light interacts with matter. Atoms, ions, and molecules exist in discrete energy states, and transitions between these states involve the emission or absorption of a photon. These changes are known as atomic transitions. As a starting point simple 2-level energy system is shown as an example.

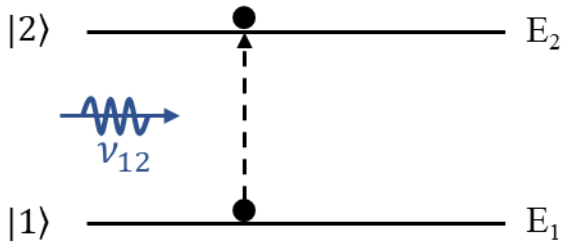

Figure 2.2. Diagram of ideal 2-level atomic systems absorption process

In 2-level energy systems, an atom can only be in one state, ground (E1) or excited (E2). The ground state is the lowest energy state that can atom occupy, while the excited state is the higher energy state that can atom reach by absorbing energy from the outer source. Excitation occurs when an atom absorbs energy, such as a photon, which has energy equal to the difference between E1 and E2. After the interaction of the atom and photon, the resident electron on the ground state makes a transition from a lower energy level to a higher energy level (figure 2.2). This optical transition is known as the absorption of light. The relation between absorbed photons and atomic energy system can be represented by;

$$E_2 - E_1 = h\nu_{12} \tag{2.1}$$

where h is Planck constant and ν_{12} is the frequency of photon. After being excited, the atom stays in the excited state E_2. The duration for which an atom remains in an excited state is referred to as its lifetime (τ). As a consequence of the instability of the E2 state, the atom will tend to return to its ground state E1 via a process known as spontaneous emission (figure 2.3). In the case of 2-level system, the emitted photon has energy equal to the energy difference between the two levels (E_2-E_1), same as absorbed photon energy. So, it has the frequency of ν_{12}.

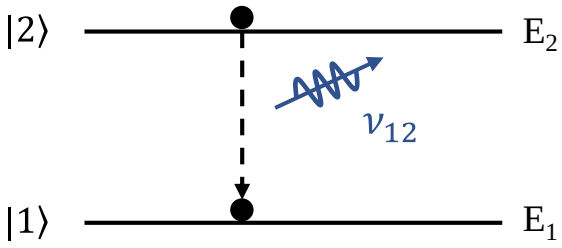

Figure 2.3. Diagram of spontaneous emission process

To gain a detailed understanding of this optical transition, it is necessary to describe the process in terms of its rates. The population of atoms in the ground state E_1 and the excited state E_2 can be denoted as N_1 and N_2 respectively. As a starting point, the rate of absorption can be expressed in terms of Einstein's coefficients, which represent the number of atoms transitioning from the ground state to the excited state at any given time. The rate of absorption is proportional to the intensity of the incident radiation and the population of atoms N_1 in the ground state. The rate of absorption can be represented as;

$$\text{Rate of absorption} = -\frac{\partial N_1}{\partial t} B_{12}\rho(h\nu_{12}) \tag{2.2}$$

where B_{12} is Einstein's coefficient of absorption, $\rho(h\nu_{12})$ is the density of atoms that has energy $h\nu_{12}$. After the absorption, the atom spontaneously decays back to the ground state by emitting photons. The rate of spontaneous emission is proportional to the population of excited atoms N_2. The rate of spontaneous emission can be represented as;

$$\text{Rate of spontaneous emission} = -\frac{\partial N_2}{\partial t} A_{21} \tag{2.3}$$

whereA_{21} is Einstein's coefficients of spontaneous emission and can be represented by the reciprocal of the lifetime $\frac{1}{\tau}$ (Eichler et al., 2018). Unlike the absorption process, there is no radiation field in the spontaneous emission. The direction and the phase of emitted photons occurs randomly.

In addition to the well-known spontaneous emission of fluorescence, Einstein proposed the existence of another mechanism for fluorescence emission. According to his

theory, the decay of an excited atom can also be triggered by an incoming photon. In other words, the excited atom, which is already in the excited state, can be knocked by incoming photons in a harmonic way. This leads amplification of incident photons. This process is known as stimulated emission.

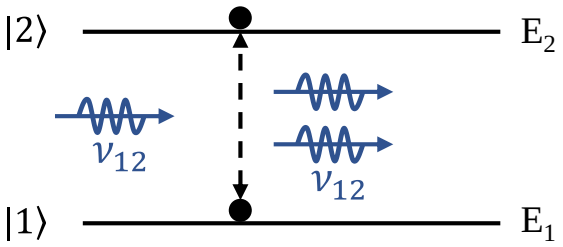

Figure 2.4. Diagram of stimulated emission process

Stimulated emission process can be represented in terms of rate by applying the Einstein's coefficient as follows,

$$\text{Rate of stimulated emission} = -\frac{\partial N_2}{\partial t} B_{21} \rho(h\nu_{12}) \tag{2.4}$$

where B_{21} is Einstein's coefficient of stimulated emission. Note that, the negative sign is coming from the decay change of a number of atoms in the related state. Photons emitted through spontaneous emission travel in various directions, while photons produced through stimulated emission propagate in the same direction with the same phase and frequency. This determines the important characteristic of laser, "coherence".

According to the system equilibrium principle, or principle of detailed balance, the transition of the kinetic systems should be equal in thermal equilibrium. In other words, the rate of transition from the ground state to the excited state must be equal to the rate of emission from the excited state to the ground state (Klein, 1955). This equality can be represented as follows,

$$\frac{\partial N_1}{\partial t} = -\frac{\partial N_2}{\partial t} \tag{2.5}$$

$$B_{12} N_1 \rho(h\nu_{12}) = A_{21} N_2 + B_{21} N_2 \rho(h\nu_{12}) \tag{2.6}$$

$$\rho(h\nu_{12}) = \frac{A_{21}}{B_{12}} \frac{N_2}{N_1} \frac{1}{\left(1 - \frac{B_{21}}{B_{12}} \frac{N_2}{N_1}\right)} \tag{2.7}$$

Further, by applying the Boltzmann statistics (eq. 2.8), which describe the probability of finding atoms in a particular energy state at thermal equilibrium (Maini, 2013).

$$\frac{N_2}{N_1} = exp\left(\frac{-(E_2 - E_1)}{kT}\right) \tag{2.8}$$

then the expression becomes,

$$\rho(h\nu_{12}) = \frac{A_{21}}{\left(B_{12}\exp\left(\frac{\Delta E}{kT}\right) - B_{21}\right)} \tag{2.9}$$

where k is the Boltzmann constant and T is temperature. From this expression by comparing Planck law of radiation (eq. 2.10), under some conditions, Einstein's coefficients can be described as,

$$\rho(\nu, T) = \frac{2h\nu^3}{c^2}\frac{1}{\left(\exp\left(\frac{\Delta E}{kT}\right) - 1\right)} \tag{2.10}$$

$$\frac{A_{21}}{B_{21}} = \frac{2h\nu^3}{c^2} \; and \; B_{12} = B_{21} \tag{2.11}$$

The relation between Einstein's coefficients is very crucial to obtain the stimulated emission of radiation. Equality between the rate of absorption and rate of stimulated emission describes the number of atoms rising to the excited state equal to the number of atoms that decays back to the ground state, which means that the system is neither amplify nor de amplify. However, in order to achieve stimulated emission of radiation, it is necessary to have a situation where the rate of stimulated emission is greater than the rate of absorption. Additionally, the relationship between the rates of spontaneous emission and stimulated emission is also crucial for laser operation. According to equation 2.11, as the frequency of photons increases, the ratio between spontaneous and stimulated emission also increases, leading to more spontaneous emission. Conversely, at lower frequencies, such as microwave frequencies, the ratio is lower, making the stimulated emission process easier. As a result of stimulated emission, the emitted photons have several properties. The emitted photon has the same energy, frequency, and direction as the incident photon that caused the stimulated emission. This is known as coherence and is what makes laser light unique compared to other sources of light. Allows laser light to be focused on a narrow spot and travels over long distances without any diffraction. Besides, stimulated emission occurs in phase with incoming photons, so the emitted photons are all in phase with each other.

In order to obtain stimulated emission, there is a condition, as mentioned in the upper paragraph, which is the number of atoms in the excited state should be larger than the number of atoms in the ground state. In other words, $N_2 > N_1$ where there is optical gain in the system. This situation is named population inversion. However, in a two-level system, it is not possible to achieve a population inversion. Considering the total number of atoms in the system remain constant, $N_1 + N_2 = N_t$, since there are two atomic levels that involve transition, N_2 and N_1 reach only equal number of atoms, which is named as saturation. Therefore, in order to achieve population inversion more than two energy

levels are required (Sennaroglu, 2010).

As an alternative to a two-level system, the three-level system can be used to obtain population inversion. In a three-level system, there are three energy levels involved in the transition process, with one additional energy state that atoms can reside in between the ground state and the excited state. This additional energy level is typically referred to as the "pump state" or the "metastable state" (E_2 in figure 2.5).

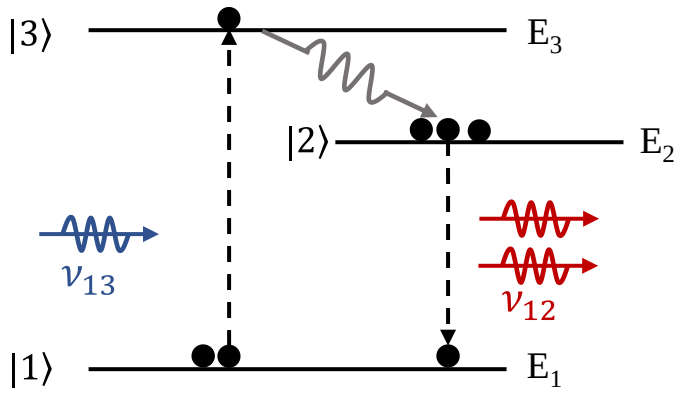

Figure 2.5. Diagram of three-level energy system

As an initial step, photons coming in excite the atoms that are in the ground state E_1 to the excited state E_3. Then, the excited atoms in the E_3 decay back to the metastable state E_2. It is important to note that during the atom transition between E_3 and E_2, there is no radiation emitted. The transition happens through a non-radiative process that takes a very short time. The energy loss caused by the transition between the excited state and metastable state is transferred to the crystal lattice by phonon emission. As will be discussed in the following chapters this energy transfer creates a heat load caused by the lattice vibration. The metastable state E_2 has a relatively long lifetime (τ) rather than the excited state E_3, meaning that atoms can remain in this state for a significant amount of time before decaying back to the ground state E_1 via a radiative process, such as spontaneous emission or stimulated emission. In other words, the radiative lifetime of the metastable state must be larger than the non-radiative lifetime of the excited state $\tau_2 \gg \tau_3$. This allows for the population of the E_2 state to exceed that of the ground state E_1, resulting in population inversion and stimulated emission. However, in a three-level system, it is difficult to maintain population inversion. Initially, in thermal equilibrium, all atoms are at the ground level. Then the excited atom, at least 50% atoms should be in a metastable state, decays back in short period of time to the metastable state. This will cause the reduction of atoms in energy levels E_1 and E_3 (Svelto, 2010). Maiman's first ruby (Cr^{+3}:Al_2O_3) laser can be shown as an example of three-level laser system (Maiman, 1960). Besides, Nd:YAG laser which has 946 nm transition another popular three-laser system (Sennaroğlu, 2010). Moreover, widely tunable alexandrite (Cr^{+3}:$BeAl_2O_4$) lasers also have a three-level transition (Walling et al., 1980).

The four-level laser systems are generally used to eliminate this sort of problem by providing favorable features such as obtaining the population inversion. In the four-level system, there is an additional atomic energy level between the ground state E_1 and

metastable state E_2 (figure 2.6), which provides additional non-radiative decay for atoms, allowing for a longer lifetime in the metastable state.

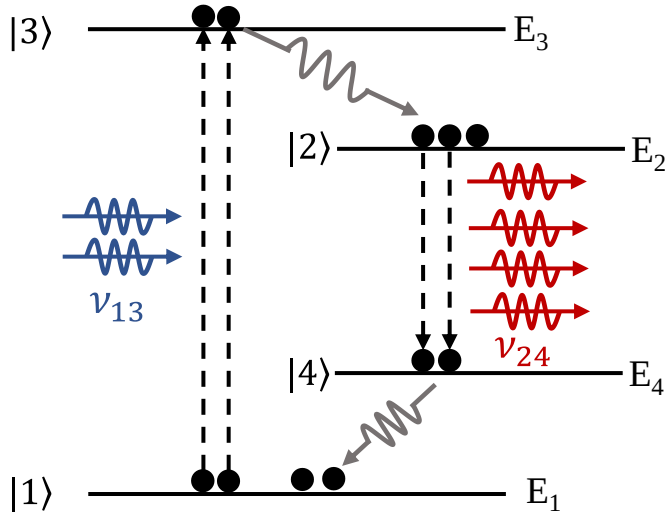

Figure 2.6. Diagram of four-level energy system

The pumping mechanism initiates the transition of atoms E1 (lower energy level) through E3 (higher energy level), and atoms rapidly decay to a slightly lower energy level E_2 by the non-radiative transition. This leads to population inversion of atoms in E_2. One condition for this transition is that the lifetime of excited energy level τ_3 must be smaller than the lifetime of the metastable energy level τ_2. In other words, to achieve population inversion on the metastable energy state, atoms must reside longer in the metastable state than in the excited state. Then transition occurs between E_2 and E_4 radiatively, which means a downward transition emits stimulated photons. After the transition, the atoms in E_4 rapidly decay back to the ground state E_1. The key difference between the four-level system and the three-level system is that in the four-level system, due to the non-radiative fast decay, the E_4 state remains empty. This continuous population inversion on the metastable state E_2 is crucial for the operation of a four-level laser system, as it ensures that there are always more atoms in the excited state E_2 than in the ground state E_1, allowing for stimulated emission to occur continuously. This results in a coherent and intense beam of laser light.

2.3. Optical Resonator

In a laser, optical amplification of light is combined with continuous oscillation to produce a highly coherent and monochromatic beam of light. This process can be achieved by combining the optical amplification and optical resonator (figure 2.7). As an amplification source, the gain medium is placed inside the two parallel highly reflective mirrors so that the emitted light travels along the mirror spacing back and forth to build up light energy.

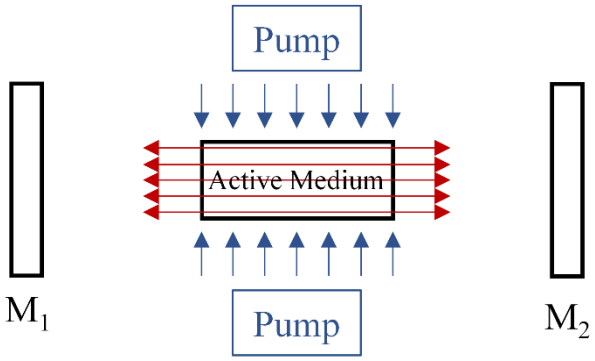

Figure 2.7. Two-mirror optical resonator

The active medium inside the optical cavity is pumped with an external energy source, such as a flash lamp or a laser diode, which causes the electrons to become excited and move to higher energy levels. When a photon passes through the active medium, it can stimulate the emission of another photon with the same energy, direction, and phase as the original photon, due to the principle of stimulated emission. The two mirrors in the optical cavity then reflect this photon back and forth between them, causing it to pass through the active medium multiple times and stimulate the emission of even more photons. A laser system with a pair of fully reflective mirrors, similar to any positive feedback system, has the potential to infinitely amplify itself. However, the feedback is limited by the losses in the cavity, which restricts the degree of amplification (Hecht, 1999). To address this issue, one of the mirrors is made partially transparent to allow some of the built-up light to escape. This partially transparent mirror shapes the output of the laser beam.

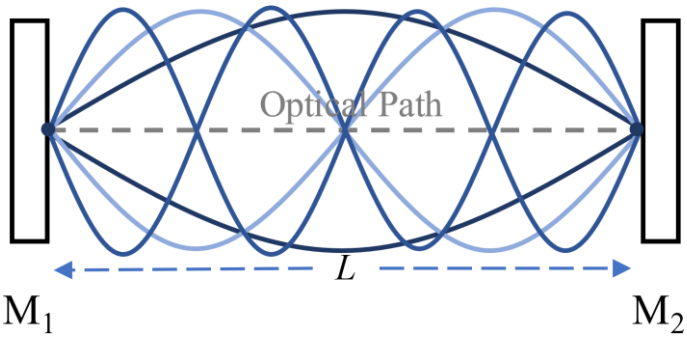

Figure 2.8. Longitudinal modes of optical resonator

In the presence of oscillation, there is resultant amplitude building. The simplest example of this can be shown as Fabry-Perot interferometer. This is a cavity consisting of two end mirrors. When light enters the Fabry-Perot interferometer, it goes through multiple reflections between the mirrors, resulting in the interference of the reflected and transmitted waves. The interference arises from the constructive and destructive interference of waves that have traveled to different optical paths within the cavity. As a result of constructive interference, multiple modes complete their round trip within a

spectral range. These modes can be found with $m = 2L / \lambda$ where m is an integer and L is the distance between two mirror and λ is the wavelength. This relation can represent in terms of frequency via $\nu = m(c/2L)$. Figure 2.8 shows the illustration of the longitudinal modes of the laser resonator.

2.4. Operation Regimes

The remarkable characteristics of lasers make it possible to employ various operational modes. While the continuous wave (cw) operation provides a stable high power uninterrupted beam of light, pulse operation provides short pulse duration, and high peak intensity of light (Eichler et al., 2018). Depending on the pulse duration, Q-switched and mode-locked (ML) lasers are generally utilized. Q-switched lasers offer high energy pulses on the microsecond (μs) to nanosecond (ns) pulses, and mode-locked lasers offer short intense light in picoseconds (ps) to femtoseconds (fs) region. In this sub-section, the different laser operation is briefly explained.

2.4.1. Continuous Wave (CW) Lasers

Continuous wave laser operation means that the laser operates continuously by non-stop emission of light. One of the important parameters here is the pump source should be kept on during the amplification process. Depending on the structure of the resonator, such as adjustment on resonator length, different spectral outputs can be controlled. However, to obtain the continuous wave laser output, there should be a condition to satisfy which is the lasing threshold. The threshold condition is defined as the minimum amount of pump power needed to achieve laser oscillation. It depends on the gain of the active medium, the losses in the cavity, and the geometry of the laser resonator. Assuming a laser system with two mirrors, which have a reflectivity of R_1 and R_2, and a gain medium length of l. Gain coefficient of gain medium can be described as g and the intensity gain factor of $e^{(gl)}$. Losses occur in the photon intensity that travels inside the cavity and gain medium due to internal scattering losses caused by the gain material, as well as losses caused by the mirrors. The round-trip gain can be expressed,

$$G = R_1 R_2 e^{(2gl)} \tag{2.12}$$

Considering the absorption losses, which is proportional to gain medium length,

$$G = R_1 R_2 e^{(g-a)2l} \tag{2.13}$$

By rearranging the equation, and from the theory of net gain should be greater than the unity to find the threshold,

$$g = \alpha + \frac{1}{2l} ln\left(\frac{1}{R_1 R_2}\right) \tag{2.14}$$

when the gain coefficient exceeds 1 then the laser action start to initiate. The gain medium starts to amplify the photons, and the photons reflect back and forth between the two

mirrors. The laser output power increases linearly with the pumping power until it reaches the saturation level, where further increase in pumping power does not lead to a significant increase in output power.

2.4.2. Q-switching

Q-switching is another laser operation used to produce high energy pulses on the scale of nanoseconds. The name Q-switching is derived from the Q-factor, which is a measure of the quality of an optical resonator (eq.2.13).

$$Q = \frac{\nu_0}{\Delta\nu} \tag{2.13}$$

where ν_0 is the centered emission frequency and $\Delta\nu$ is the spectral width. This can be described as the ratio of the energy stored in the cavity to the energy loss per optical cycle. To put it simply, increasing the losses in a laser cavity leads to a decrease in its quality, while decreasing the losses leads to an increase in its quality. In Q-switching, the Q-factor of the laser cavity is modified to allow the buildup of energy before releasing it as a high-energy pulse. In other words, by increasing the cavity losses during the continuous population inversion, build up a much more population inversion inside the gain medium, and after a short period of time by decreasing the losses the Q factor of the cavity rapidly switching back to the high position. As a result of this switch mechanism high-energy laser pulses were obtained. The Q-switching operation is typically achieved using an active device such as an optical switch or acousto-optic modulator in the cavity that can be controlled externally and a passive device as a saturable absorber (Paschotta, 2008b). For example, one of the earliest demonstrations of pulse operation was achieved with a ruby crystal using Kerr cell switching, which resulted in the generation of 0.2 μs pulses (McClung & Hellwarth, 1962).

2.4.3. Mode-Locking

Mode-locking is another technique to create laser pulses in the range of picosecond (10^{-12}) to femtosecond (10^{-15}) pulse width and named as ultrashort lasers. Unlike the Q-switching laser, in a mode-locked laser the pulse duration is generally shorter than the cavity round-trip time. The laser cavity is designed to support many longitudinal modes that are closely spaced in frequency by $\Delta\nu = \frac{c}{2L}$ where c is the speed of light and L is the cavity length. These randomly phased longitudinal modes interfere with each other to produce a train of short pulses that are separated by the cavity round-trip time. The resulting pulse duration is determined by the spectral width of the modes. In other words, all the longitudinal modes inside the cavity have a different phase while circulating inside the cavity. At a point inside the cavity depending on the cavity length, the modes are interfered with each other and as a result of this interference create signal with random amplitudes. This leads to random fluctuation in the electric field intensity of the generated laser. On the other hand, when all longitudinal modes come in the same phase, this will create constructive interference and high-intensity laser pulses (figure 2.9). The separation of the locked pulses in a mode-locked laser is directly related to the

cavity round trip time. The round-trip time is the time it takes for a light pulse to travel from one end of the laser cavity to the other and back again. In a mode-locked laser, the pulse train is locked to the cavity round-trip time, which means that the separation between the pulses is equal to the round-trip time divided by the number of pulses in the train. This relationship is expressed mathematically as:

$$\Delta T_p \cong \frac{1}{\Delta v} \cong \frac{2L}{c} \tag{2.14}$$

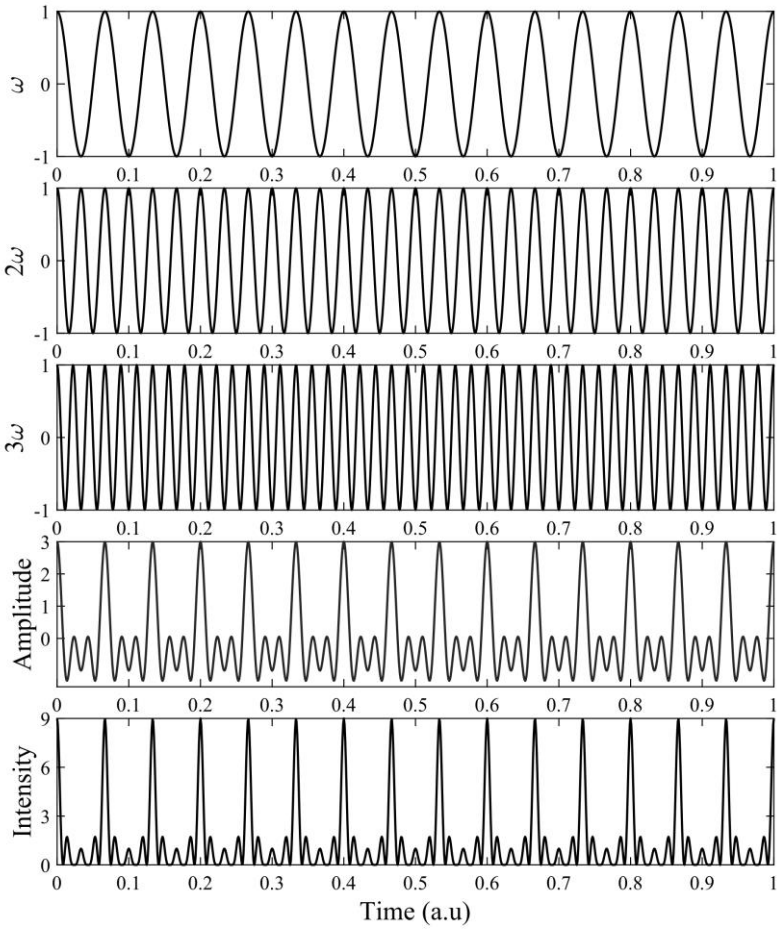

Figure 2.9. Illustration of three different modes that are in phase and their sum of Amplitude and Intensity (Silfvast, 2004)

In a mode-locked laser, the pulses are very short, typically in the picosecond or femtosecond range. The duration of these pulses is determined by the spectral bandwidth of the laser output and the shape of the pulse in the time domain. The spectral bandwidth of the laser output is determined by the gain bandwidth of the laser material and the cavity length. The shorter the cavity length, the broader the gain bandwidth and the wider the

spectral bandwidth of the laser output. In general, the duration of the laser pulses is expressed mathematically as:

$$\Delta t_p \cong \frac{1}{N\Delta v} \cong \frac{2L}{Nc} \tag{2.15}$$

The pulses that are obtained are referred to as transform limited. Different approximations were applied to obtain pulse duration depending on the experimental setup and cavity design. Table 2.3 presents various pulse shapes and their corresponding bandwidth products. Both active and passive methods can be utilized to achieve mode-locking. In active mode-locking, an external device similar to an acousto-optic modulator (AOM) or electro-optic modulator (EOM) is used to actively modulate the cavity, as in the Q-switching, resulting in the production of mode-locked pulses. The first ever active mode-locked was reported from He-Ne lasers (Hargrove et al., 1964). Passive mode-locking, on the other hand, relies on the inherent nonlinear properties of the laser gain medium and optical elements within the cavity to produce mode-locked pulses. Passive mode-locking can be achieved using techniques such as Kerr-lens mode-locking (Spence et al., 1991), and semiconductor saturable absorber mode-locking (SESAM) (Keller et al., 1996).

Table 2.3. Different pulse-shapes and corresponding time bandwidth products

Pulse Shape	**Fourier Transform**	**Pulse Width**	**Time-Bandwidth Product**
$A(t)$	$A(\omega) = \int_{-\infty}^{\infty} a(t)e^{-j\omega t}\,dt$	Δt_p	$\Delta t_p \cdot \Delta v$
Gaussian: $e^{-\frac{t^2}{2\tau^2}}$	$\sqrt{2\pi}\tau e^{-\frac{1}{2}\tau^2\omega^2}$	$2\sqrt{ln2}\,\tau$	0.441
Hyperbolic Secant: $\mathrm{sech}\left(\frac{t}{\tau}\right)$	$\frac{\tau}{2} sech\left(\frac{\pi}{2}\tau\omega\right)$	$1.7627\,\tau$	0.315
Rect-Function: $\begin{cases}1, \lvert t\rvert \le \tau/2\\ 0, \lvert t\rvert > \tau/2\end{cases}$	$\tau\frac{\sin(\tau\omega/2)}{\tau\omega/2}$	τ	0.886
Lorentzian: $\frac{1}{1+(t/\tau)^2}$	$2\pi\tau e^{-\lvert\tau\omega\rvert}$	$1.287\,\tau$	0.142

2.5. Brief Literature Review of Cr:LiCAF Lasers

Trivalent chromium (Cr^{3+}) doped $LiCaAlF_6$ (Lithium Calcium Aluminum Fluoride) is a gain medium which is a member of the Cr:Colquiriite family. It has a broad absorption band at 650 nm and a broad emission band around 800 nm which makes it potential competitor to Ti:Saphhire lasers. Cr:LiCAF was discovered in 1988 by S. A. Payne and colleagues, and has been identified as a promising new laser (Payne et al., 1988). In the initial years after its discovery, Cr:LiCAF lasers did not receive much attention and fewer studies were reported compared to another member of the colquiriite family, Cr:LiSAF (Lithium Strontium Aluminum Fluoride) (Demirbas, 2010). These

studies include flash lamp pumps (Payne et al., 1990), first-time Q-switched operation (Scheps et al., 1990), kerr-lens mode-locking (Gabel et al., 1998), and self-mode locking (LikamWa et al., 1992).

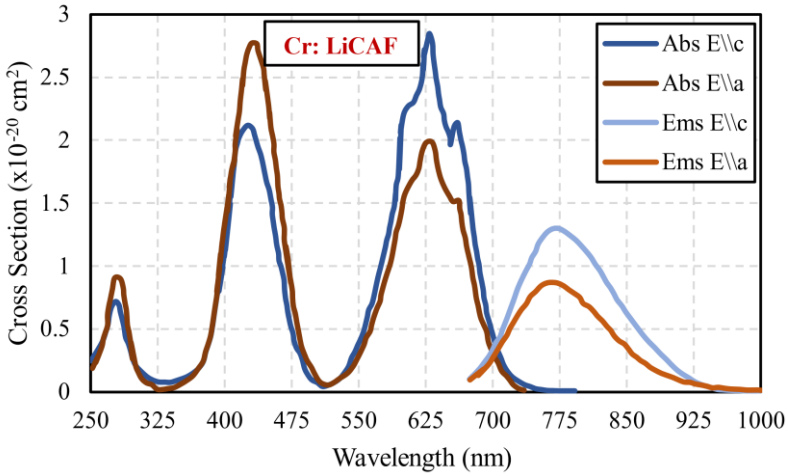

Figure 2.10. Measured room-temperature absorption and emission spectrum of Cr: LiCAF gain medium (Payne et al., 1990)

The lack of attention was primarily due to higher parasitic losses (~2%) resulting from its production stage (Demirbas et al., 2009a). The laser performance is affected by the crystal structure's disorientation, which depends on the LiCAF crystal's growing techniques (Klimm et al., 2005; Lacayo et al., 1999; Yoreo et al., 1991; Klimm et al., 1999; Klimm et al., 1998). On the other hand, recent technological improvements have enabled the growth of LiCAF crystals with lower passive losses ~0.2% (Klimm et al., 2000). Compared to other members of the colquiriite family, Cr:LiCAF crystal exhibits superior physical properties. It has a higher intrinsic slope efficiency (67%) (Payne et al., 1988; Demirbas et al., 2009b), better thermal conductivity (Aterton et al., 1993), less thermal lensing (Eichenholz & Richardson, 1998; Woods et al., 1991), lower quantum defect ($1-\lambda_p/\lambda_l$), reduced excited state absorption (ESA) (Payne et al., 1989), and lower auger upconversion rate (Jabczyński et al., 2001). In addition, it has a temperature of thermal quenching of fluorescence at 255 °C, which is most effective for high-power applications (Stalder et al., 1992).

In the early years there were studies on pulse generation from Cr:LiCAF lasers. The first operation on ultrashort pulse generation of Cr:LiCAF laser produced 170 fs pulses with 100 mW average output power and 90 MHz repetition frequency (LikamWa et al., 1992). The first Q-switched laser demonstration produced 247 ns output pulse with 3 kHz repetition frequency (Scheps et al., 1990). The shortest pulse obtained from Cr:LiCAF laser was demonstrated by Wagenblast et al, with Ti:sapphire pumped kerr-lens mode-locked laser, which produced 9 fs at 220 mW average output power with a repetitions frequency of 97 MHz (Wagenblast et al., 2002). In 2003 the group obtained 10 fs at 40 mW average output power with a repetitions frequency of 110 MHz via diode-pumped system (Wagenblast et al., 2002). In 2007, Demirbas et al, demonstrated the first diode pumped SBR\SESAM mode-locked Cr:LiCAF laser, and obtained 67 fs pulses at

300 mW average output power with 120 MHz repetition frequency results 2.5 nJ pulse energy (Demirbas et al., 2007). Besides, they demonstrated single-spatial mode diode-pumped system and obtained the continuous wave slope efficiency 54% and in mode-locking 72 fs pulses with average power 178 mW (Demirbas et al., 2008). 101 kW pulse peak power was obtained by employing a multipass cavity with single mode diode-pumped system in 2009 (Demirbas et al., 2009c). The same research group also demonstrated the performance of a Cr:LiCAF laser with tapered diode systems. They have obtained 220 fs pulses with a repetition frequency of 77 MHz (Demirbas et al., 2011). The first, self Q-switched operation demonstrated by Beyatli et al, by single mode diode-pumped system and obtained 5 us pulses with repetition rates between 10 and 30 kHz (Beyatli et al., 2013).

The highest continuous-wave output power reported for a diode-pumped Cr:LiCAF laser is 2.54 W (Demirbas et al., 2015). This was achieved using four multimode diodes with a power of 1.8 W each. In addition to the high continuous wave output power achieved with the diode-pumped system, the researchers also performed intracavity frequency doubling using a BBO (Barium Borate) crystal. They were able to obtain a blue output power of around 0.9 W at a wavelength of 402 nm using this technique (Demirbas et al., 2015). Cr:LiCAF lasers have been used as tunable sources due to their emission bandwidth. The reported infrared tunability range can extend up to a range of 140 nm (746-887 nm) while maintaining a reasonable output power regime and in the ultraviolet region extended more than 50 nm (375-433 nm) (Demirbas et al., 2012). In addition to the previous studies, there have also been investigations into the use of femtosecond Cr:LiCAF lasers for multiphoton microscopy (Sakadžić et al., 2008). All of these studies demonstrate the potential applications of Cr:LiCAF lasers. As crystal growth technologies continue to improve, it has the potential to become a viable option for laser applications due to its favorable properties, such as low-cost sustainability.

3. FINDINGS AND ARGUMENTS

This chapter provides an overview of the experimental results obtained from the various laser operations conducted during the research. Including a detailed description of the experimental setup, as well as the procedures and techniques used to achieve the desired laser behavior.

Figure 3.1. Cr:LiCAF crystals produced with different physical properties in bulk phase

Before presenting the findings, it is important to provide information about the solid-state laser crystal that was used throughout the study. Solid-state laser crystals are required to produce high technological equipment. They are typically produced through a process called crystal growth or crystal synthesis. The exact method can vary depending on the type of laser crystal being produced. The process starts with the selection of the materials. As mentioned in section 2.1 there were different host materials varied for the desired operating wavelength. Then, the prepared materials are melted at high temperatures, typically in a crucible made of a suitable refractory material. Afterward, the crystal growth process starts to initiate. There were different methods used for crystal growth. One of the most popular ones is Czochralski Method. In this method, a seed crystal is dipped into the molten solution and slowly pulled out while rotating. Figure 3.1 shows the produced bulk crystals. After the production stage, crystals were cut as desired. Figure 3.2 shows the Brewster cut, polished Cr:LiCAF crystals. In some applications, there were also applied antireflection coating to increase performance.

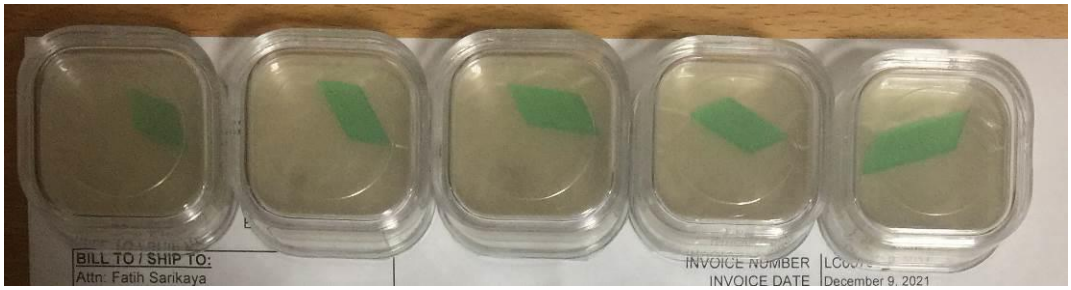

Figure 3.2. Brewster-cut Cr:LiCAF crystals

3.1. Doping Estimation of Cr:LiCAF Gain Medium

In the first step of the study, the characterization of the Cr:LiCAF crystal process was carried out. To achieve this, the chromium doping concentration of the crystals was determined. There were crystals of different lengths used for the characterization, ranging from 10, 12.5, 15 (2 pieces), and 20 mm in length. To obtain the doping concentration of each crystal, there was a method that used. For the first step, the simple experimental setup was built as in figure 3.3 for absorption measurements.

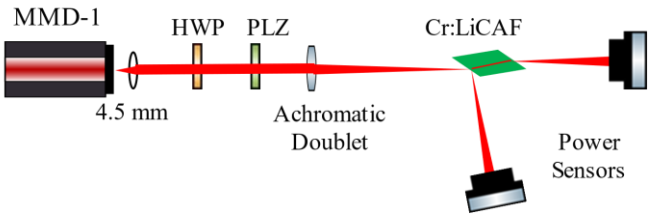

Figure 3.3. Schematics of absorption measurement setup, MMD: multimode diode, HWP: half-wave plate, PLZ: polarizer

A linearly polarized 655 nm multimode diode was used as the pump source, which was collimated using a 4.5 mm focal length aspherical lens to correct for diffraction. To adjust the polarization of the incoming light, a halfwave plate (HWP) and polarizer were used. An achromatic doublet was placed in the setup to focus the light inside the Cr:LiCAF crystal. The crystals were Brewster-cut to prevent Fresnel reflection losses from the surface. The incoming power was measured using a power sensor and recorded. To prevent losses caused by the high-power incident, the power was kept at a lower level of around 30 mW. The reflected and transmitted power was also measured and recorded. This process was repeated for both TM (p) and TE (s) polarization states by adjusting polarization states with HWP. For the 5 different crystals the measurements were repeated, and the results were recorded. In the calculation part firstly, the absorption coefficient calculated with the following expression;

$$\alpha = ACS \times N_{i1\%} \times doping \tag{3.1}$$

where ACS is absorption cross section, which was obtained from figure 2.10 at 655 nm, $N_{i1\%}$ is number of ion density in 1% doping, which was calculated using eq. 3.2, and the doping that was taken from the datasheet.

$$N_{i1\%} = \frac{Number\ of\ ion\ occupied \cdot Density\ of\ Crystal}{(Total\ Atomic\ Mass) \cdot Atamic\ Mass\ Constant} \tag{3.2}$$

In the following, the expected absorption of crystal calculated depending on the crystal length by using following expression;

$$A = 1 - e^{-\alpha l} \tag{3.3}$$

by using the same expression, the actual doping was estimated via inserting the measured absorption values of crystal. Equation 3.4 used for absorption calculation;

$$A_{ms} = 1 - \frac{P_{tr}}{P_{in} - P_{ref}} \tag{3.4}$$

where P_{in}, P_{tr}, and P_{ref} is measured incident, transmitted, and reflected power respectively. The estimated doping was calculated using Equation 3.5 based on the measured absorption of the gain crystal.

$$doping = -\frac{ln\left(1 - \frac{A_{ms}}{100}\right)}{ACS \times N_{i1\%} \times l} \tag{3.5}$$

Measurements and calculations were performed on five different length crystals, where two crystals had the same length of 15 mm and were labeled as "15a" and "15b" to differentiate between them. The comparison showed that the doping values that were described on the datasheet are not the same. However, one can obviously say that the measurement method can also have errors. Nonetheless, the gain medium crystal has a sufficient doping concentration to maintain adequate gain during laser operation.

Table 3.1. Estimated doping concentration of Cr:LiCAF crsytals

	ACS (cm^2)	**Doping (%)**	**$N_{i1\%}$ (cm^{-3})**	**α (cm^{-1})**	**Length (cm)**	**A (%)**	**A_{ms} (%)**	**Est. Doping (%)**
E//c	2.10	1.5	0.950	2.9925	1	94.98	91.53	1.24
E//a	1.55	1.5	0.950	2.9925	1	89.02	84.06	1.25
E//c	2.10	1.5	0.950	2.9925	1.25	97.63	96.94	1.40
E//a	1.55	1.5	0.950	2.9925	1.25	93.68	93.49	1.48
E//c	2.10	1.5	0.950	2.9925	1.5 (a)	98.88	97.58	1.24
E//a	1.55	1.5	0.950	2.9925	1.5 (a)	96.36	95.09	1.36
E//c	2.10	1.5	0.950	2.9925	1.5 (b)	98.88	97.49	1.23
E//a	1.55	1.5	0.950	2.9925	1.5 (b)	96.36	94.86	1.34

E//c	1.55	1.5	0.950	2.9925	2	98.35	98.11	1.00
E//a	2.10	1.5	0.950	2.9925	2	98.79	97.19	1.21

3.2 Continuous Wave operation of Cr:LiCAF Laser

Among the Cr:Colquiriite gain medium family Cr:LiCAF has distinguish properties which make it favorable for high power application. The superior thermal properties enable to the application of more than 6 W of pump power without any crystal fracture. Additionally, the upper state lifetime of Cr:colquiriites temperature dependent and for the Cr:LiSAF and Cr:LiSGAF laser, the room temperature fluorescence lifetime reduces by half at 69 °C and 88°C (Isemann & Fallnich, 2003). On the other hand Cr:LiCAF upper state lifetime is mostly constant over a wide temperature range of 255 °C. Despite, the high power suitability of Cr:LiCAF, one of the main disadvantages is low ECS which leads to low optical round-trip gain. In this chapter detailed continuous wave results presented. The Cr:LiCAF laser was operated in continuous wave mode by using four commercially available nLight C-mount multimode diodes with narrow emission at approximately 655 nm, which were selected as suitable pump sources according to the maximum ACS of the Cr:LiCAF. Figure 3.4 shows the emission spectrum and output power characteristics of the laser diodes.

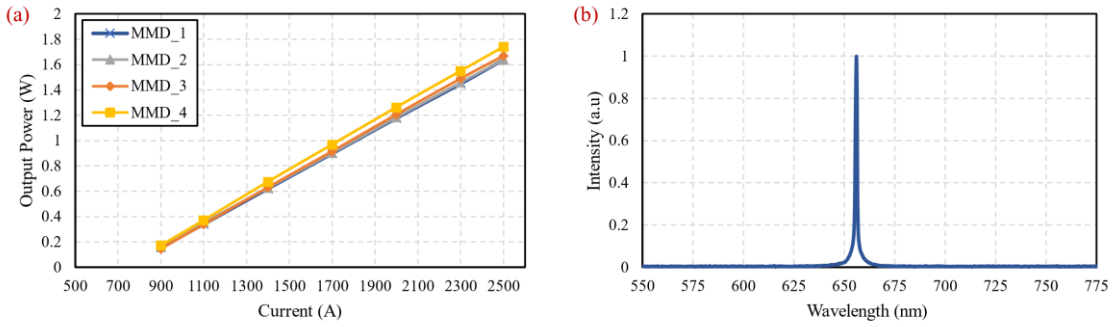

Figure 3.4. Characteristics of diodes that are used in the experimental studies a) Output optical power with respect to applied current; b) Emission spectrum of laser diodes

Selected four linearly polarized single emitter laser diodes was provide optical power up to 1.7 W under the operation current of a maximum of 2.5 A. Single emitter multimode diodes had an emitter size of 1x150 μm (sagittal x tangential) with a diffraction limited output in the sagittal axis and beam quality of M^2 10 in the tangential axis. To maintain the output power stability, the diodes holder kept at 20 °C temperature.

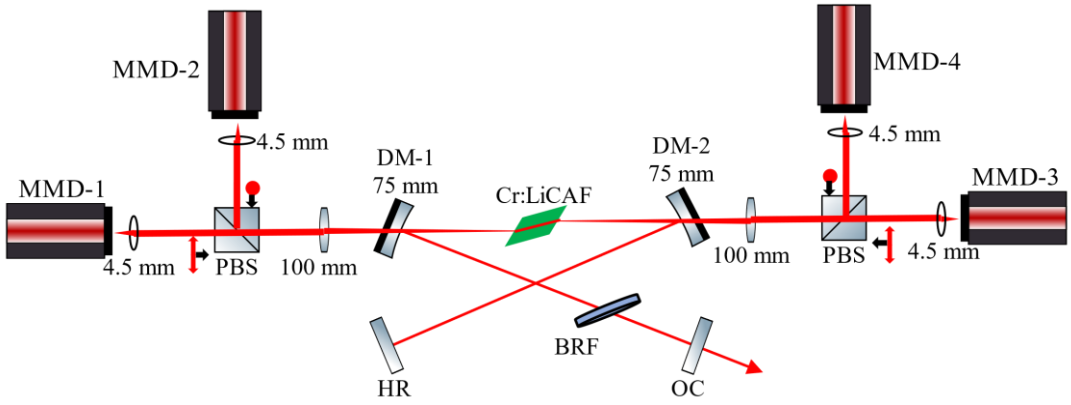

Figure 3.5. Schematic of the four multimode diode pumped Cr:LiCAF laser. HR: high reflector, BRF: birefringent filter, OC: output coupler, PBS: polarizing beam splitter

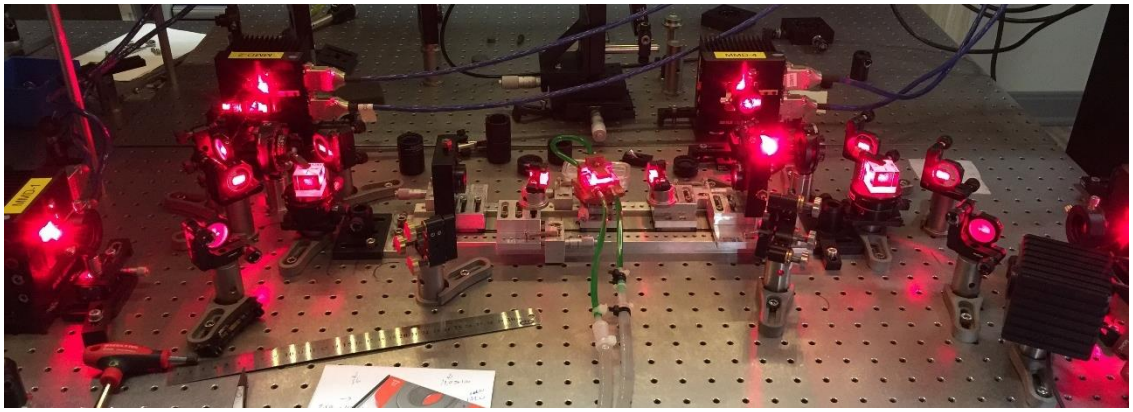

Figure 3.6. Cr:LiCAF laser system installed in ABU-LTL for use in continuous wave experiments. Four multimode diodes placed two side equally

Figure 3.5 shows the schematics of the multimode diode-pumped Cr:LiCAF laser cavity used to perform the cw lasing experiment. Figure 3.6 represents the installed laser system in ABU-LTL. On two sides, all the components that were used to build laser system carefully placed and their position arranged as required. The multimode diodes output first collected and collimated with aspherical lens of a focal length of 4.5 mm. Two of the diodes (MMD-2 & MMD-4) were combined with a polarizing beam splitter to pump crystal with one side. HWP utilized the alter the polarization of the diodes (MMD-2 & MMD-4) from TM(p) to TE(s). The collected beam focused with 100 mm focal length achromatic doublets inside the crystal. Astigmatically compensated x-folded cavity consists of two 75 mm radius of curvature curved pump mirror (DM-1 & DM-2), a high reflective mirror (HR) and an output coupler (OC) placed. BRF plate, were placed for the tuning experiments. Starting with the 10 mm 1.24% chromium-doped gain medium, five different crystals (10 mm 1.24%, 12.5 mm 1.4, 15 mm 1.25 %, 15 mm 1.25 %, 20 mm 1%) were tested for continuous wave (cw) operation. Crystals were mounted with indium foil in a copper crystal holder and cooled with water flow at 15 °C constant temperature to eliminate the thermal effects. For the 10 mm gain medium cavity arm's

lengths were 18 cm and 20 cm, and a respected cavity mode size was 24x30 μm obtained inside the crystal. The crystal absorbed 91% and 83% of the TM and TE polarized incident pump light at 655 nm respectively.

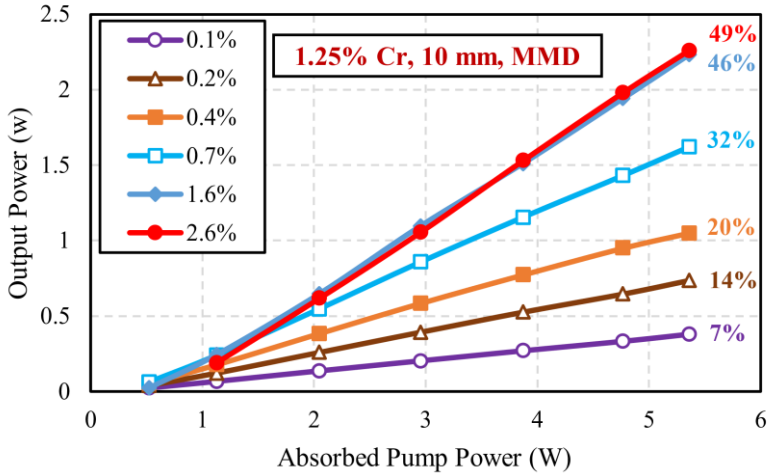

Figure 3.7. CW efficiency curves for the MMD pumped 10 mm 1.25% Cr doped Cr:LiCAF laser. Data taken with 0.1%, 0.2%, 0.4%, 0.7%, 1.6% and 2.6% output couplers. Next to the lines, the corresponding slope efficiencies was given

Figure 3.7 shows the measured cw performance of the multimode diode pumped 10 mm 1.25% Cr doped Cr:LiCAF laser. Data were taken with 0.1%, 0.2%, 0.4%, 0.7%, 1.6% and 2.6% output couplers. The free-running output wavelength was around 795 nm. The best performance was obtained using the 2.6% output coupler. This output coupler enabled output power up to 2.22 W at the absorbed power of 5.35 W. The slope efficiency obtained as 49% for 2.6% output coupler. This shows that the high mode matching obtained inside the crystal between the laser and pump modes. In 2015 Demirbas obtained the 49% efficiency with the same configuration system and reached the 2.54 W output power (Demirbas et al.,2015). However, the gain medium that was used in the experiment had length of 4 mm and 5% Cr doping and they observed cracking inside the crystal due to the thermal stress on the high-power pumping. Comparing the results, one can conclude that 10 mm 1.25% Cr doping showed better performance in a thermal perspective rather than 4 m long 5% doping gain medium.

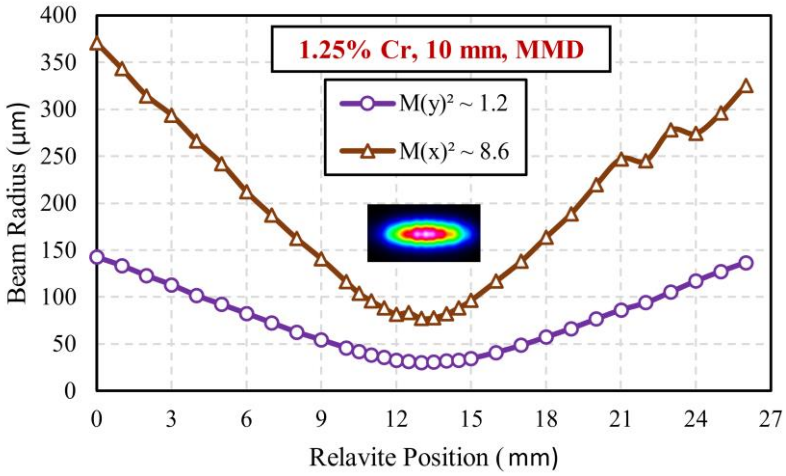

Figure 3.8. M^2 measurement of multimode diode pumped 10 mm 1.25% Cr:LiCAF sample. Measurements were made at 1.98 W output power by focusing with achromatic doublets. Inside figure shows the beam profile of respected output

Figure 3.8 shows the measured variation of output beam spot size for both sagittal and tangential axis. The data was collected by focusing the output beam of the laser, while operating at around 1.98 W, using achromatic doublets and observing the resulting change in spot size. Minimum spot size obtained from the laser used to calculate M^2 factor of output laser beam via eq. 3.6,

$$M^2 = \frac{\pi w_0}{z_R \lambda} \tag{3.6}$$

Table 3.2. Measured M^2 of 10 mm 1.25% doped Cr:LiCAF laser for different output power

Output Power (W)	Tangential axis M^2 (x)	Sagittal axis M^2 (y)	Beam Profile
0.61	4.67	1.19	
1.05	5.86	1.33	
1.53	6.03	1.27	
1.98	8.69	1.3	

Table 3.2 shows the M^2 of Cr:LiCAF output beam with respect to different output power. At an output power of around 0.6 W, the M2 values for the tangential and sagittal beam quality were 4.67 and 1.19, respectively. As the output power was increased, the beam quality on the tangential axis decreased. At an output power of 1.98 W, the beam quality on the tangential axis was around 8.69 and 1.3 on the sagittal axis. The laser diodes

used for pumping the crystal had an emitter size of 1x150 on the sagittal and tangential axes, respectively. Therefore, only a one-tenth change in beam quality was observed on the sagittal axis. Additionally, under the high-power effect the laser diodes emission area widens to provide sufficient power. This also leads to additional diffraction on the tangential axis. Beam profiles show that diffraction. While at low power pumping the output beam was in single mode, at high power pumping output beam became multimode.

The experimental setup consisted of a system of four multimode diodes used to pump different gain media with varying doping and crystal length. The purpose was to observe the laser's performance under the same conditions but with different crystal configurations. With this way the laser performance of the low-ion doped crystals would have been spotted clearly. Figure 3.9 shows the cw performance of 12.5 mm 1.4% Cr doped gain media. The crystal absorbed the 96% and 93% of TM and TE polarized incident pump light at 655 nm respectively. The laser crystal yielded an output power of 1.62 W at an absorbed pump power of 5.76 W and a slope efficiency of 34%, while using an output coupler of 2.6%. Moreover, with 1.6% output coupler 1.61 W of output power and 33% of slope efficiency attained. The increase on the crystal length affects the absorbed pump light inside the gain medium. Equitation 3.3 explains this relation mathematically. According to the obtained results, introducing external losses into the cavity resulted in a significant reduction of both gain and output power, indicating the presence of high passive losses of crystal.

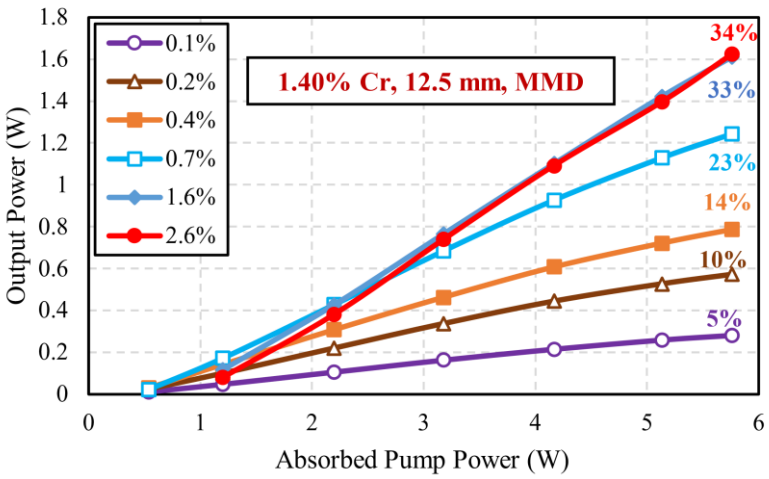

Figure 3.9. CW efficiency curves for the MMD pumped 12.5mm 1.40% Cr doped Cr:LiCAF laser

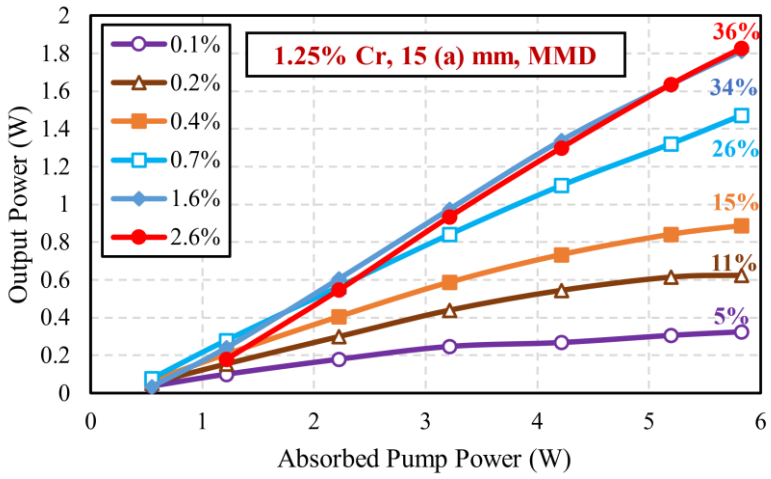

Figure 3.10. CW efficiency curves for the MMD pumped 15 (a) mm 1.25% Cr doped Cr:LiCAF laser

Figure 3.10 shows the cw efficiency curves of MMD pumped 15 (a) mm 1.25% Cr doped Cr:LiCAF laser. The gain medium absorbed the 97% and 95% of TM and TE polarized incident pump light at 655 nm respectively. 1.82 W output power obtained at 5.82 W absorbed pump power. Corresponding slope efficiency was 36% with 2.6% output coupler. Figure 3.11 represents the cw results of multimode diode pumped 15 (b) mm 1.25% Cr doped Cr:LiCAF laser. Similar to the same length 15 (a) mm sample this gain medium absorbed the 97% and 95% of TM and TE polarized incident pump light. Maximum output power observed as 1.85 W with 2.6% output coupler and corresponding slope efficiency of 38%. Based on the comparison of two gain mediums with the same length, it was found that their efficiency characteristics were almost the same. However, the results obtained from sample b were slightly better than sample a.

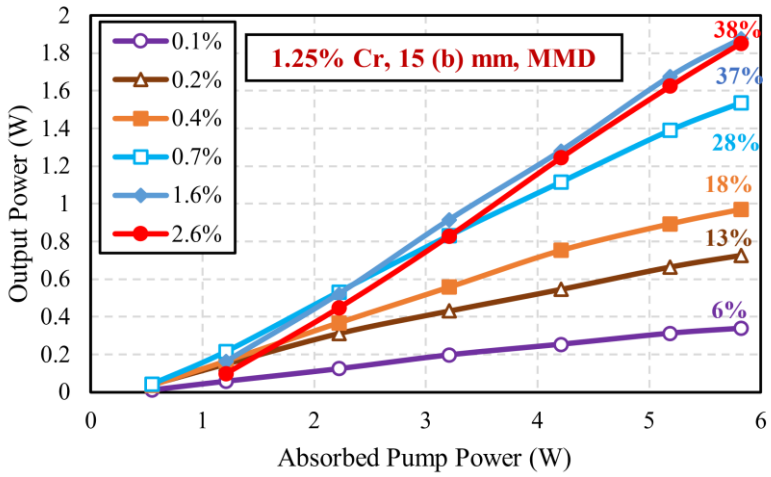

Figure 3.11. CW efficiency curves for the MMD pumped 15 (b) mm 1.25% Cr doped Cr:LiCAF laser

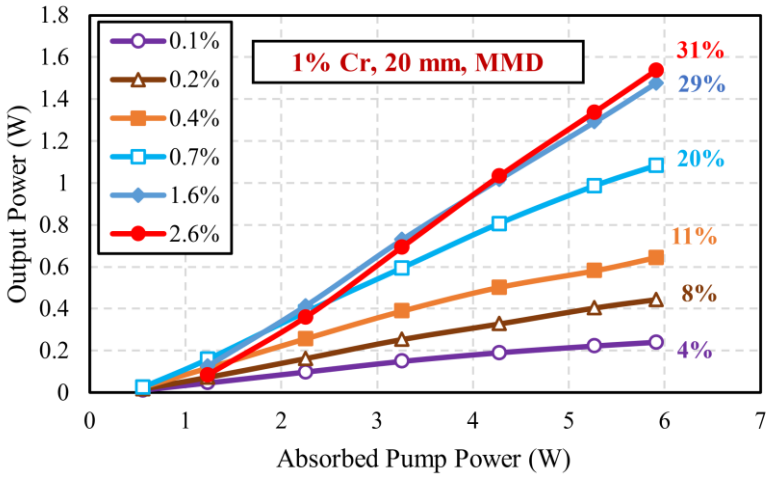

Figure 3.12. CW efficiency curves for the MMD pumped 20 mm 1% Cr doped Cr:LiCAF laser

Figure 3.12 shows the cw results of MMD pumped 20 mm 1% Cr doped Cr:LiCAF laser. 20 mm Cr:LiCAF crystal absorbed 98% and 97% of TM and TE polarized incident pump light. At 5.9 W absorbed power measured output power was 1.53 W with 2.6% output coupler. A low doping concentration can lead to a lower gain in the gain medium, resulting in insufficient amplification of the optical signal and lower output power. Overall, the results obtained with the four MMD pumped system showed output powers of 2.22 W, 1.63 W, 1.82 W, 1.85 W, and 1.53 W for 10 mm, 12.5 mm, 15 (a) mm, 15 (b) mm, and 20 mm gain mediums, respectively. Six different output coupling rates between 0.1% to 2.6% were tested and maximum output power was obtained with 2.6%. Table 3.3 shows the results obtained with 2.6% output coupler for five different lengths and doped gain medium. The output coupling rate used in the high-power results falls within the reported optimum range for Cr:LiCAF, but is still higher than what has been reported in previous studies (Demirbas et al., 2008; Isemann & Fallnich, 2003). Interestingly, the results also show that using an output coupler with a rate of 1.6% still resulted in high output power.

Table 3.3. Measured output power variation of different length and doping Cr:LiCAF gain mediums with 2.6% output coupler

Crystal Doping (%)	Crystal Length (mm)	Output Power at 2.6% OC (W)
1.25	10	2.22
1.40	12.5	1.63
1.25	15	1.82
1.25	15	1.85
1.00	20	1.53

3.2.1 Loss Analysis of Cr:LiCAF Laser

Loss analysis is an important tool to estimate the losses in the cavity and gain medium, which can help in predicting the potential applications of the laser. By knowing the losses, it is possible to optimize the laser system to achieve the desired output power and beam quality. Resonator losses can be estimated using the Caird analyses (Caird et al., 1988). The slope efficiency of the laser at certain transmission output coupling can be calculated by the following formula;

$$\eta = \eta_P \frac{\lambda_p}{\lambda_l}\left(1 - \frac{\sigma_{ESA}}{\sigma_e}\right) \cdot \frac{T}{T + L} \tag{3.7}$$

where η_P is pumping efficiency, λ_p and λ_l is pumping and lasing wavelength respectively, σ_{ESA} is excited state absorption cross-section, σ_e emission cross-section, T is output coupler transmission and L is cavity loss per pass. Figure 3.13 shows the experimentally measured inverse slope efficiency with respect to different output coupling inverse transmission of Cr:LiCAF laser. Employing the linear fit to the measured values, the cavity loss and intrinsic slope efficiency were estimated as 0.3±0.1% and 65% respectively.

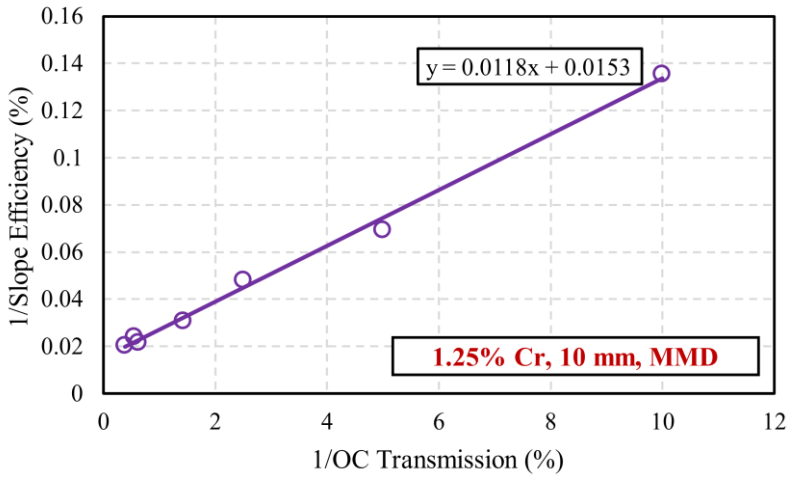

Figure 3.13. Ciard analysis for multimode diode pumped Cr:LiCAF laser. Crystal loss estimated to 0.3% using Caird analyses.

Another method that can be used to estimate cavity losses is the Findlay-Clay analysis (Findlay & Clay, 1966). The Findlay-Clay analysis indicates that the threshold power for lasing is proportional to the total losses in the cavity, which includes both the internal losses of the gain medium and the coupling losses at the cavity mirrors. This relation can be expressed as;

$$P_{th} = \frac{\pi\left(w_p^2 + w_c^2\right)h\nu_p}{4(\sigma_e - \sigma_{ESA})\tau_f \eta_p}\left(2A_g + T + L\right) \tag{3.8}$$

where w_p^2 and w_c^2 is the pump and cavity beam waist respectively, h is the Planck constant, v_p pump photon frequency, τ_f is the upper state fluorescence lifetime, A_g is the ground state absorption. Figure 3.14 shows the measured threshold values of Cr:LiCAF laser at a wavelength of 795 nm with respect to different output couplers. The linear fit of the data shows that all values lie on the solid line. By applying the theory, multimode diode-pumped Cr:LiCAF laser total cavity losses were estimated as 0.4±0.1%.

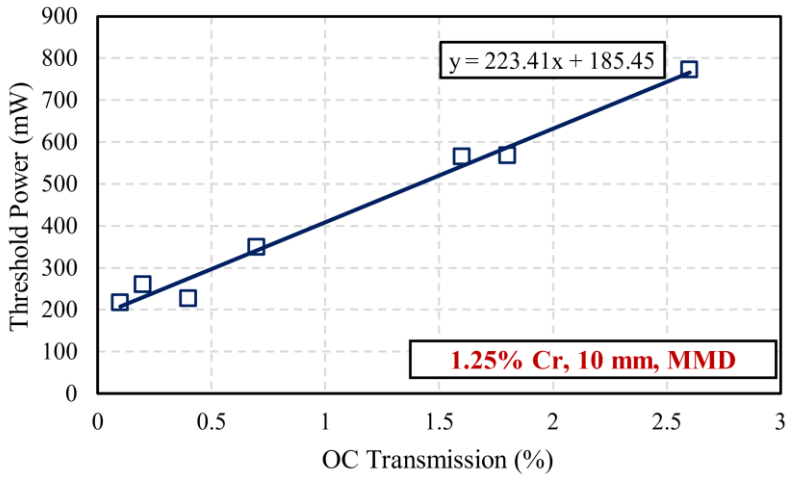

Figure 3.14. Findlay-Clay analysis for multimode diode pumped Cr:LiCAF laser. Crystal loss estimated to 0.4% using Findlay-Clay analysis.

Here should be noted that the used mirror is assumed lossless. However, there could be errors caused by this assumption and experimental measurements. Nonetheless, for 10 mm long 1.25% Cr doped crystal, Caird analysis and Findlay-Clay analysis shows good agreement on loss level around 0.3±0.1%. Comparing the obtained result with the reported a 4 mm 5% doped gain medium (Demirbas et al., 2015) and a 2 mm 10% doped gain medium (Demirbas et al., 2009a), it can be seen that the passive losses of both high-doped crystals were 0.1% and 0.3%, respectively. So, one can conclude that, for a longer crystal this level of passive losses shows good agreement in terms of crystal quality. Table 3.4 shows the obtained losses of five different gain mediums by Caird analysis. For 10 mm, 12.5 mm, 15 (a) mm, 15 (b) mm and 20 mm gain medium, loss per cm measured as 0.36%, 0.43%, 0.35, 0.29% and 0.35% respectively. However, the lowest loss per crystal was obtained with 10 mm. Comparing the results 15 (b) mm has the second lowest loss parameter. In continuous wave results, the second highest output power was 1.85 W with 15 (b) mm crystal. The power difference between the 10 mm and 15 (b) mm gain medium can be explained by crystal losses and mode matching between pump and laser modes. Mode mismatching inside the crystal causes additional heat load and extra losses.

Table 3.4. Measured and calculated doping and loss parameter for different Cr:LiCAF crystal

Crystal Doping (%)	Crystal Length (mm)	Crystal Loss @800 nm (%)	Crystal Loss per cm (%)
1.25	10	0.36	0.36
1.40	12.5	0.54	0.43
1.25	15	0.53	0.35
1.25	15	0.44	0.29
1.00	20	0.69	0.35

3.2.2 Continuous Wave Tuning Results

As shown in figure 3.5 a 2 mm thick crystalline quartz birefringent filter (BRF) was inserted cavity for continuous wave tuning measurements. BRF was inserted at Brewster angle to eliminate Fresnel reflection from the surface of the crystal. In this manner, there was no loss of power in the output beam. In the first set of measurements, four MMD pumped 10 mm 1.25% Cr doped gain medium tuning performance tested. The tuning ranges varied from 744-860 nm to 741-874 nm, depending on the output coupler used. The most achievable tuning range was obtained with the 0.1% output coupler since the decreased loss pushed the emission limit further. However, it comes with drawbacks such as lower output power.

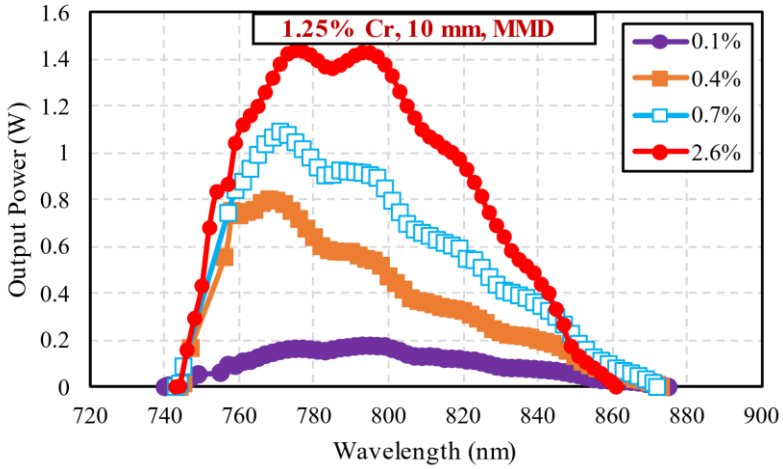

Figure 3.15. Continuous wave tuning curves of 10 mm 1.25% Cr doped gain medium taken with output coupler 0.1%, 0.4%, 0.7% and 2.6%

Figure 3.16 shows the continuous wave tuning curves of 15 (b) mm length gain medium pumped with four MMD system. As well as in 10 mm measurements BRF plate was utilized by rotating around optic axis. Tuning range extended between 747-870 nm by using 0.1% output coupler. Comparing the result, 10 mm crystal tuned more than 15 (b) mm crystal about 5 nm. Reported studies show that Cr:LiCAF tunable range between 720-887 nm (Payne et al.,1988; Demirbas et al, 2012). The results obtained in this study were within the reported range. On the short wavelength side self-absorption losses and

a decreased emission cross-section (figure 2.10) on the long wavelength side could be possible reasons for this.

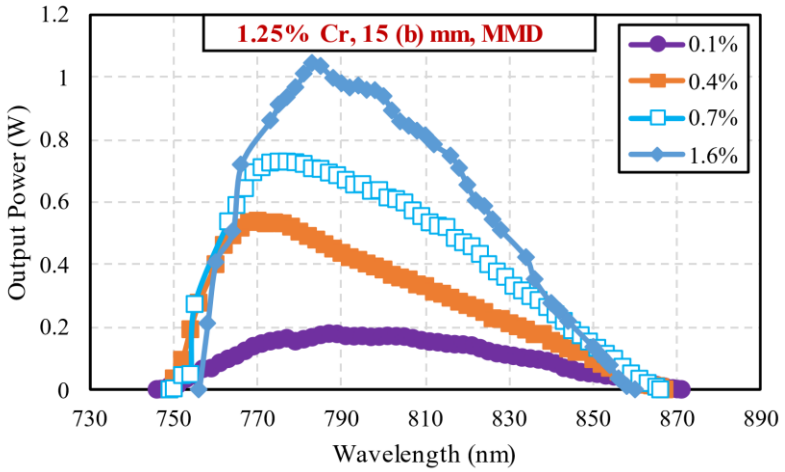

Figure 3.16. Continuous wave tuning curves of 15 mm 1.25% Cr doped gain medium taken with output coupler 0.1%, 0.4%, 0.7% and 1.6%

3.3. Quasi CW and Gain Switch Cr:LiCAF Laser

In this section, the investigation focused on quasi-continuous wave and gain-switched Cr:LiCAF lasers. In quasi-continuous wave and gain-switched operation, pumped diodes operate in pulsed mode. These lasers operate by providing pumping for a specific period and then turning off to allow the crystal to cool. Pulse mode operation increases the laser performance by decreasing thermal loading caused from continuous wave pumping. Quasi-continuous wave operation can be described as using a pump source in pulse mode. On the other hand, while the pump pulse duration is shorter than the upper state lifetime, the laser operates in gain-switch mode to produce pulse outputs. Studies have been conducted using Cr:LiSAF lasers in quasi-continuous wave (cw) and gain-switched modes, which have shown improvements in the output power level (Demirbas & Acar, 2016). The glass-like thermomechanical properties of Cr:LiSAF make it particularly suitable for pulse pumping, which has proven to be effective in continuous wave operations. Based on this, quasi-continuous wave and gain switched performance of Cr: LiCAF laser were examined.

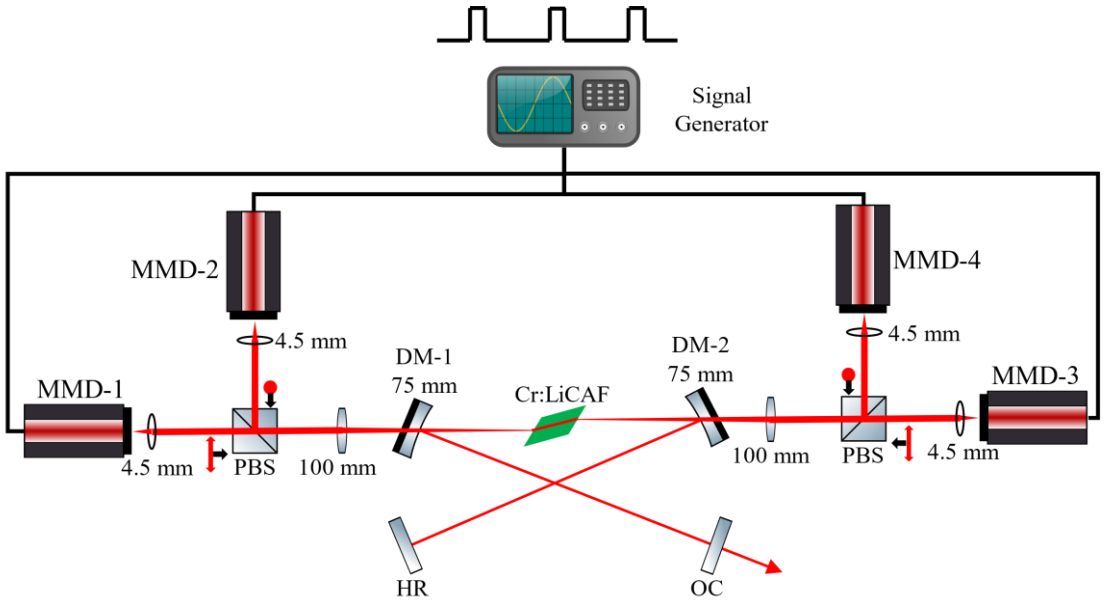

Figure 3.17. Schematic of the four multimode diode pumped Cr:LiCAF laser. Diodes connected to signal generator to drive in pulse mode

Figure 3.17 shows the schematic for multimode diode-pumped Cr:LiCAF laser driven in pulse mode. An arbitrary signal generator was employed to generate pulse pumping signals and control the duty cycle of the pulses in the experimental setup. The signal generator (AATech, AWG-1020) was connected to diode drivers through a coaxial cable, allowing for precise timing and control of the pumping pulses. To monitor the generated signals, a digital oscilloscope (Tektronix, DPO 3054) was utilized to visualize and analyze the waveform. This setup enabled accurate control and characterization of the pulse pumping process in the Cr:LiCAF laser system. 10 mm 1.25% Cr:LiCAF crystal was used for this experiment. Figure 3.18 shows the measured variation of the Cr:LiCAF laser outputs for the gain-switched and quasi-continuous wave mode of operation at different trigger pulse width values. For clear understanding trigger pulse and diode response were also included in the figures.

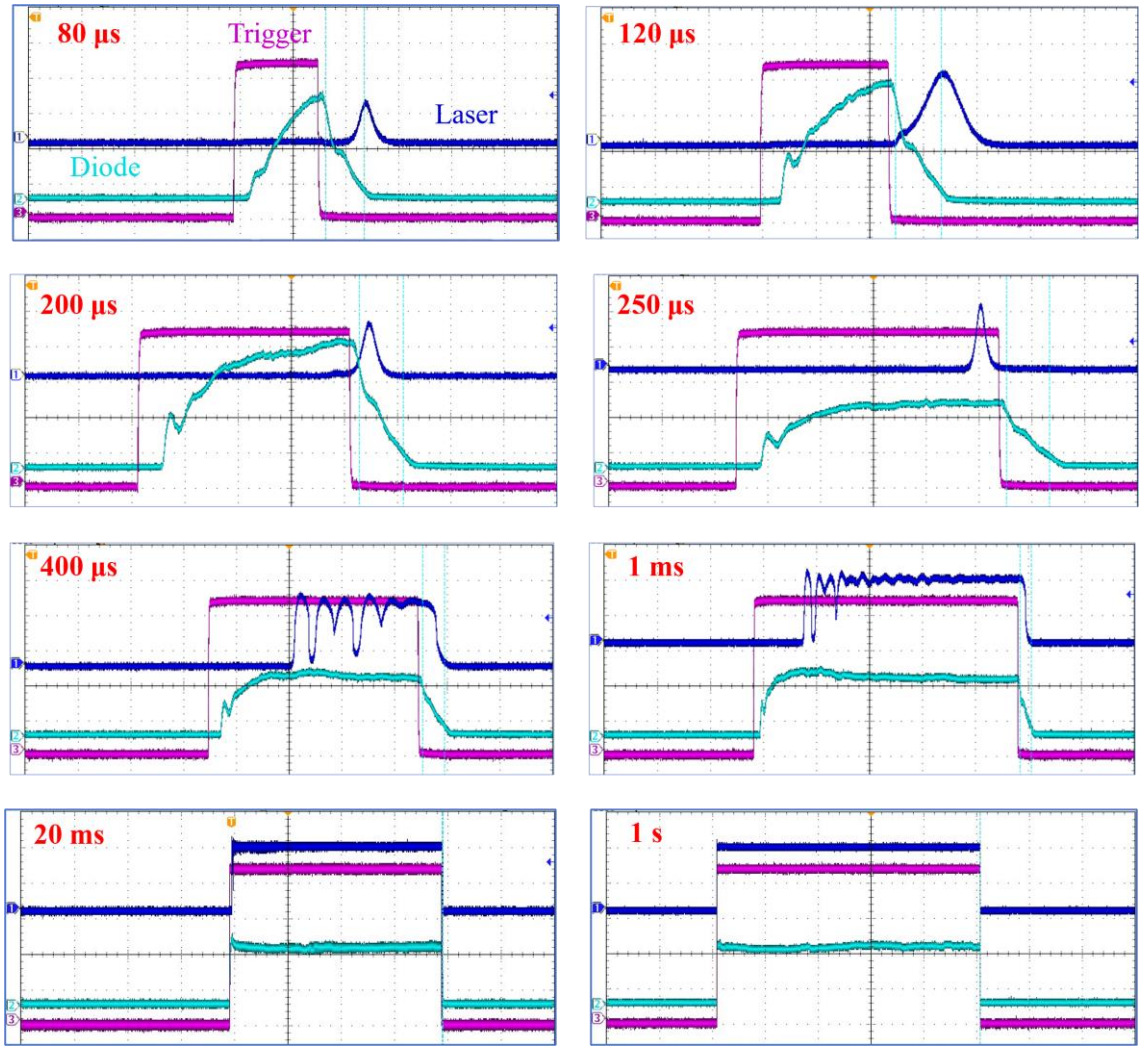

Figure 3.18. Measured variation of the Cr:LiCAF laser outputs for the gain switched and quasi continuous wave mode of operation at different trigger pulse width values. The pulse period for each trigger signal is indicated. The data was taken at 20% duty cycle of pulse periods

For different trigger pulse periods of 80 µs, 120 µs, 200 µs, 250 µs, 400 µs, 1 ms, 20 ms, and 1 s laser output was measured. As mentioned, the duty cycle of 20% were applied for trigger pulses, which is corresponding 16 µs pulse with for 80 µs pulse period. Under the period of 250 µs Cr:LiCAF laser generates pulses. The shortest pulse duration obtained from the laser was measured as 4.3 µs. Over the 250 µs pulse periods Cr:LiCAF laser started the reach steady-state and follow the pump pulse. Figure 3.19 shows the measured quasi-continuous wave performance of Cr:LiCAF laser by different pump pulse duty cycle. During the measurements pump pulse period were employed as 10 ms. The measurements were made with 2.6% output coupler.

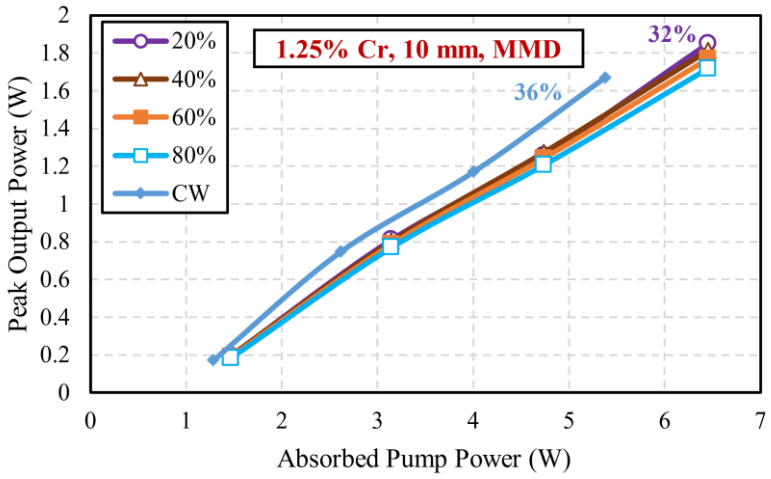

Figure 3.19. Quasi continuous wave laser performance of the Cr:LiCAF laser for different pump pulse duty cycle. Pump pulse period 10 ms used for the measurements

As a first step starting from 20% duty cycle, output power measured. During the pulse pumping operation crystal absorbed more peak power than the continuous wave operation. Also, the output power of the Cr:LiCAF laser increased depending on the duty cycle. However, superior thermal properties of Cr:LiCAF showed better performance according to the slope efficiencies. An increase in the absorbed power lower the slope efficiency. When the duty cycle approaches 100%, meaning that the laser operates in continuous wave (CW) mode, the output power of the laser tends to decrease due to thermal effects.

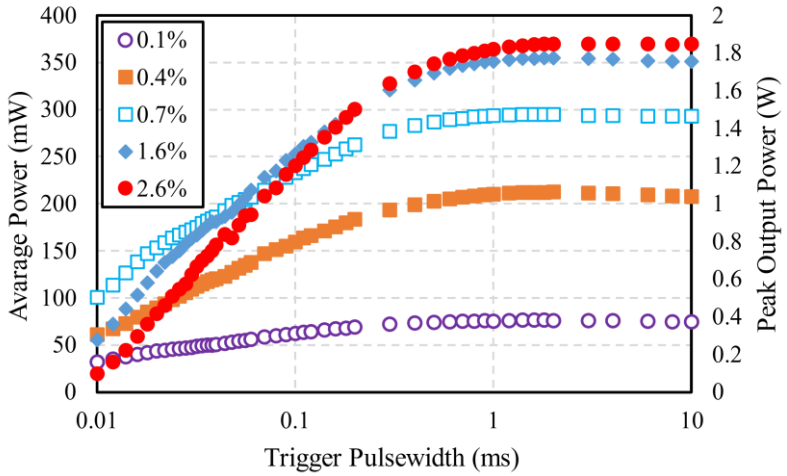

Figure 3.20. Measured average power and peak power results of Cr:LiCAF as a function of different trigger pulse widths

Additionally, the laser output performance increased by about 18%, while the laser operated in quasi-continuous wave on 20% percent duty cycle pumping. Measured

output power increased from 1.67 W to 1.85 W. Figure 3.20 shows the measured variation of Cr:LiCAF quasi-continuous wave peak power and average power results with respect to trigger pulse duration. The duty cycle was set to 20% and the pulse duration varied from 10 μs to 10 ms. For the measurements, output couplers with transmission rates of 0.1%, 0.4%, 0.7%, 1.6%, and 2.6% were used. The laser output power showed an increase until around 600 μs trigger pulse with, reaching its maximum around 1 ms. However, after 1 ms, thermal effects started to impact the lasing process, resulting in a decrease in output power.

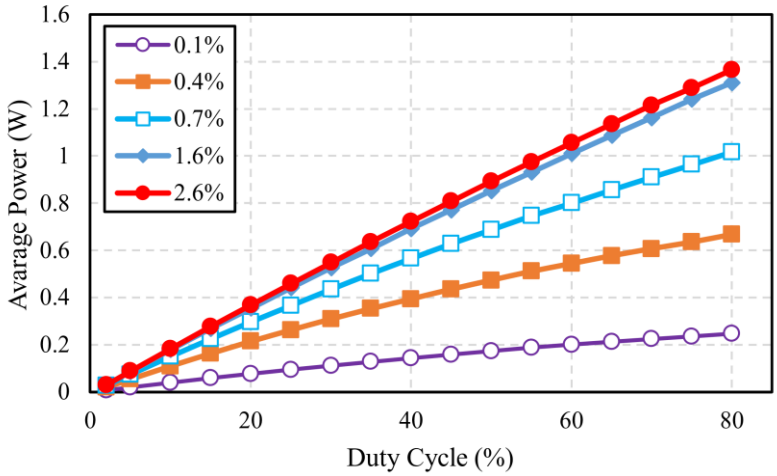

Figure 3.21. Measured average power results of Cr:LiCAF as a function of duty cycle

Figures 3.21 and 3.22 show the Cr:LiCAF laser average power and peak power changing depending on the trigger pulse duty cycle. Measurements were conducted using a pulse period of 10 ms, while the duty cycle was varied between 2% and 80%. For the measurements, output couplers with transmission rates of 0.1%, 0.4%, 0.7%, 1.6%, and 2.6% were utilized. It is evident that the average power level was consistently increased as the duty cycle increased. On the other hand, peak power levels decreased once the duty cycle reached 15%. One can conclude that the Cr:LiCAF laser operates at higher peak power levels with 1.5 ms trigger pulses. However, beyond that point, the increase in thermal effects leads to a reduction in power efficiency. Nevertheless, this reduction stayed at reasonable levels due to the superior thermal properties of Cr:LiCAF laser.

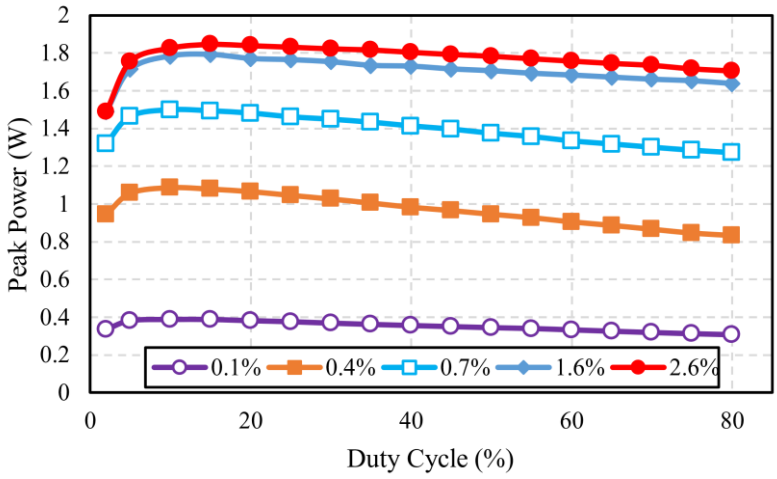

Figure 3.22. Measured peak power results of Cr:LiCAF as a function of duty cycle

3.4. Intracavity Second Harmonic Generation in Cr:LiCAF Laser

In this section, intracavity second harmonic generation in Cr:LiCAF laser experiment were presented. Second harmonic generation (SHG) is an optical phenomenon that involves the nonlinear interaction of two photons of identical frequency within a nonlinear material, resulting in the production of a photon with double the frequency. This process occurs when the incident light wave passes through a nonlinear crystal or material with high optical intensity.

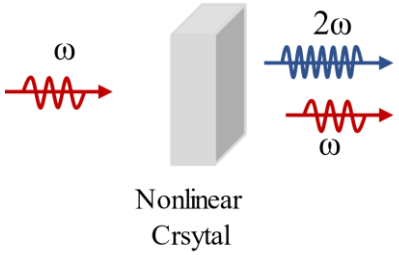

Figure 3.23. Simple illustration of second harmonic generation with nonlinear crystal

To maximize the intensity of the second harmonic radiation, it is important for the induced polarization wave and the generated light wave propagates through the medium with the same phase velocity. In other words, proper phase matching increases the achievable conversion efficiency. By exploiting the natural birefringence of biaxial or uniaxial nonlinear crystal, fundamental and second harmonic generation wave phase matching can be ensured. Birefringence refers to the property of a crystal to have different refractive indices for different polarization directions. By carefully adjusting the crystal orientation and polarization of the input beam, it becomes feasible to achieve phase matching, which leads to improved efficiency in the second harmonic generation.

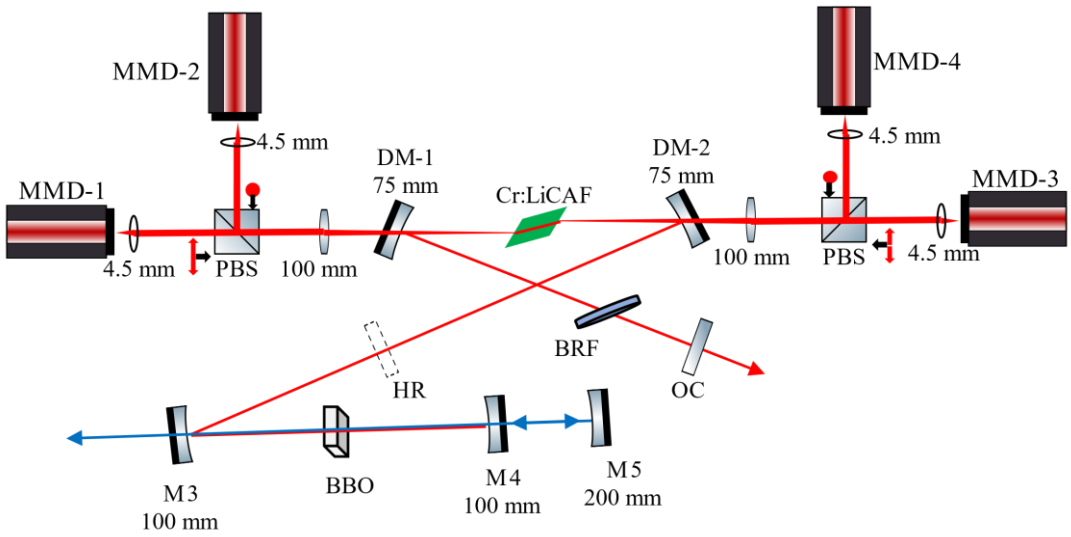

Figure 3.24. Schematics of the continuous wave Cr:LiCAF laser that was used in second harmonic generation experiments. BBO: Beta-Barium Borate nonlinear crystal

Figure 3.24 shows the schematics of Cr:LiCAf laser that was used in the second harmonic generation experiment. In contrast to continuous wave (cw) operation, the high reflectivity (HR) mirror is removed in order to allow for higher intensity in the nonlinear crystal. To achieve this, a second cavity is inserted into the setup. 15 (b) mm 1.25% doped Cr:LiCAF crystal used as gain medium. As a nonlinear crystal, 0.5 mm 800-400 nm, 2 mm 800-400 nm, 4 mm 800-400 nm, 2 mm 825-412 nm, 2 mm 775-387 nm Beta-Barium Borate (BBO) and 10 mm 800-400 nm Bismuth Borate (BiBO) utilized. Two highly reflective curved mirrors (M_3 and M_4) with a radius of curvature 100 mm were used to generate second focus inside the nonlinear crystal. The mirrors had around 90% reflectance on the 400 nm and act as OC. To prevent the loss and increase the power level another curved mirror with a radius of curvature 200 mm was used for the reflect back the transmitted light. A crystalline quartz birefringent plate was inserted to cavity to obtain the wavelength tuning of second harmonic emission. Finally, to boost the intracavity intensity and the conversion efficiency, output coupler inside the cavity was replaced with the HR mirror.

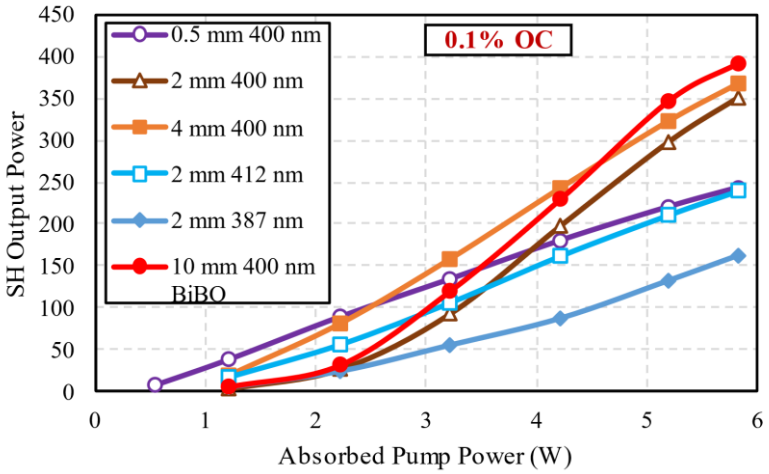

Figure 3.25. Intracavity generated continuous wave power efficiency curves. Data taken with different various nonlinear crystal. As an output coupler 0.1% utilized

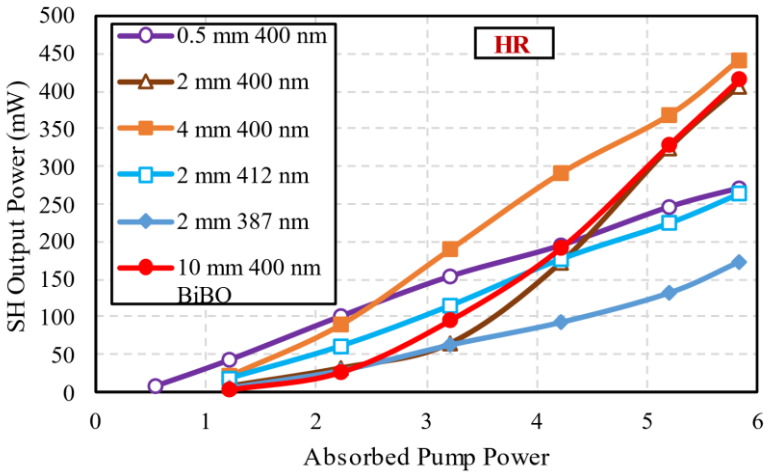

Figure 3.26. Intracavity generated continuous wave power efficiency curves. Data taken with different various nonlinear crystal. To boost the intracavity power HR utilized

Figure 3.25 shows the measured variation of intracavity generated second harmonic power efficiency as a function of absorbed pump power. During the measurement, different nonlinear crystals were inserted into the cavity. These included a 0.5 mm crystal with a conversion wavelength of 800-400 nm, a 2 mm crystal with 800-400 nm, a 4 mm crystal with 800-400 nm, a 2 mm crystal with 825-412 nm, a 2 mm crystal with 775-387 nm BBO, and a 10 mm crystal with 800-400 nm BiBO. After each crystal was placed in the cavity, a fine alignment process was conducted to achieve optimal phase matching for an efficient second harmonic generation. To minimize intracavity loss and increase the conversion efficiency, an output coupling of 0.1% was

used. This choice of output coupling allowed for the maximum intensity of power within the cavity, reducing losses and maximizing the efficiency of the second harmonic generation process. Varying the nonlinear crystal operation wavelength and length, the maximum second harmonic power measured as 392 mW with a 10 mm BiBO crystal. The lowest power was obtained with 2 mm 387 nm crystal. To improve the intracavity power 0.1% OC was replaced with HR. Figure 3.26 shows the measured variation of intracavity generated second harmonic power efficiency as a function of absorbed pump power. The replacement of the output coupler significantly boosted the nonlinear conversion efficiency, resulting in a measured second harmonic blue power of 441 mW with the 4 mm 400 nm nonlinear crystal. Once again, the lowest power was measured with the 2 mm 387 nm crystal. This possibly caused the fundamental nonlinear effects lowering at 775 nm.

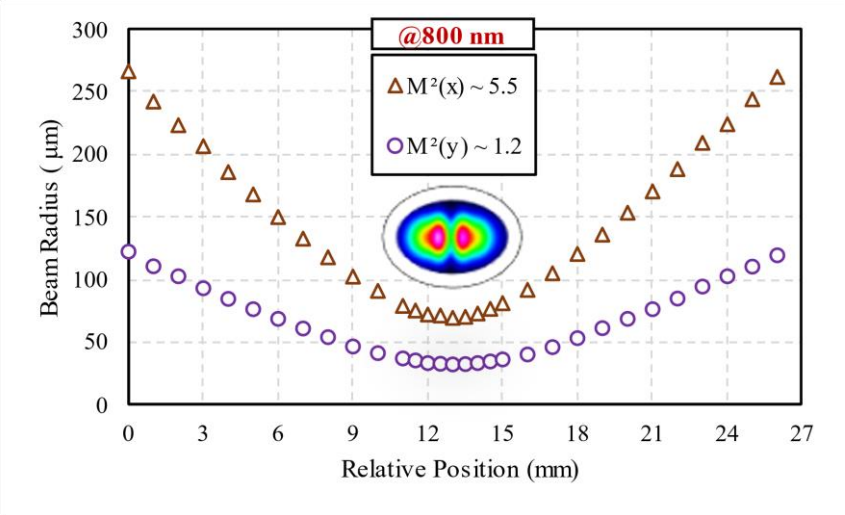

Figure 3.27. Measured output beam quality M^2 of Cr:LiCAF laser at 800 nm fundamental wavelength. Beam profile of output laser presented inside figure

Figures 3.27 and 3.28 show the measured variation of output beam quality M^2 factor of Cr:LiCAF laser at fundamental and second harmonic wave respectively. The beam quality on the sagittal axis for the 800 nm wavelength was measured to be 1.2, while for the 400 nm wavelength, it was measured to be 1.9. On the other hand, for the tangential axis, as mentioned in section 3.2 diffracted beam was observed. Beam quality was measured as 5.5 and 12.2 for 800 nm and 400 nm respectively. Additionally, during the second harmonic generation, on the fundamental beam the transverse beam mode converted to TEM_{10} (figure 3.27 inside).

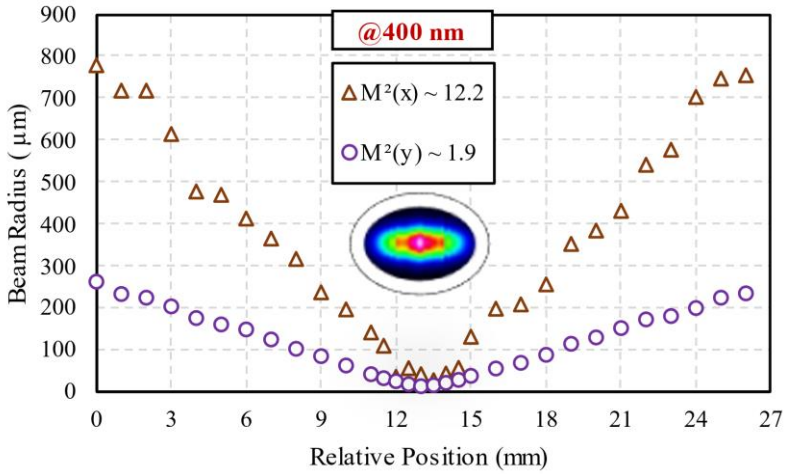

Figure 3.28. Measured output beam quality M^2 of Cr:LiCAF laser at 400 nm fundamental wavelength. Beam profile of output laser presented inside figure

Figure 3.29 illustrates the continuous wave second harmonic tuning range of the Cr:LiCAF laser. The experiment involved the use of three different BBO crystals with wavelengths of 387 nm, 400 nm, and 412 nm. Furthermore, a 10 mm long 400 nm BiBO crystal was also tested for tuning. 2 mm thick birefringent plate was utilized for the tuning. Each crystal was placed into the cavity carefully and aligned for each wavelength. The obtained tuning range in the experiment was between 377 nm and 424 nm. This range is consistent with the reported frequency doubled range of 375 nm to 433 nm as stated in the work by Demirbas et al. in 2014. On the other hand, 400 nm 10 mm BiBO crystal showed better tuning performance between 380-418 nm. One possible reason for the difference in wavelength tuning range could be attributed to the antireflective coatings applied on the crystals. It is likely that the 10 mm sample had a broader antireflective coating, allowing it to cover a wider range of wavelengths compared to the other samples.

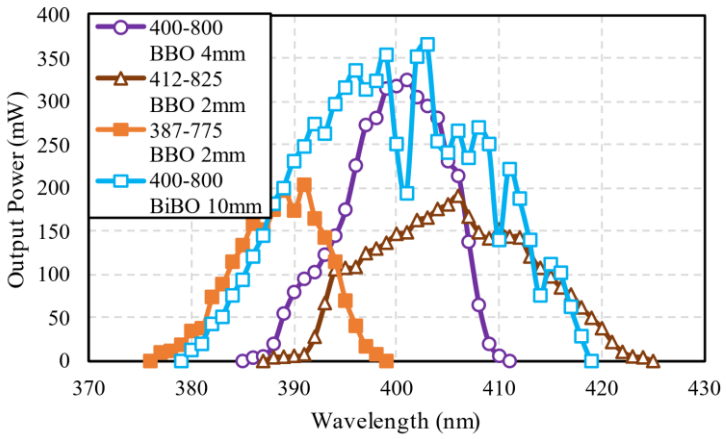

Figure 3.29. Measured frequency doubled Cr:LiCAF tuning range. 387-412 nm nonlinear crystals utilized for the tuning measurements

One of the significant drawbacks of the intracavity frequency doubling process is the occurrence of output power fluctuations. These fluctuations arise from the nonlinear operations involved in the second harmonic conversion, leading to significant variations in the output power. Figure 3.30 shows the measured second harmonic intensity with respect to time. The output power was measured continuously for a duration of 600 seconds, and the relative standard deviation of the data was found to be 1.12%. This indicates that there was a relatively low level of fluctuation in the output power over time.

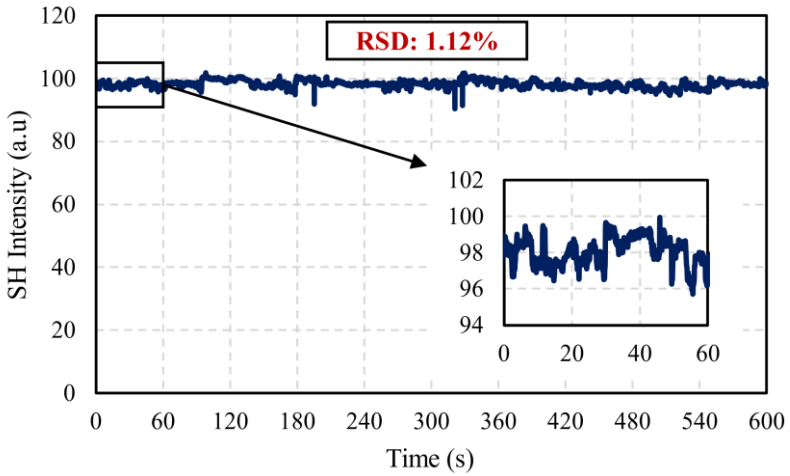

Figure 3.30. Measured variation of second harmonic intensity over time. RSD of second harmonic intensity measured as 1.12%

3.5. Q-Switched Operation of Cr:LiCAF Laser with SESAM/SBR

In this section, the results of a passively Q-switched Cr:LiCAF laser are presented. The laser operation was achieved by using a Saturable Bragg Reflector (SBR) as the passive Q-switching element. Figure 3.31 shows the schematics of a passively Q-switched Cr:LiCAF laser system. The same laser system used for continuous wave operation was utilized for the passively Q-switched operation with the replacement of the HR mirror. To create a larger focus spot size and prevent high-intensity focusing that could lead to mode-locking or Q-switched mode-locking, a curved mirror with a radius of curvature of 150 mm was placed in the laser cavity. An SBR with a central wavelength of 800 nm was used to enable Q-switching operation and generate pulsed output from the laser. 10 mm 1.25% Cr doped crystal utilized as the gain medium.

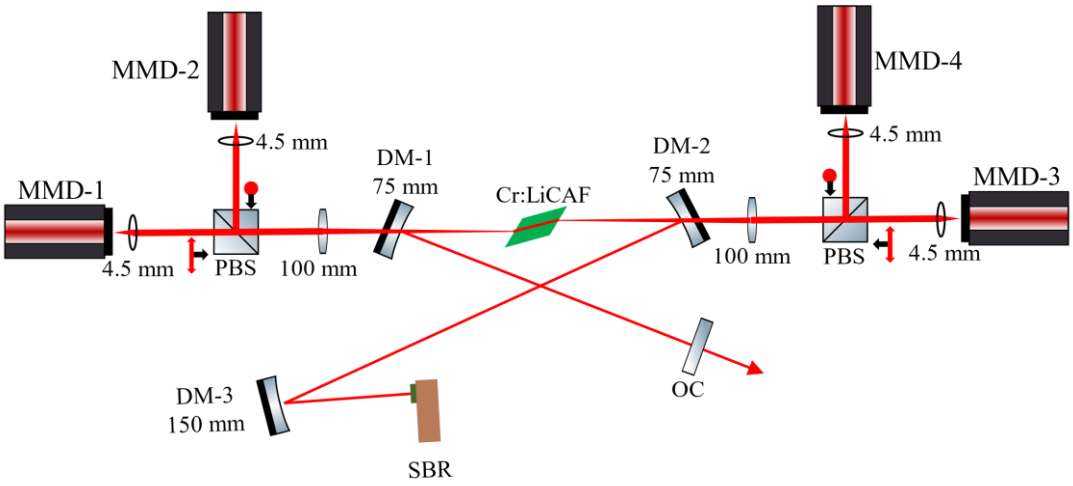

Figure 3.31. Schematics of passive Q-switched Cr:LiCAF laser cavity

Figure 3.32, shows the recorded pulse trains of Q-switched Cr:LiCAF lasers. During the measurements, high-speed photodetector used. Pulsed laser operation was measured in the following time windows: 40 ms, 4 ms, 400 µs, and 40 µs. These time windows represent the durations of the oscilloscope seconds per division scale. A single clean pulse with a measured pulse width of 1.52 µs was obtained in the experiment.

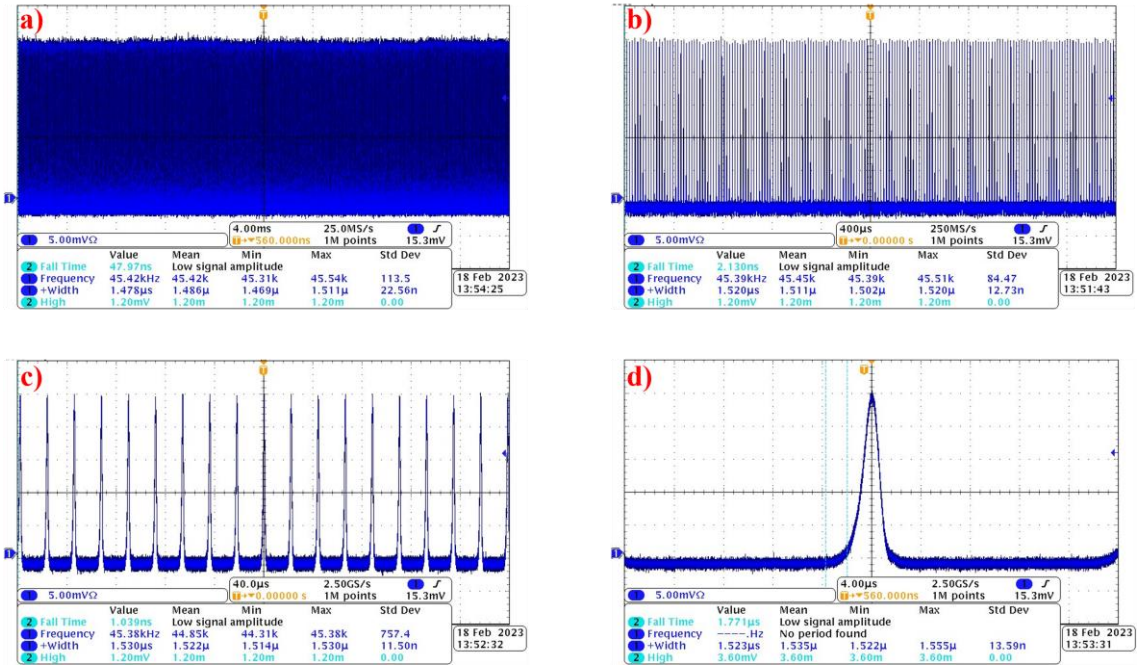

Figure 3.32. Recorded pulse trains of Q-switched Cr:LiCAF laser. Figures shows the pulse train in a) 40 ms window; b) 4 ms; c) 400 µs; d) 40 µs

Figure 3.33 and 3.34 shows the measured variation of pulse repetition rate and pulse width as a function of absorbed pump power. Data taken with 0.1%, 0.4%, 0.7%, 1.6% and 2.6% OC. Highest repetition frequency obtained with 1.6% around 42 kHz. The overall repetition frequency within the range of 15-30 kHz range.

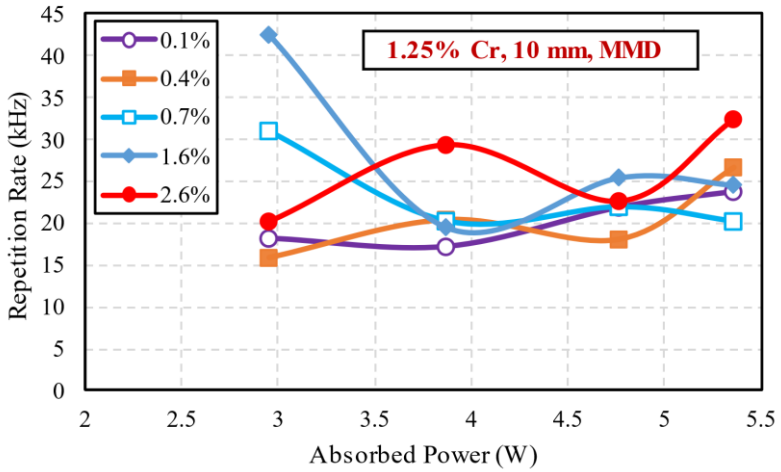

Figure 3.33. Q-switched repetition rate of a Cr:LiCAF laser measured with varying output couplers

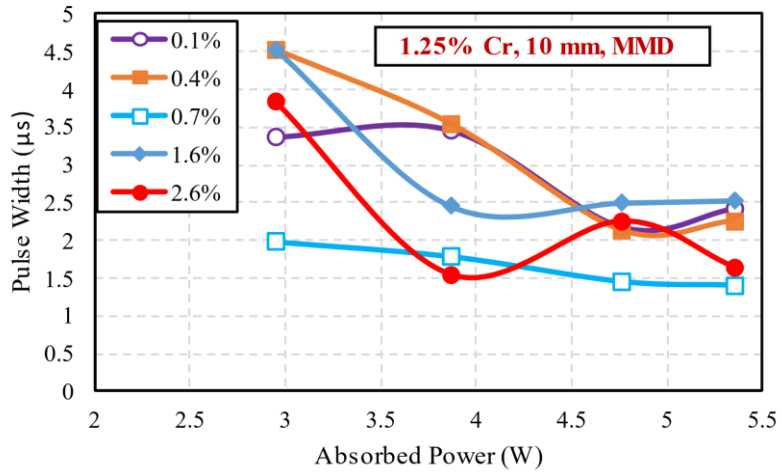

Figure 3.34. Q-switched pulse width of a Cr:LiCAF laser measured with varying output couplers

However, Okuyucu et al., reported that the increase on the repetition frequency should be linearly upward (Okuyucu et al., 2021). To achieve the desired linear upward trend in the repetition rate of pulses, a more careful cavity design should be taken into consideration. On the other hand, the pulse width characteristics show a linear downward trend depending on the absorbed pump power level. The measured pulse widths showed a decrease with all OC. The shortest pulse widths were obtained with a 0.7% OC, measuring at 1.4 µs. Also, the longest pulse widths were obtained with a 1.6% OC,

measuring at 4.52 μs. Figure 3.35 and figure 3.36 shows the measured variation of Q-switched pulses peak power and pulse energies as a function of absorbed pump power.

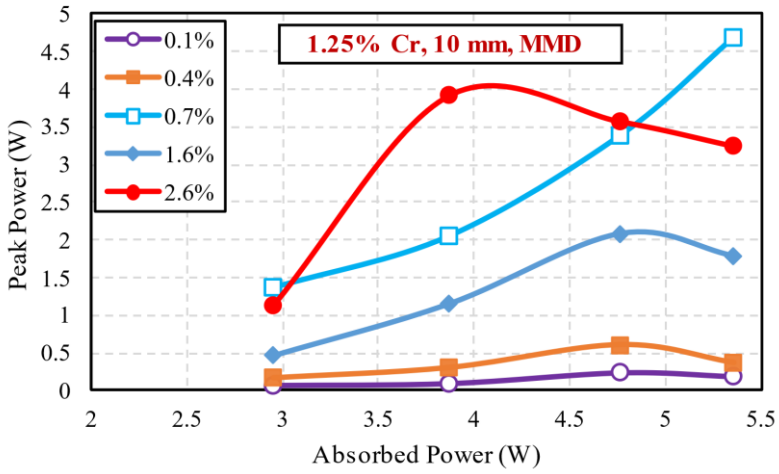

Figure 3.35. Q-switched peak powers of a Cr:LiCAF laser measured with varying output couplers

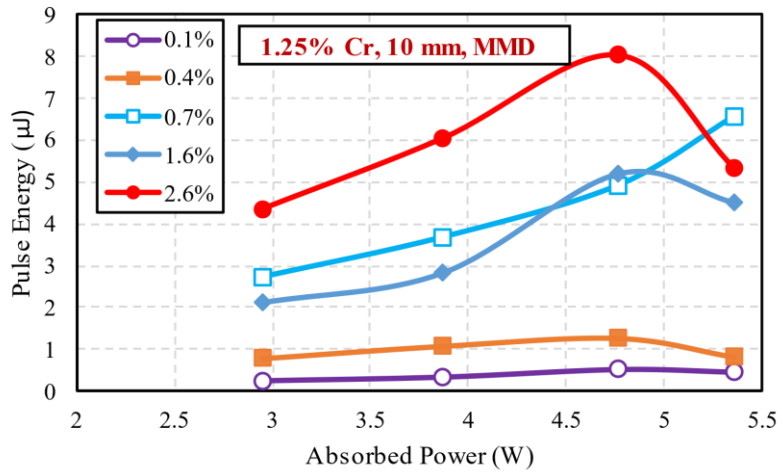

Figure 3.36. Q-switched pulse energy of a Cr:LiCAF laser measured with varying output couplers

Based on the pulse withs and repetition frequency, peak powers can be estimated via following expression;

$$P_{peak} = \frac{P_{avg}}{\tau_p f_{rep}} \tag{3.9}$$

where P_{avg} was measured average power, τ_p was pulse width, and f_{rep} was repetition frequency. The peak power of pulses varied between 177 mW to 4.6 W. The minimum and maximum peak power obtained with 0.1% and 0.7% OCs respectively. As expected,

the 0.1% C) resulted in the lowest peak powers due to the reduced output power. Further, the pulse energy of pulses can be estimated via following expression;

$$E_{pulse} = \frac{P_{avg}}{f_{rep}} \tag{3.10}$$

Measurements showed that the pulse energies increased with respect to absorbed pump power. The maximum pulse energy obtained with the 2.6% OC was measured as 8 μJ. Moreover, there was a linear increase in the pulse energy when using the 0.7% OC. The obtained pulse energy can be increased with a finely aligned cavity design. This is because the measured continuous wave average power reached around 250 mW. However, despite the increase in pulse energy, clean pulses were not sustained.

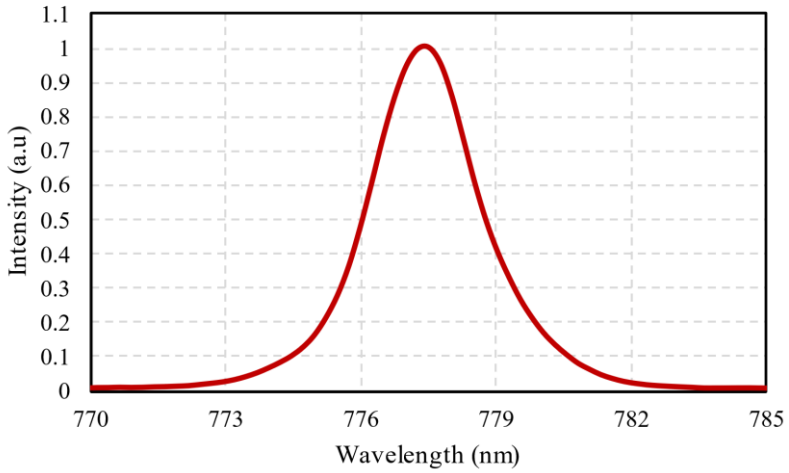

Figure 3.37. Measured optical spectrum of Q-switched Cr:LiCAF laser with 2.6% OC

Figure 3.37 shows the measured optical spectrum of the Q-switched Cr:LiCAF laser. Data taken with 2.6% OC. The optical spectrum full width at half-maximum was (FWHM) measured as 2.7 nm. During the measurements with an increase in the OC transmission peak wavelength shifted through the shorter wavelength. The observed optical spectrum with a FWHM of 2.7 nm is likely a result of increased overall losses in the laser cavity, which pushed the lasing operation towards a higher gain region. The characteristics of the output coupler coating may also have influenced the spectral properties of the laser emission.

3.6. Passively Mode-Locked Cr:LiCAF Laser

Passively mode-locked Cr:LiCAF laser results were presented in this section. Semiconductor saturable bragg reflector used to initiate stable mode-locked pulse trains. Figure 3.38 shows the cw mode-locking cavity setup of Cr:LiCAF laser. In this set of experiments single-mode diode (SMD) pumped system was used rather than MMD system. Two 660 nm single spatial mode, TM (p) polarized commercial laser diode as a

pump source. The SMD diodes provide up to 240 mW of output power at a 20 °C operating temperature. Incident light collimated with 4.5 mm focal length aspherical lens. Achromatic doublets with a focal length of 60 mm were used to focus the beam inside the gain medium. 15 (b) mm 1.25% Cr doped gain medium placed the copper holder at ambient temperature. The gain medium absorbed the 97% incident TM (p) polarized light.

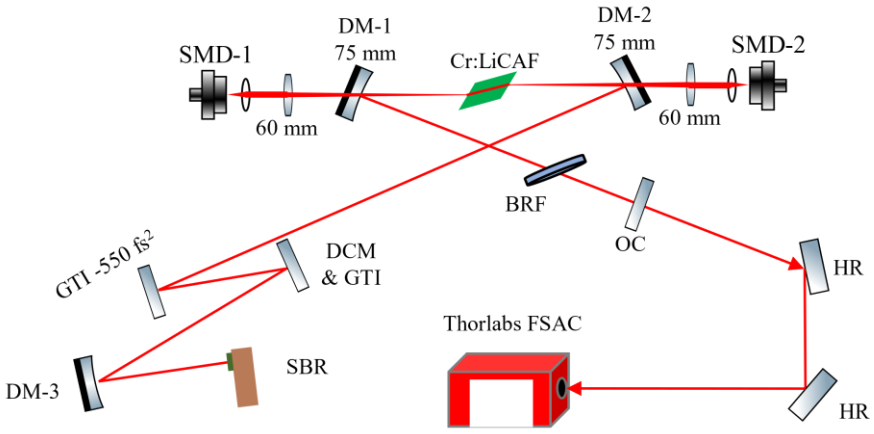

Figure 3.38. Schematics of single mode diode pumped cw mode-locking operation setup of Cr:LiCAF laser. SMD: Single mode diode, GTI: Gires-Tournois Interferometer mirror, DCM: Double-chirped mirror, FSAC: Femtosecond autocorrelation

An X-folded cavity was employed for the experiment. Two curved mirrors with a radius of curvature 75 mm were used to create a secondary focus inside the gain medium. The Gires-Tournois Interferometer mirror (GTI) and double-chirped mirror (DCM) were utilized for the dispersion compensation. GTI and DCM mirrors had a group velocity dispersion (GVD) value -550, -50, and -150 fs^2. Moreover, Cr:LiCAF crystal itself provides +25 fs^2/mm group GVD. During the experiment total cavity dispersion estimation varied between -450 fs^2 and -1026 fs^2. A 75 mm and 100 mm radius of curvature curved mirror (DM-3) was used to create focus on SBR. A birefringent filter placed the cavity at Brewster's angle for output wavelength tuning operation. Commercial femtosecond interferometric autocorrelator (Thorlabs, FSAC), was measure the mode-locked Cr:LiCAF laser pulse duration. The output beam aligned with two broadband dielectric mirrors has a reflectivity of around 99% in 750-1100 nm, inside through autocorrelator. Figure 3.39 shows the recorded pulse trains of stable continuous wave mode-locked Cr:LiCAF laser. On the continuous wave regime, the oscilloscope showed only continuous energy level. However, while the mode-locking was initiated, there were fluctuations observed. The increase on the power level and change on the oscilloscope give pure mode-locking pulse trains. During measurements, depending on the intensity of the focus beam on SBR there was Q-switched mode-locking observed. The pulse trains given in the figure were operating at around 137 MHz repetition rate.

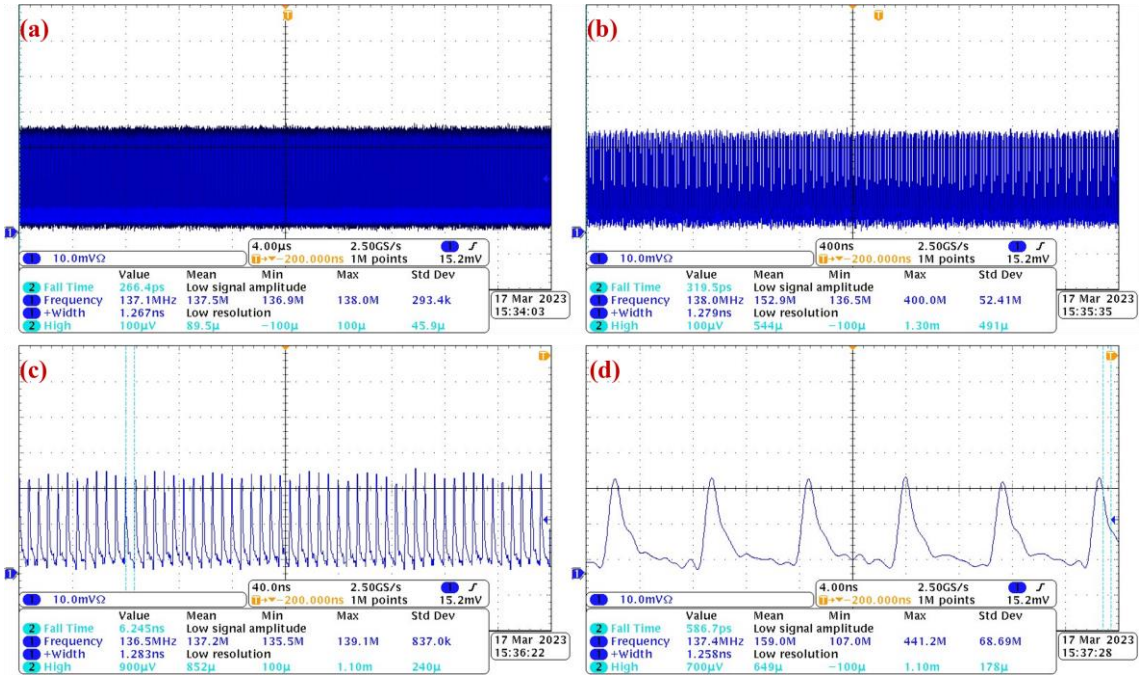

Figure 3.39. Recorded pulse trains of cw mode-locked Cr:LiCAF laser. Figures show the pulse train in a) 40 μs window; b) 4 μs; c) 400 ns; d) 40 ns

Figure 3.40 shows the measured shortest pulse properties of passively mode-locked Cr:LiCAF laser. The obtained intensity autocorrelation trace with an FWHM of 100 *fs* suggests a pulse duration of approximately 65 *fs* assuming a $sech^2$ pulse shape. The measured average output power of 35 mW corresponds to a peak power of 3.9 kW and pulse energy of 0.25 nJ when the pump power was 430 mW. The optical spectrum centered around 797 nm with an FWHM of 15 nm. The repetition frequency of the pulses, as measured by the frequency spectrum analyzer, was approximately 139 MHz. Different pulse durations were measured depending on the specific configuration of the cavity such as cavity length. The dispersion compensation and the focused intensity of the beam on the saturable bragg reflector (SBR) played a crucial role in determining the pulse duration.

Table 3.5. Measured mode-locked pulse duration of Cr:LiCAF laser

P_{out} (mW)	τ_{ac} (*fs*)	$sech^2$ τ_p (*fs*)	Frep (MHz)	Optical FWHM (nm)	Peak Power (kW)	Pulse Enrgy (nJ)
35	100	64.8	139	15.1	3.9	0.25
31	110	71.3	136	10.6	3.2	0.22
51	137	88.8	137	8.4	4.2	0.37
48	196	127	134	3.4	2.8	0.35

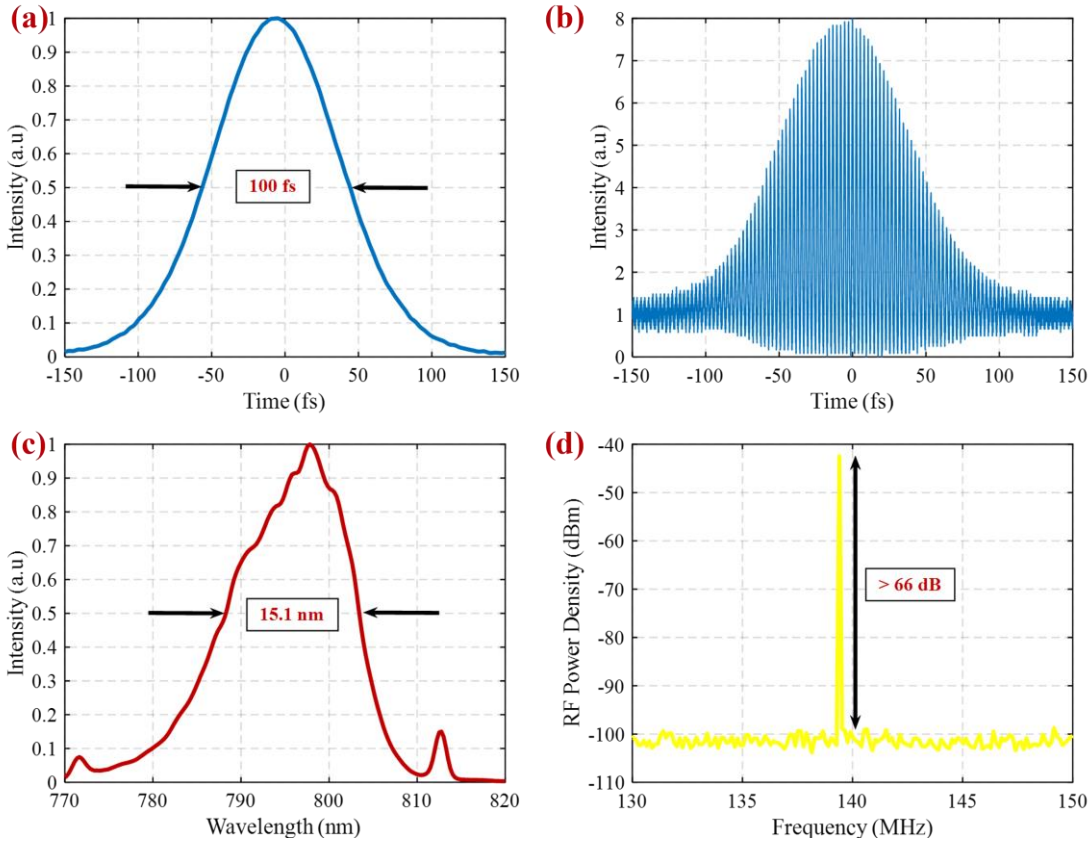

Figure 3.40. Measured properties of mode-locked Cr:LiCAF laser. a) measured intensity autocorrelation trace; b) interferometric autocorrelation signal; c) optical spectrum FWHM of 15.1 nm; d) measured radio frequency spectrum at 139 MHz repetition rate

Table 3.5 shows the measured different cw mode-locking pulse durations of Cr:LiCAF. Obtained pulses varied between 127 *fs* to 65 *fs*. The pulse energies were around 0.3 nJ for the all-stable mode-locked pulses. As an output coupler 0.7% was used during the measurements due to increase in the intracavity intensity. In order to achieve stable cw mode-locking, the SBR needed to be saturated. The intensity of the beam on the SBR was controlled by the focusing mirror and OC, which determined the level of saturation. However, in certain cases, the SBR could be damaged due to the high energy focused on it. To reduce the risk of damaging the SBR while maintaining stable cw mode-locking, a 0.7% OC was used in combination with a focusing mirror with a radius of curvature of either 75 mm or 100 mm. This choice of focusing mirror helped control the intensity of the beam and prevent excessive energy from being focused on the SBR.

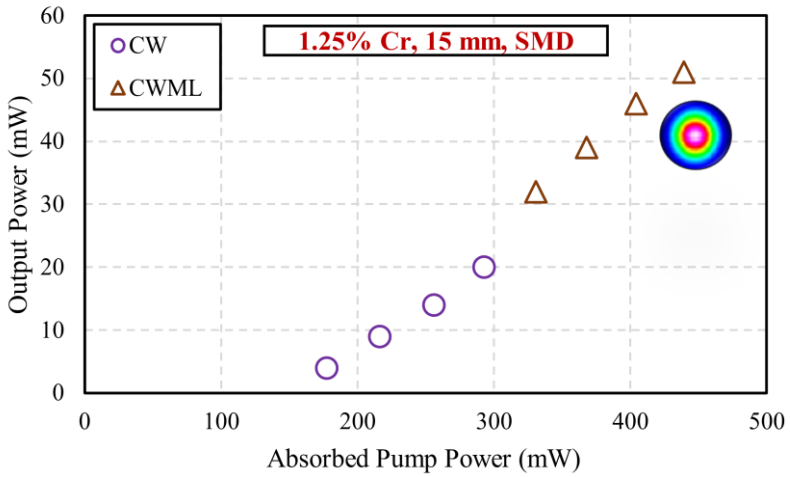

Figure 3.41. Measured variation of Cr:LiCAF cw mode-locking efficiency curves. Shows the different operation regimes depending on absorbed pump power

Figure 3.41 shows the efficiency curves of the cw mode-locking Cr:LiCAF laser. Using an output coupler of 0.7% transmission self-starting stable mode-locking was obtained. A cw mode-locked pulse train was observed when the absorbed pump power reached 300 mW. Below 300 mW the laser was working in cw regime. The inside figure shows output beam profile of single-mode diode-pumped mode-locked Cr:LiCAF laser. Beam profile was in the TM_{00} mode operation during mode-locking. In figure 3.42 cw mode-locking tuning performance is presented. A 16 mm birefringent plate was inserted cavity to achieve continuous tunability of the mode-locked laser. tuning range between 794 nm to 801 nm achieved. Along the short and long wavelengths, the tuning limited due to the bandwidth of GTI and DCM mirror.

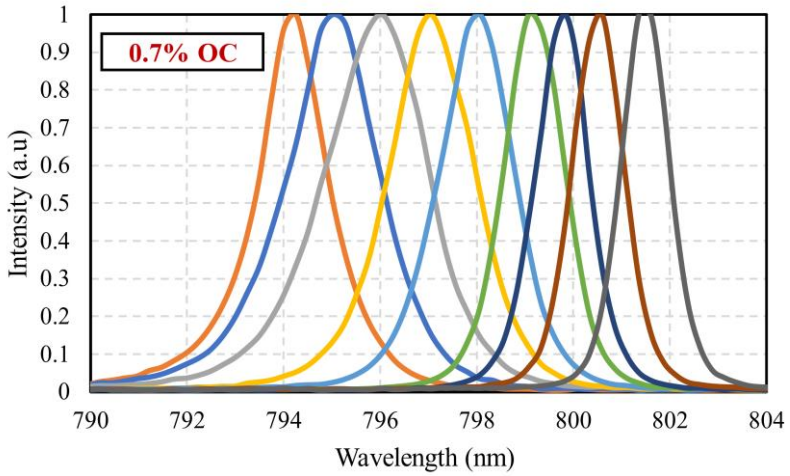

Figure 3.42. Measured cw mode-locking tuning performance of Cr:LiCAF laser

3.7. Thermal Analysis of Cr:LiCAF Laser

In this section, studies that were carried out for temperature estimation and thermal analysis inside the Cr:LiCAF laser crystal during continuous wave operation are presented. In order to estimate the temperature in the system, an optical probing method and finite element simulation were employed. The optical probing method utilized the emission characteristics of Cr:LiCAF at different temperatures to measure and analyze the system. Below, we provide more detailed explanations of the methods used for optical probing to measure temperature in the Cr:LiCAF material.

3.7.1. Temperature Probing Method

To perform temperature probing, a four multimode-diode pumped laser system was employed, utilizing a 15 mm Cr:LiCAF crystal as the gain medium. Figure 3.43 shows the experimental setup of emission measurements depending on temperature. Firstly, MMDs were connected to a function generator to drive in pulsed mode. The function generator was adjusted to operate at 1Hz repetition frequency with 10 ms pulse duration with connected four MMD diodes.

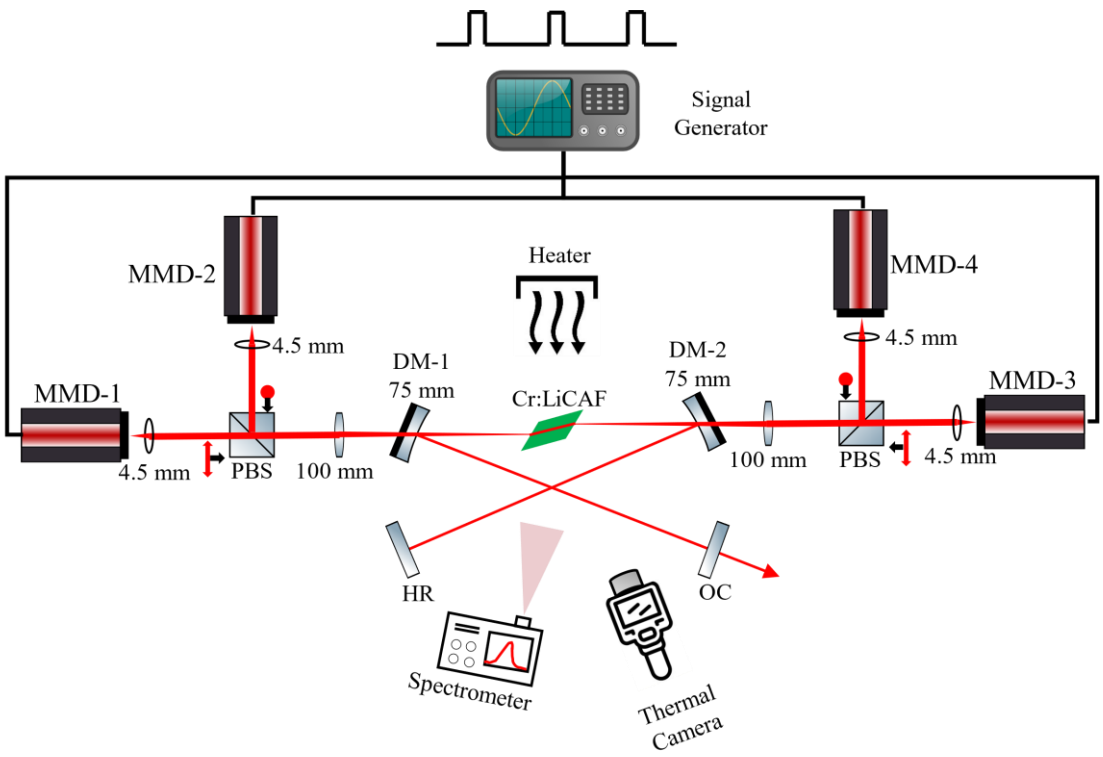

Figure 3.43. Schematics of temperature probing experimental setup, to obtain learning curve from fluorescence emission with spectrometer. MMD's driven in pulsed mode. Temperature of the crystal was monitored with thermal camera during heating.

This setting provided around 30 mW pump power on each pulse. To introduce heat to the crystal and simulate temperature changes, a soldering blower and crystal holder chiller was utilized. The temperature range was arranged between 10-100 °C.

Crystal holder chiller used to control the temperature between 10-40 °C and above that temperature soldering blower activated. The soldering blower was directed towards the top of the crystal holder, allowing controlled heating of the crystal. Spectrometer placed where fluorescence emission of Cr:LiCAF crystal has higher intensity. To monitor the temperature changes during the heating process, a thermal camera was positioned to capture the side surface of the crystal. The thermal camera provided real-time thermal imaging, allowing for the observation and measurement of temperature variations in the crystal. Fluorescence emissions from the crystal were recorded with a high-resolution spectrometer, capturing the emission spectra at small temperature intervals of 0.5 °C. This fine temperature resolution helped to minimize measurement errors and accurately track the changes in fluorescence characteristics with temperature.

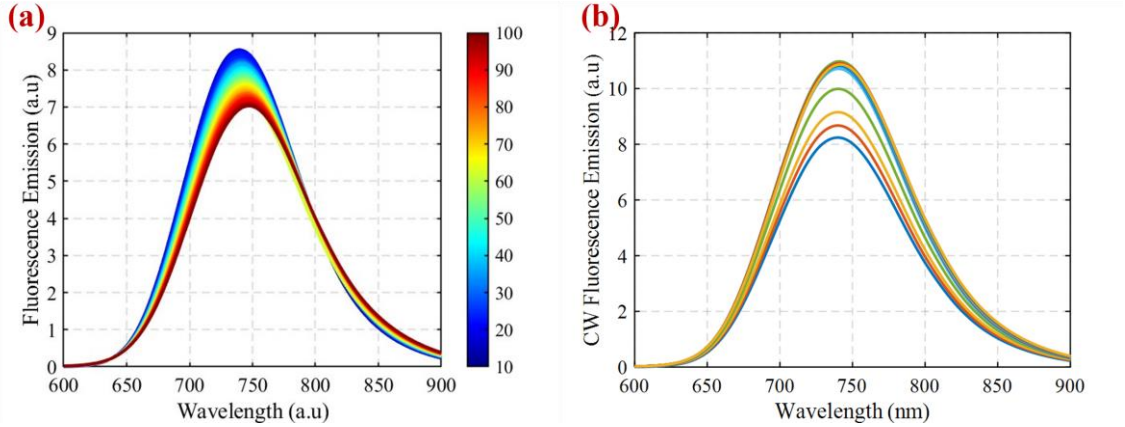

Figure 3.44. Measured fluorescence emission characteristics of Cr:LiCAF crystal a) temperature depending between 10-100°C; b) during continuous wave lasing depending on diode current

Figure 3.44 shows the measured fluorescence emission characteristics of Cr:LiCAF between 10-100 °C and during continuous wave lasing emission. Inevitably, during measurements the spectrometer captured the pump and lasing emission too. With a MATLAB post-processing the unwanted pump and lasing emissions were removed, and data smoothed with curve fitting toolbox as required. Furthermore, while the laser was operating in continuous wave (cw) mode, the fluorescence emission was captured as a function of the diode current. During the temperature dependent measurements, it was observed that as the temperature increased, there was a decrease in fluorescence emission and a shift in the wavelength of the emitted light. This phenomenon was observed also in emission cross-section measurements as reported (Okuyucu et al., 2023). In the post-processing phase, the emission peaks of the measured data were extracted based on the studies reported for the temperature probing methods (Demirbas et al., 2020).

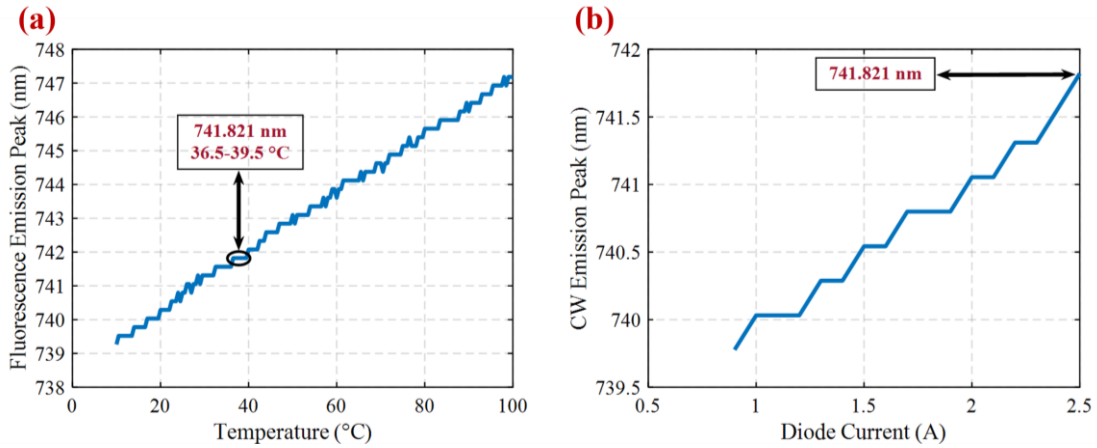

Figure 3.45. Measured fluorescence emissions characteristics emission peaks for a) temperature depending between 10-100 °C; b) cw emission as a function of diode current

Figure 3.45 represents the obtained Cr:LiCAF crystal fluorescence emission peaks at different temperatures and cw emission with different diode currents. Extracted emission peaks of temperature dependent data were used as learning. The same process was applied for cw emission at different diode operation currents. Figure 3.45 (b) shows the cw emission peak characteristic of Cr:LiCAF laser. At the maximum pump power of 6W, achieved by setting the diode current to 2.5 A, the cw fluorescence emission peak was observed at a wavelength of 741.821 nm. The obtained peak was paired with the corresponding point on the learning curve to estimate the temperature. This pairing result showed that the emission peak was observed between 36.5-39.5 °C. At this particular point, the temperature inside the crystal during full pump power of 6W can be estimated to be around 38±1.5 °C. On the other hand, figure 3.46 shows the captured thermal image of Cr:LiCAF crystal during cw operation. The maximum temperature recorded at the beam entrance face of the crystal was approximately 70.5 °C, while on the side face around 42.5 °C. Due to the nature of the thermal camera, which collects infrared radiation from the surface of an object, it is expected that the temperature reading at the pump light entrance face of the crystal, where the radiation reflection is more distinct, would be higher than at the side face. However, here should be noted that there should be more specific studies carried out to obtain a more accurate temperature of an Cr:LiCAF laser. One of the challenging parts that was faced was the post-processing methods. Depending on the used methods, to process measured emission data obtained results showed various results. Here, one of the accurate ones was used.

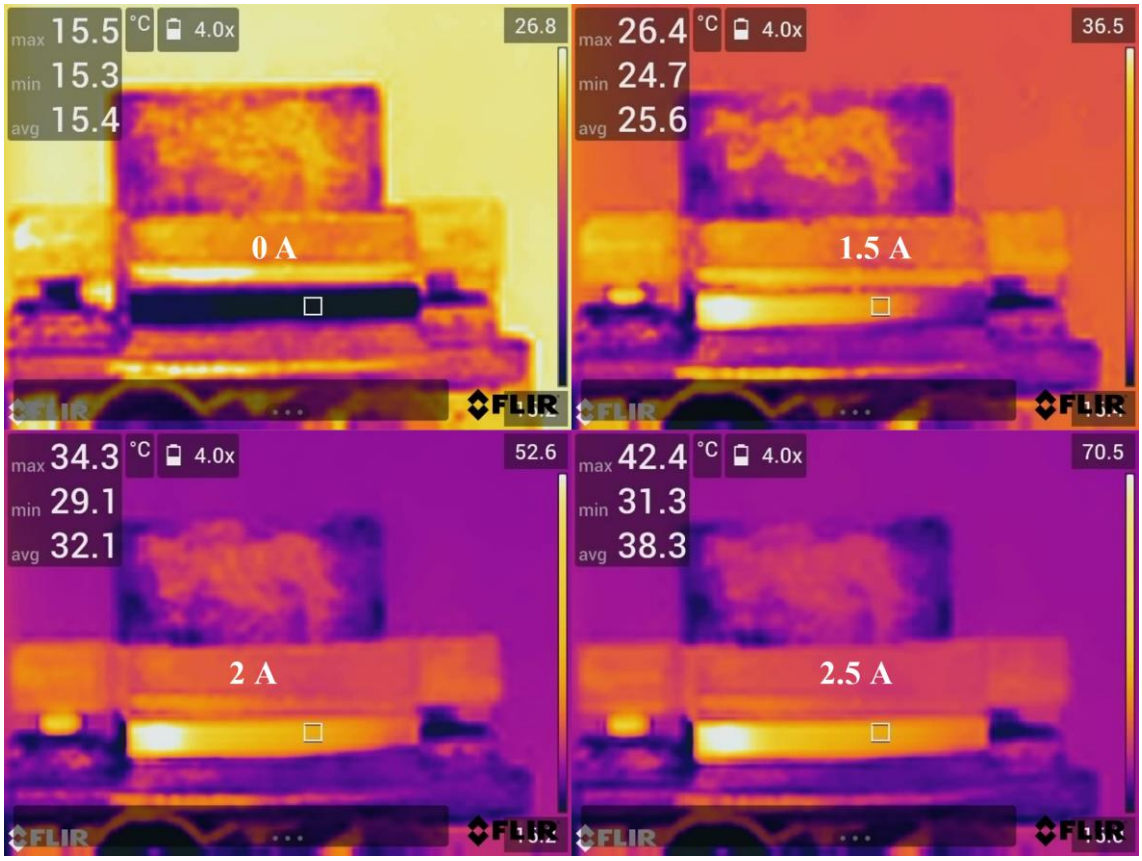

Figure 3.46. Real-time thermal image of Cr:LiCAF crystal while working in cw lasing. Images captured at different diode operation current indicated inside

3.7.2. Thermal analysis with COMSOL FEA Software

Another method that could be used to estimate the temperature inside the Cr:LiCAF crystal was using a finite element analysis software simulation. During the simulations, COMSOL multiphysics, FEA software, was used. By applying the required pumping configuration, temperature could be calculated. Firstly, the thermal load mechanics of the Cr:LiCAF laser should be understood. Excessive heat load inside the crystal during population inversion can be attributed to four mechanisms: quantum defect, thermal quenching of the upper laser level, excited state absorption, and auger upconversion (Demirbas, 2019). The quantum defect can be described as the energy difference between pump and laser photon. Thermal quenching is caused by the increased temperature of the crystal, decreasing the fluorescence lifetime duration. During the absorption of photons, in the excited state ions absorb another photon the energy and reach another upper level. The back transaction to upper level occurs non-radiatively so that creates heat load. Auger upconversion prosses create heat load where two excited photons exchange energy and promoted to upper level. The decay of that photon creates non-radiative lattice vibrations and causes heat load. These mechanisms were introduced to simulation numerically.

Table 3.6. Opto-mechanical properties of Cr:LiCAF

Parameter	Symbol	Value
Pump Wavelength	λ_p	660 nm
Lasing Wavelength	λl	795 nm
Doping	Dp	%1.25
Absorption Coefficient	a	249.37 m^{-1} (Demirbas, 2019)
Specific Heat Capacity	Cp	0.935 J/(g*K) (Woods, 1991)
Density	rho	2.988 g/cm^3 (Woods, 1991)
Thermal Conductivity	k	5.14 //c 4.58 //a W/(mK) (Atherton, 1993)
Depth	K	10 mm
Length	L	15 mm
Height	M	2 mm
Mode Matching Factor	MMF	0.8
Refractive Index	n	1.39
Beam Waist (Tangential)	wT_0	186 um
Beam Waist (Sagital)	wS_0	12 um
Bem Focus	z_0	7.5 mm
Young's Modulus	E	96 GPa (Woods,1991)
Poisson Ratio	v	0.25 (Woods,1991
Thermal Expansion Coefficient	αe	3.1//c 21//a 10^{-6} 1/K (Peterson, 1999)
Tensile Strength	TenS	62 MPa (Demirbas, 2018)

Opto-mechanical properties of Cr:LiCAF given in table 3.6. The heat source density was applied to the crystal based on the configuration of the laser pump beam. In this study, pump beam assumed as elliptical beam. Provide heat source as an elliptical beam following expression used (Fu et al., 2013);

$$Q(x,y,z) = \frac{2(n_{heat})P_{in}alpha}{\pi\big(wS(z) * wT(z)\big)} \text{Exp}\left[-\frac{2(x^2+y^2)}{wS(z)^2 * wT(z)^2}\right] Exp[-az] \tag{3.11}$$

where n_{heat} is heat load, P_{in} in input power. To calculate tangential and sagittal cavity beam waist following expressions used:

$$wT(z) = wT_0\sqrt{1+\left[\frac{M^2\lambda_p(z-z_0)}{n\pi wT_0^2}\right]^2} \tag{3.12}$$

$$wS(z) = wS_0\sqrt{1+\left[\frac{M^2\lambda_p(z-z_0)}{n\pi wS_0^2}\right]^2} \tag{3.13}$$

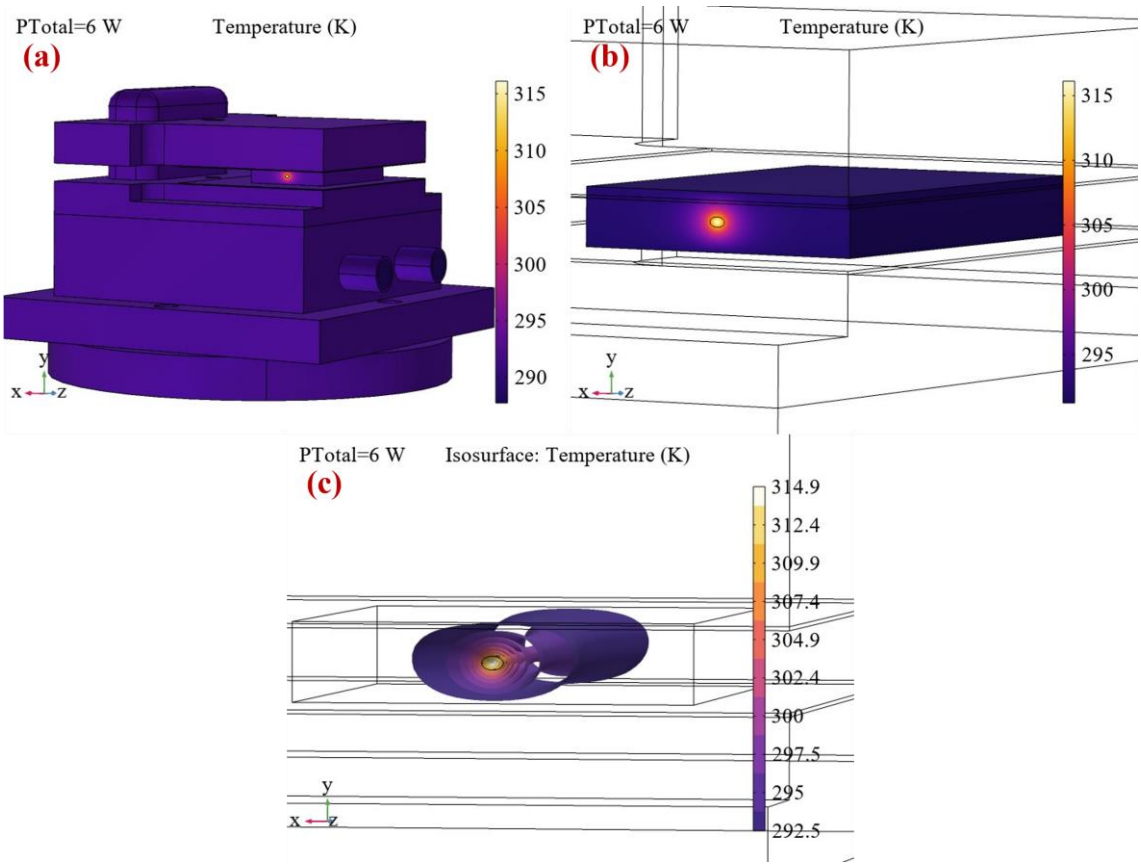

Figure 3.47. Simulation results of 15 mm Cr:LiCAF crystal inside copper holder during 6 W of pump power. a) shows the general temperature distribution over the holder; b) shows the crystal temperature distribution; c) shows the isothermal contours along pump beam

Simulation results were obtained at 6 W pump power, since 15 mm 1.25% Cr doped gain medium absorbed around 5.8 W of pump power. To perform more realistic calculations, with the help of the multiphysics properties of simulation software, water cooling at 15 °C was provided alongside the pipeline. Figure 3.47, shows the 3D temperature distribution of Cr:LiCAF gain medium under the 6 W pump power. In figure (a) the crystal holder that was used during the laboratory experiments was designed with a realistic size. As seen on figure 3.47 (c) the temperature of the gain medium along the pump beam reached up to 315 K (42 °C). Figure 3.48 represents this temperature change along the beam axis inside the crystal. As expected, an increase on the pump power creates more heat load on the crystal. However, around the middle of the pump beam gets smaller and due to the low absorption around the focus point heat load decreases.

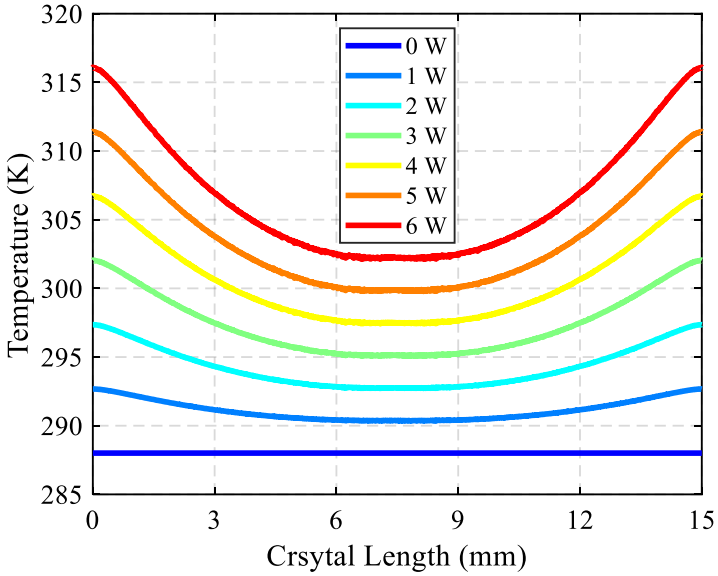

Figure 3.48. Temperature distribution along the pump beam axis of Cr:LiCAF crsytal with different pump power

Finally, the maximum temperature of Cr:LiCAF crystal as a function of pump power is given in figure 3.49. The temperature increases linearly up to 63 W, after which a breakdown occurs, and all the power is dissipated as heat load. That creates an enormous amount of temperature increase. That breakdown is caused by the thermal quenching of fluorescence lifetime. As Okuyucu measured in 2023, after crystal temperature reaches 563 K, the fluorescence lifetime typically decreases to half of the radiative lifetime. Which leads to non-radiative transaction and cause excessive heat load.

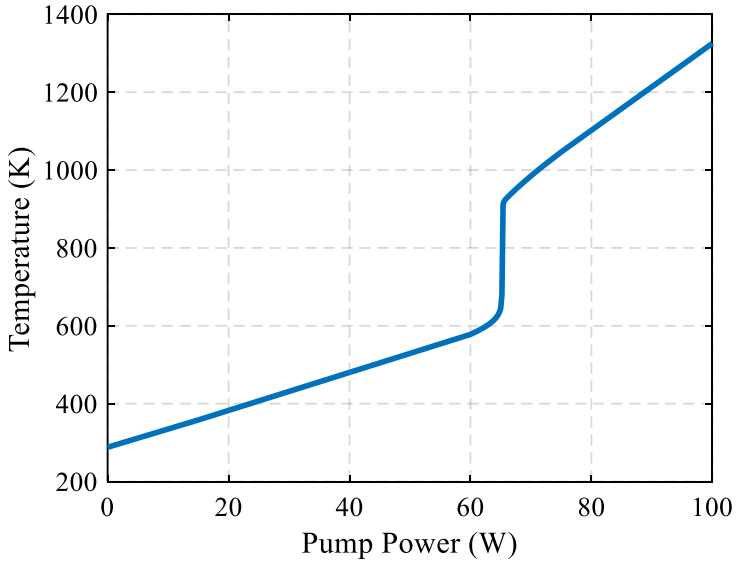

Figure 3.49. Calculated maximum temperature as of Cr:LiCAF crystal as a function of pump power between 0-100 W

As a conclusion, for the temperature estimation of Cr:LiCAF two different methods were performed. During the first method experimentally fluorescence emission of Cr:LiCAF gain medium measured between the 10-100 °C interval. The peak points of the measured emission were extracted and compared with the cw peak point. In the second method, the numerical calculation of temperature was performed with a finite element model. One can say that the first method, experimental measurements and post-processing can be improved to obtain more accurate results. For the simulation, the results obtained can be supported with additional simulations to compare the results accuracy. Nevertheless, temperature of 15 mm Cr:LiCAF laser under the 6 W pump power could be estimated at around 40 °C.

3.8. Two-Color Cr:LiCAF Laser

In this section, the two-color (dual wavelength) Cr:LiCAF lasers were investigated. A crystalline quartz birefringent filter (BRF) was utilized to employ two-color lasing. Two-color lasers have become more popular lately. Their potential application in various fields such as terahertz (THz) generation and remote sensing. Two-color lasing achieved with different methods including dual-crystal cavity. Another method to obtain dual wavelength is using the birefringent filter. Here the two-color lasing performance of birefringent filter has been tested. To do that, in two different diving angles (σ) with 90° named as on surface and 25° named as off-surface, various thickness BRF plates utilized. For on-surface BRF 2 mm, 4 mm, 8 mm, and for off-surface BRF 2 mm, 4 mm, and 8 mm plates compared. As a starting point the theoretical calculation made for the understand background of experimental studies.

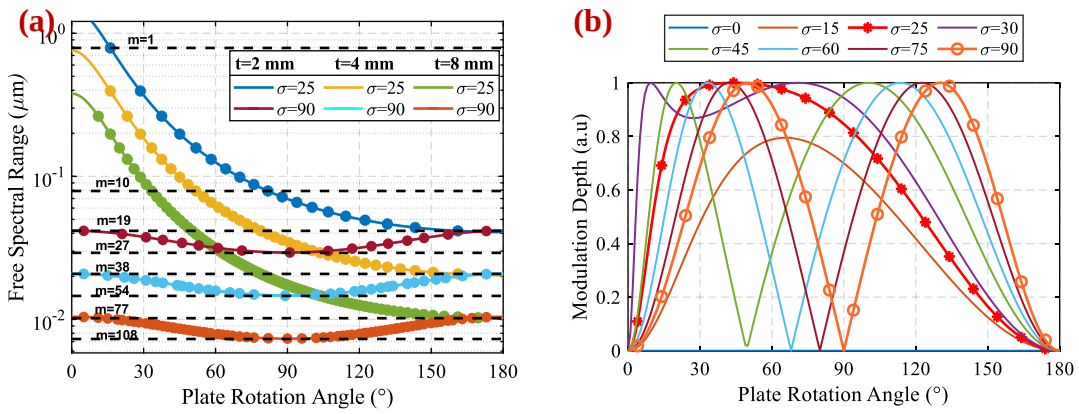

Figure 3.50. Calculated variation of (a) free spectral range as a function of plate rotation angle for on surface and off surface BRF plate; (b) modulation depth as a function plate rotation angle for different diving angle plates

Figure 3.50 shows the variation of calculated of free spectral range (FSR) for on-surface and offsurface BRF plates as a function of plate rotation angle. Calculations were performed for plates with thicknesses of 2 mm, 4 mm, and 8 mm. The on-surface, BRF plates FSR range limited only the 7-41 nm range. On the other hand, off-surface BRF

provides achievable FSR 10-790 nm range. The FSR of BRF calculated via (Demirbas, 2017);

$$FSR = \frac{\lambda^2 \cos(\beta)}{t\Delta n sin^2(\gamma)} \tag{3.14}$$

where λ fundamental wavelength and t is BRF thickness, Δn is birefringence, β is the internal Brewster's angle, and γ is the angle between optic axis and beam propagation direction. Figure 3.50 (b) shows the calculated modulation depth of BRF plate for different diving angles as a function of plate rotation angle. Modulation depth of BRF calculated via;

$$MD = 4\, cos^2(\theta) sin^2(\theta) \tag{3.15}$$

where θ is angle between TM-polarized electric field and ordinary refractive axis of BRF. Calculated results show that, while diving angle at 25°, there is smooth modulation depth of BRF observed. This shows that off-surface BRF especially diving angle equal 25° can provide broader tuning range at 790 nm central wavelength.

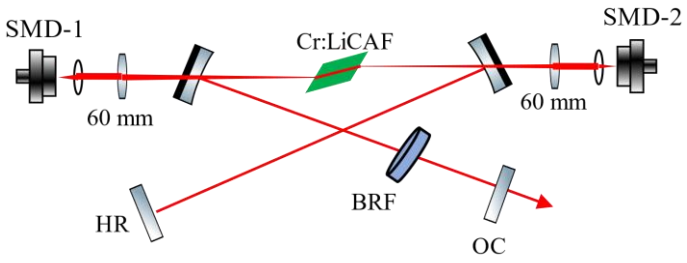

Figure 3.51. Schematics of two-color lasing experimental cavity

In the experimental part, off-surface BRF plates inserted cavity and measured the respected results. 2 mm, 4 mm, and 8 mm, off-surface BRF plates tested for the two-color lasing. Figure 3.52 shows the measured two-color lasing results of off-surface (σ=25°) BRF plates with a thickness of 2 mm, 4 mm, and 8 mm. The 2 mm BRF plates successively provided 12 pairs of two-color lasing. The two-color pair wavelength range varied between 750-848 nm and 772-812 nm. On the other hand, 4 mm BRF had more pairs compared to 2 mm. Achieved successive pair recorded as 31. The two-color wavelength separation varied between 20-96 nm. Lastly, with 8 mm thick BRF, 70 wavelength pairs were obtained. The wavelength range varied between 10-99 nm. By utilizing thicker BRFs, the overlap between the gain bandwidth of the laser crystal and the available free-spectral range values increases. This expanded overlap leads to a wider range of possibilities for two-color lasing operations. Specifically, for the 2 mm, 4 mm, and 8 mm thick BRFs, FSR values within the ranges of 40-790 nm, 20-395 nm, and 10-263 nm, respectively, are accessible. The results clearly show that an off-surface birefringent plate has various benefits for tuning experiments.

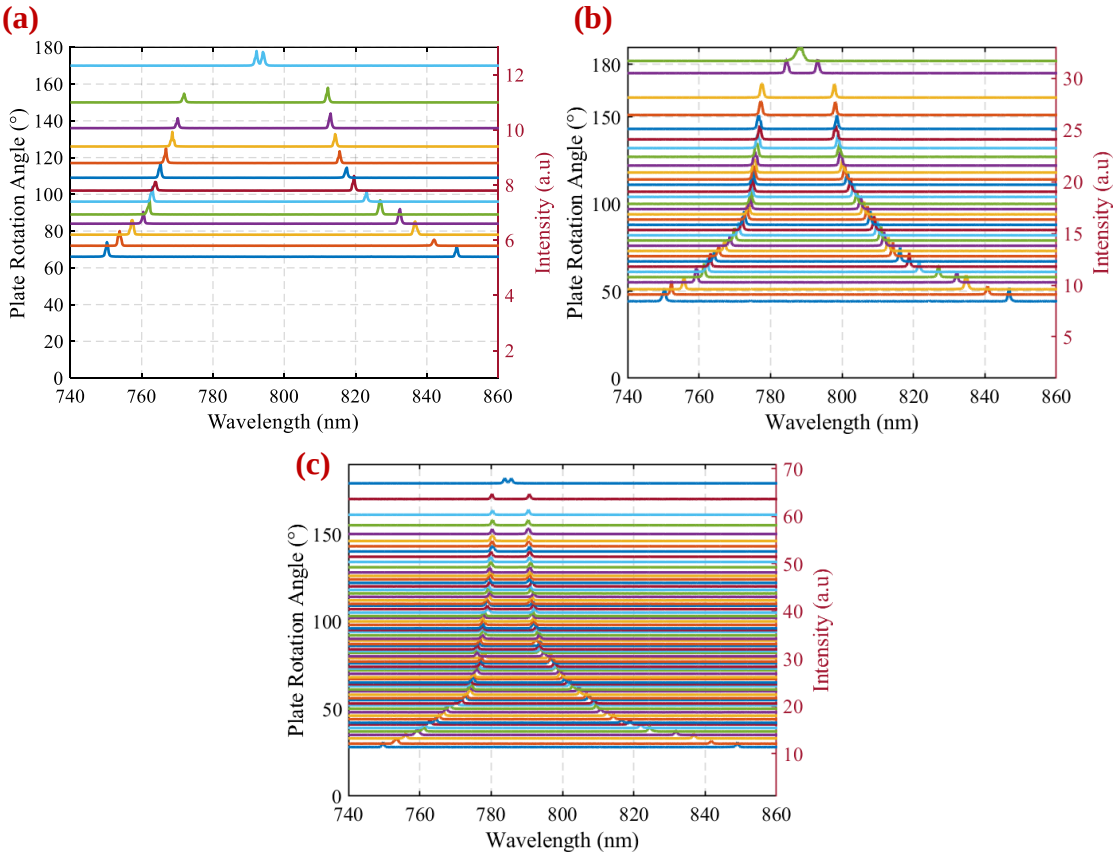

Figure 3.52. Measured two color lasing results for a) 2 mm; b) 4 mm; and c) 8 mm off surface BRF

4. CONCLUSIONS AND SUGGESTIONS

With an ignition that Theodore Harold Maiman started, over the years the position of the light in our life has been altered enormously. Lasers have found applications in diverse fields including technology, defense, and healthcare. In this thesis, one of the solid-state laser family member of Cr:LiCAF laser performance investigated in different operation regimes. To do that low-ion doped gain mediums utilized. As a starting point, doping characterization was performed for 5 samples with lengths of 10 mm, 12.5 mm, 15 (2) mm and 20 mm. As a result of the characterization, the doping concentration for 10 mm, 12.5 mm, 15 (a) mm, 15 (b) mm, and 20 mm were determined as 1.25%, 1.40%, 1.25%, 1.25% and 1%, respectively.

All these samples were tested for potential power scaling application in four multimode diode pumped system. The 10 mm sample with a 1.25% concentration yielded a maximum output power of 2.22 W, while the absorbed pump power was 5.35 W. This corresponded to 49% slope efficiency and 41% optical-to-optical conversion efficiency. Obtained results indicated that the potential of low-ion doped Cr:LiCAF gain mediums possesses optimum laser performance compared to the higher ion doped gain mediums. Furthermore, these findings create opportunities for the development of high-power applications. It can be stated with clarity that crystals of this kind low-ion doped can be effectively employed at pump powers exceeding 10 W. The broadband wavelength tuning results showed that for the related gain medium, 741-874 nm tunability performance was obtained. Despite this, with a low-loss, shorter length (~8 mm), and antireflective coated crystal, the tunability can be extended even further, showcasing a range of 133 nm.

Gain switch and quasi continuous wave experiments employed for the Cr:LiCAF laser to examine the reaction under the pulse pumping. There was an 18% increase on the output power and on the lower pulse duration (<250 us) around 4.3 μs pulsed lasers obtained. In further studies this experimental configuration could be employed to test the quasi continuous wave mode-locking Cr:LiCAF lasers. In intracavity second harmonic generation experiments, different length and conversion wavelength nonlinear crystals are placed inside the cavity. The highest second harmonic power obtained with 4 mm 800-400 nm BBO crystal as 441 mW. Moreover, the second harmonic tuning range measured as 377-424 nm. The short wavelength tuning performance can be extended by utilizing antireflective coated nonlinear crystals. On the contrary, for achieving long wavelength tuning performance, another member of the colquiriite family, namely Cr:LiSAF laser, could be utilized, offering a broader range of tunability.

Following, pulse operations were conducted with an SBR. In passive Q-switching experiments, shortest pulse measured as 1.4 μs and maximum pulse energy assumed as 8 uJ. On the other hand, in passive mode-locking experiments pulse duration varied between 127-65 *fs* with a pulse energy between 0.37-0.22 nJ. In mode-locking experiments, obtained pulse durations could be shorter, regarding the dispersion mirrors variations. However, this should be noted that the longer. Adjustability in dispersion compensation may present this opportunity.

Lately, with a temperature estimation studies low-ion doped Cr:LiCAF lasers potentially used in power scaling operation. Multiphysics simulations and cw operation

results show that Cr:LiCAF crystals come through around 50 W pump power. On the final part, two-color performance of Cr:LiCAF laser examined and off surface BRF filter benefits reported. Further, studies will be carried out to perform two-color mode-locking performance of Cr:LiCAF lasers. Overall, all these results give an insight into the low-ion doped Cr:LiCAF lasers, for further studies.

REFERENCES

Books

Denker, B., & Shklovsky, E. (Eds.). (2013). *Handbook of solid-state lasers: materials, systems and applications*. Elsevier.

Eichler, H. J., Eichler, J., & Lux, O. (2018). Lasers: basics, advances and applications.

Hecht, J. (1999). *The Laser Guidebook.* McGraw-Hill Education.

Koechner, W. (2006). *Solid-state laser engineering*. Springer.

Maini, A. K. (2013). *Lasers and optoelectronics: fundamentals, devices and applications*. John Wiley & Sons.

Paschotta, R. (2008a). *Field guide to lasers* (Vol. 12). Bellingham, WA: SPIE press.

Paschotta, R. (2008b). Field guide to laser pulse generation, no. FG14 in SPIE field guides.

Sennaroglu, A. (2010). *Photonics and laser engineering: principles, devices, and applications*. McGraw-Hill.

Silfvast, W. T. (2004). *Laser fundamentals*. Cambridge university press.

Sorokin, E. (2004). Solid-state materials for few-cycle pulse generation and amplification. *Topics in Applied Physics*, *95*, 3-72.

Svelto, O., & Hanna, D. C. (2010). *Principles of lasers* (Vol. 1). New York: Springer.

Weber, M. J. (2000). *Handbook of lasers* (Vol. 18). CRC press.

Weber, M. J. (Ed.). (2018). *Handbook of laser wavelengths*. CRC press.

Articles

Atherton, L. J., Payne, S. A., & Brandle, C. D. (1993). Oxide and fluoride laser crystals. *Annual Review of Materials Science*, *23*(1), 453-502. https://doi.org/10.1146/annurev.ms.23.080193.002321

Beyatli, E., Sennaroglu, A., & Demirbas, U. (2013). Self-q-switched cr: licaf laser. *JOSA B*, *30*(4), 914-921.

Bruce W. Woods, Stephen A. Payne, John E. Marion, Robert S. Hughes, and Laura E. Davis, "Thermomechanical and thermo-optical properties of the $LiCaAlF_6$:Cr^{3+} laser material," J. Opt. Soc. Am. B **8**, 970-977 (1991) https://doi.org/10.1364/JOSAB.8.000970

Caird, J. A., Payne, S. A., Staver, P. R., Ramponi, A. J., & Chase, L. L. (1988). Quantum electronic properties of the Na3Ga2Li3F12: Cr3+ laser. *IEEE Journal of Quantum Electronics*, *24*, 1077-1099. 10.1109/3.231

Chaoyang, L., Yong, B., Feng, Y., Zhichao, W., Yiting, X., Yuanbin, W., ... & Zuyan, X. (2010). 106.5 W high beam quality diode-side-pumped Nd: YAG laser at 1123 nm. *Optics Express*, *18*(8), 7923-7928. https://doi.org/10.1364/OE.18.007923

De Yoreo, J. J., Atherton, L. J., & Roberts, D. H. (1991). Elimination of scattering centers from Cr: LiCaAlF6. *Journal of crystal growth*, *113*(3-4), 691-697. https://doi.org/10.1016/0022-0248(91)90106-F

Demirbas, U. (2010). *Low-cost, highly efficient, and tunable ultrafast laser technology based on directly diode-pumped Cr: Colquiriites* (Doctoral dissertation, Massachusetts Institute of Technology, Department of Electrical Engineering and Computer Science). http://hdl.handle.net/1721.1/60097

Demırbas, U. (2017). Off-surface optic axis birefringent filters for smooth tuning of broadband lasers. *Applied optics*, *56*(28), 7815-7825. https://doi.org/10.1364/AO.56.007815

Demirbas, U. (2018). Power scaling potential of continuous-wave Cr: LiSAF and Cr: LiCAF lasers in thin-disk geometry. *Applied Optics*, *57*(35), 10207-10217. https://doi.org/10.1364/AO.57.010207

Demirbas, U. (2019). Cr: Colquiriite Lasers: Current status and challenges for further progress. *Progress in quantum electronics*, *68*, 100227. https://doi.org/10.1016/j.pquantelec.2019.100227

Demirbas, U., & Acar, D. A. E. (2016). Continuous-wave, quasi-continuous-wave, gain-switched, and femtosecond burst-mode operation of multi-mode diode-pumped Cr: LiSAF lasers. *JOSA B*, *33*(10), 2105-2113. https://doi.org/10.1364/JOSAB.33.002105

Demirbas, U., Baali, I., Acar, D. A. E., & Leitenstorfer, A. (2015). Diode-pumped continuous-wave and femtosecond Cr: LiCAF lasers with high average power in the near infrared, visible and near ultraviolet. *Optics Express*, *23*(7), 8901-8909. https://doi.org/10.1364/OE.23.008901

Demirbas, U., Li, D., Birge, J. R., Sennaroglu, A., Petrich, G. S., Kolodziejski, L. A., ... & Fujimoto, J. G. (2009b). Low-cost, single-mode diode-pumped Cr: Colquiriite lasers. *Optics Express*, *17*(16), 14374-14388. https://doi.org/10.1364/OE.17.014374

Demirbas, U., Schmalz, M., Sumpf, B., Erbert, G., Petrich, G. S., Kolodziejski, L. A., ... & Leitenstorfer, A. (2011). Femtosecond Cr: LiSAF and Cr: LiCAF lasers pumped by tapered diode lasers. *Optics Express*, *19*(21), 20444-20461. https://doi.org/10.1364/OE.19.020444

Demirbas, U., Sennaroglu, A., Benedick, A., Siddiqui, A., Kärtner, F. X., & Fujimoto, J. G. (2007). Diode-pumped, high-average-power femtosecond Cr 3+: LiCAF laser. *Optics letters*, *32*(22), 3309-3311.

Demirbas, U., Sennaroglu, A., Kärtner, F. X., & Fujimoto, J. G. (2009a). Comparative investigation of diode pumping for continuous-wave and mode-locked Cr 3+: LiCAF lasers. *JOSA B*, *26*(1), 64-79. https://doi.org/10.1364/JOSAB.26.000064

Demirbas, U., Sennaroglu, A., Kärtner, F. X., & Fujimoto, J. G. (2008). Highly efficient, low-cost femtosecond Cr 3+: LiCAF laser pumped by single-mode diodes. *Optics letters*, *33*(6), 590-592. https://doi.org/10.1364/OL.33.000590

Demirbas, U., Sennaroglu, A., Kärtner, F. X., & Fujimoto, J. G. (2009c). Generation of 15 nJ pulses from a highly efficient, low-cost multipass-cavity Cr 3+: LiCAF laser. *Optics letters*, *34*(4), 497-499. https://doi.org/10.1364/OL.34.000497

Demirbas, U., Thesinga, J., Kellert, M., Kärtner, F. X., & Pergament, M. (2020). Comparison of different in situ optical temperature probing techniques for

cryogenic Yb: YLF. *Optical Materials Express*, *10*(12), 3403-3413. https://doi.org/10.1364/OME.411331

Demirbas, U., Uecker, R., Klimm, D., & Wang, J. (2012). Low-cost, broadly tunable (375–433 nm & 746–887 nm) Cr: LiCAF laser pumped by one single-spatial-mode diode. *Applied Optics*, *51*(35), 8440-8448. https://doi.org/10.1364/AO.51.008440

Demirbas, U., Uecker, R., Klimm, D., Sumpf, B., & Erbert, G. (2014). Intra-cavity frequency-doubled Cr: LiCAF laser with 265 mW continuous-wave blue (395–405 nm) output. *Optics Communications*, *320*, 38-42. https://doi.org/10.1016/j.optcom.2014.01.045

Einstein, A. (1905). On a heuristic viewpoint of the creation and modification of light. *Ann. d. Phys*, *17*, 133-148.

Einstein, A. (1917). On the quantum mechanics of radiation. *Physikalische Zeitschrift*, *18*(121.128).

Findlay, D., & Clay, R. A. (1966). The measurement of internal losses in 4-level lasers. *Physics Letters*, *20*(3), 277-278. https://doi.org/10.1016/0031-9163(66)90363-5

Fu, X., Hong, K. H., Chen, L. J., & Kärtner, F. X. (2013). Performance scaling of high-power picosecond cryogenically cooled rod-type Yb: YAG multipass amplification. *JOSA B*, *30*(11), 2798-2809. https://doi.org/10.1364/JOSAB.30.002798

Gäbel, K. M., Rußbüldt, P., Lebert, R., & Valster, A. (1998). Diode pumped Cr3+: LiCAF fs-laser. *Optics communications*, *157*(1-6), 327-334. https://doi.org/10.1016/S0030-4018(98)00526-4

Gensic, J. E., Marcos, H. M., & Van Uitert, L. G. (1964). Laser oscillations in Nd-doped Yttrium aluminium, Yttrium gallium and Gadolinium garnet. *Appl Phys Lett*, *4*, 182. https://doi.org/10.1063/1.1753928

Gordon, J. P., Zeiger, H. J., & Townes, C. H. (1955). The maser—new type of microwave amplifier, frequency standard, and spectrometer. *Physical review*, *99*(4), 1264. https://doi.org/10.1103/PhysRev.99.1264

Hargrove, L. E., Fork, R. L., & Pollack, M. A. (1964). Locking of He–Ne laser modes induced by synchronous intracavity modulation. *Applied Physics Letters*, *5*(1), 4-5. https://doi.org/10.1063/1.1754025

Isemann, A., & Fallnich, C. (2003). High-power Colquiriite lasers with high slope efficiencies pumped by broad-area laser diodes. *Optics Express*, *11*(3), 259-264. https://doi.org/10.1364/OE.11.000259

J. M. Eichenholz and M. Richardson, "Measurement of Thermal Lensing in Cr3+ doped Colquiriites.," in *Advanced Solid State Lasers*, W. Bosenberg and M. Fejer, eds., Vol. 19 of OSA Trends in Optics and Photonics Series (Optica Publishing Group, 1998), paper CS26. https://doi.org/10.1364/ASSL.1998.CS26

Jabczyński, J. K., Zendzian, W., Mierczyk, Z., & Frukacz, Z. (2001). Chromium-doped LiCAF laser passively Q switched with a V 3+: YAG crystal. *Applied optics*,

40(36), 6638-6645. https://doi.org/10.1364/AO.40.006638

Keller, U., Weingarten, K. J., Kartner, F. X., Kopf, D., Braun, B., Jung, I. D., ... & Der Au, J. A. (1996). Semiconductor saturable absorber mirrors (SESAM's) for femtosecond to nanosecond pulse generation in solid-state lasers. *IEEE Journal of selected topics in QUANTUM ELECTRONICS*, *2*(3), 435-453. 10.1109/2944.571743

Klein, M. J. (1955). Principle of detailed balance. *Physical Review*, *97*(6), 1446

Klimm, D., & Reiche, P. (1998). Nonstoichiometry of the new laser host LiCaAlF6. *Crystal Research and Technology: Journal of Experimental and Industrial Crystallography*, *33*(3), 409-416.

Klimm, D., & Reiche, P. (1999). Ternary colquiriite type fluorides as laser hosts. *Crystal Research and Technology: Journal of Experimental and Industrial Crystallography*, *34*(2), 145-152.

Klimm, D., Lacayo, G., & Reiche, P. (2000). Growth of Cr: LiCaAlF6 and Cr: LiSrAlF6 by the Czochralski method. *Journal of crystal growth*, *210*(4), 683-693. https://doi.org/10.1016/S0022-0248(99)00762-9

Klimm, D., Uecker, R., & Reiche, P. (2005). Melting behavior and growth of colquiriite laser crystals. *Crystal Research and Technology: Journal of Experimental and Industrial Crystallography*, *40*(4-5), 352-358. https://doi.org/10.1002/crat.200410350

Lacayo, G., Hähnert, I., Klimm, D., Reiche, P., & Neumann, W. (1999). Transmission electron microscope study of secondary phases in Cr3+: LiCaAlF6 single crystals. *Crystal Research and Technology: Journal of Experimental and Industrial Crystallography*, *34*(9), 1221-1227.

Maiman, T. H. (1960). Stimulated optical radiation in ruby. *Nature*, *4736*, 493-494. https://doi.org/10.1038/187493a0

McClung, F. J., & Hellwarth, R. W. (1962). Giant optical pulsations from ruby. *Applied Optics*, *1*(101), 103-105. https://doi.org/10.1364/AO.1.S1.000103

Moulton, P. F. (1986). Spectroscopic and laser characteristics of Ti: Al 2 O 3. *JOSA B*, *3*(1), 125-133. https://doi.org/10.1364/JOSAB.3.000125

Okuyucu, S., Ozturk, Y., & Demirbas, U. (2021). Passively Q-switched Cr: LiCAF laser with a saturable Bragg reflector. *Applied Physics B*, *127*(4), 54. https://doi.org/10.1007/s00340-021-07593-x

Okuyucu, S., Thesinga, J., Tanaka, H., Ozturk, Y., Kärtner, F. X., Pergament, M., & Demirbas, U. (2023). Temperature dependence of the emission cross-section and fluorescence lifetime in Cr: LiCAF, Cr: LiSAF, and Cr: LiSGaF between 78 K and 618 K. *Optical Materials Express*, *13*(5), 1211-1227. https://doi.org/10.1364/ASSL.2022.JTu6A.8

P. LiKamWa, B. H. T. Chai, and A. Miller, "Self-mode-locked Cr^{3+}:$LiCaAlF_6$ laser," Opt. Lett. 17, 1438-1440 (1992) https://doi.org/10.1364/OL.17.001438

Payne, S. A., Chase, L. L., Newkirk, H. W., Smith, L. K., & Krupke, W. F. (1988). LiCaAlF/sub 6: Cr/sup 3+: a promising new solid-state laser material. *IEEE*

Journal of Quantum Electronics, *24*(11), 2243-2252. 10.1109/3.8567

Payne, S. A., Chase, L. L., Smith, L. K., & Chai, B. H. (1990). Flashlamp-pumped laser performance of LiCaAIF 6: Cr 3+. *Optical and quantum electronics*, *22*, S259-S268.

Payne, S. A., Chase, L. L., Smith, L. K., Kway, W. L., & Newkirk, H. W. (1989). Laser performance of LiSrAlF6: Cr3+. *Journal of Applied Physics*, *66*(3), 1051-1056. https://doi.org/10.1063/1.343491

Peterson, R. D., Pham, A. T., Jenssen, H. P., Cassanho, A., & Castillo, V. (1999, January). Thermo-optical comparison of LiSAF, LiCAF, and LiSGaF. In *Advanced solid state lasers* (p. TuB6). Optica Publishing Group. https://doi.org/10.1364/ASSL.1999.TuB6

Philipp Wagenblast, Richard Ell, Uwe Morgner, Felix Grawert, and Franz X. Kärtner, "Diode-pumped 10-fs Cr^{3+}:LiCAF laser," Opt. Lett. **28**, 1713-1715 (2003) https://doi.org/10.1364/OL.28.001713

R. Scheps, J. F. Myers and S. A. Payne, "CW and Q-switched operation of a low threshold Cr/sup +3/:LiCaAlF/sub 6/ laser," in *IEEE Photonics Technology Letters*, vol. 2, no. 9, pp. 626-628, Sept. 1990, doi: 10.1109/68.59352. 10.1109/68.59352

Sakadžić, S., Demirbas, U., Mempel, T. R., Moore, A., Ruvinskaya, S., Boas, D. A., ... & Fujimoto, J. G. (2008). Multi-photon microscopy with a low-cost and highly efficient Cr: LiCAF laser. *Optics express*, *16*(25), 20848-20863. https://doi.org/10.1364/OE.16.020848

Schawlow, A. L., & Townes, C. H. (1958). Infrared and optical masers. *Physical Review*, *112*(6), 1940. https://doi.org/10.1103/PhysRev.112.1940

Spence, D. E., Kean, P. N., & Sibbett, W. (1991). 60-fsec pulse generation from a self-mode-locked Ti: sapphire laser. *Optics letters*, *16*(1), 42-44. https://doi.org/10.1364/OL.16.000042

Stalder, M., Bass, M., & Chai, B. H. (1992). Thermal quenching of fluorescence in chromium-doped fluoride laser crystals. *JOSA B*, *9*(12), 2271-2273. https://doi.org/10.1364/JOSAB.9.002271

Wagenblast, P. C., Morgner, U., Grawert, F., Schibli, T. R., Kärtner, F. X., Scheuer, V., ... & Lederer, M. J. (2002). Generation of sub-10-fs pulses from a Kerr-lens mode-locked Cr 3+: LiCAF laser oscillator by use of third-order dispersion-compensating double-chirped mirrors. *Optics letters*, *27*(19), 1726-1728. https://doi.org/10.1364/OL.27.001726

Walling, J. C., Peterson, O., Jenssen, H., Morris, R. C., & O'Dell, E. (1980). Tunable alexandrite lasers. *IEEE Journal of Quantum Electronics*, *16*(12), 1302-1315. 10.1109/JQE.1980.1070430

Wenqi Li, Zebiao Gan, Lianghong Yu, Cheng Wang, Yanqi Liu, Zhen Guo, Lu Xu, Min Xu, Yin Hang, Yi Xu, Jianye Wang, Pei Huang, He Cao, Bo Yao, Xiaobo Zhang, Lingru Chen, Yunhai Tang, Shuai Li, Xingyan Liu, Shanming Li, Mingzhu He, Dinjun Yin, Xiaoyan Liang, Yuxin Leng, Ruxin Li, and Zhizhan Xu, "339 J high-energy Ti:sapphire chirped-pulse amplifier for 10 PW laser facility," Opt. Lett. 43, 5681-5684 (2018) https://doi.org/10.1364/OL.43.005681

VITA

List of Publication;

- **Z. Erturk,** S. Okuyucu, M. Kilinc, Y. Ozturk, M. Pergament, F. X. Kärtner, and U. Demirbas, "Broadly tunable two-color lasing of Cr:LiCAF with on-surface and off-surface optical axis birefringent filters: performance comparison," Appl. Opt. 61, 10735-10743 (2022)
- Y. Ozturk, M. Kilinc, **Z. Erturk,** H. Buzcu. "Termal analiz ve iyileştirilmiş tutucu tasarımı ile 1.5 W Lazer Diyot çift-uç pompalı levha geometrisine sahip Cr:Nd:GSGG lazer sistemi". Gazi Üniversitesi Mühendislik Mimarlık Fakültesi Dergisi 38 (2023): 2347-2358
- **Z. Erturk**, S. Okuyucu, M. Kilinc, E. Beyatli, Y. Ozturk, U. Demirbas "Challenges in power scaling of Cr:LiCAF lasers: effect of passive losses", in preparation for Applied Optics.